The Philosophical Magazine

FIRST PUBLISHED IN 1798

A Journal of Theoretical Experimental and Applied Physics

Vol. 5 February 1960 No. 50
Eighth Series

25s. 0d., plus postage
Annual Subscription £13 10s. 0d., payable in advance

ALERE FLAMMAM

Printed and Published by
TAYLOR & FRANCIS LTD
RED LION COURT, FLEET STREET, LONDON, E.C.4

THE PHILOSOPHICAL MAGAZINE

Authors wishing to submit papers for publication in the Journal should send manuscripts directly to the Publishers.

Manuscripts should be typed in *double* spacing on one side of quarto (8×10 in.) paper, and authors are urged to aim at absolute clarity of meaning and an attractive presentation of their texts.

References should be listed at the end in alphabetical order of authors and should be cited in the text in terms of author's name and date. Diagrams should normally be in Indian ink on white card, with lettering in soft pencil, the captions being typed on a separate sheet.

A leaflet giving detailed instructions to authors on the preparation of papers is available on request from the Publishers.

Authors are entitled to receive 25 offprints of a paper in the Journal free of charge, and additional offprints can be obtained from the Publishers.

The *Philosophical Magazine* and its companion journal, *Advances in Physics*, will accept papers for publication in experimental and theoretical physics. The *Philosophical Magazine* publishes contributions describing new results, letters to the editor and book reviews. *Advances in Physics* publishes articles surveying the present state of knowledge in any branch of the science in which recent progress has been made. The editors welcome contributions from overseas as well as from the United Kingdom, and papers may be published in English, French and German.

The de Haas–van Alphen Effect in Copper, Silver and Gold†

By D. Shoenberg
Royal Society Mond Laboratory, Cambridge

[Received January 5, 1960]

Abstract

Measurements of the de Haas–van Alphen effect in copper, silver and gold suggest strongly that the Fermi surfaces of these metals make contact with the hexagonal faces of the Brillouin zone. The areas of cross section of the main part of the Fermi surface and of the contact have been determined. Some provisional values of effective masses have also been obtained.

When the de Haas–van Alphen effect in copper was discovered a year ago by the impulsive field technique (Shoenberg 1959), the hope was expressed that this would open the way to a detailed study of the electronic structure of the monovalent metals. As far as copper, silver and gold are concerned this hope was been amply fulfilled and there is now little doubt that supplemented by guidance from studies by other methods, the de Haas–van Alphen effect will yield very detailed information about the Fermi surfaces of these metals. Since, however, it is clear that further progress will require certain improvements of experimental technique followed by systematic measurements which will inevitably take some time, it seems worth while giving a brief survey of the results obtained to date, even though many details are still incomplete.

The results strongly suggest that the Fermi surfaces for copper, silver and gold make contact with the eight [111] faces of the Brillouin zone (B.Z.). Thus the de Haas–van Alphen effect demonstrates that the general shape of Fermi surface proposed by Pippard (1957) for copper applies also to silver and gold. Except when the small departures from sphericity are of importance a convenient simplified model of this surface is a sphere (the 'belly') with eight short cylinders ('necks') protruding from it along the [111] directions to meet the hexagon faces of the B.Z. normally. The B.Z. can of course be thought of as the unit cell of an infinite lattice in which each cell contains a Fermi surface of the kind just described. We thus have a complicated multiply-connected surface and corresponding to any closed circuit of extremal area (which encloses either holes or electrons) produced by planes cutting the surface normally to the magnetic field direction, there should be de Haas–van Alphen oscillations of a period

† Communicated by the Author.

inversely proportional to the extremal area. It turns out that there is quite a variety of possible extremal circuits and the corresponding de Haas–van Alphen oscillations for some of these have been observed.

The predominant period observed in most directions is that due to the belly and this period gives an area of cross section within a few per cent of that of the diametral section of a free electron sphere. Thus the belly periods vary between copper, silver and gold almost exactly as the two-thirds power of the atomic volumes, with a constant of proportionality appropriate to the assumption of one free electron per atom. In principle the multiple connectivity of the Fermi surface could be demonstrated by the absence of the belly period over certain restricted ranges of field directions for which no extremal closed circuit round the belly can exist. In fact some such ranges of field directions have been observed, and these are consistent with the hypothesis of multiple connectivity. However, no thorough study of these 'absent' ranges has yet been made and in any case lack of observed oscillations is not in itself conclusive evidence, because amplitude may become small for a variety of reasons; more direct evidence for multiple connectivity is presented below.

The variation of the belly period with field direction is slight, because the area of cross section is evidently rather insensitive to even quite appreciable departures from sphericity. In order to study this slight variation of period two methods have been used which are rather more precise than the direct and absolute method of measuring the change of 1/H for a given number of periods. These are (*a*) measurement of the separation of the two resonant peaks which occur when the oscillations are amplified by a resonant circuit; because of the parabolic time variation of the field close to the maximum field this separation is directly proportional to the period and provides a rapid comparison method with a relative accuracy of order 1% in favourable conditions, (*b*) measurements of beats between the oscillations of two specimens of different orientations; in favourable conditions differences of period of 3% can be measured with an accuracy of 2 or 3% giving a relative accuracy of 0·1% or better. A summary of the results on belly periods is given in table 1; the most detailed results have been obtained for copper; those for silver and gold are based on far fewer experiments and should be regarded as somewhat provisional. The difference between the periods in [111] and [100], which has been determined rather precisely for copper, appears to be at variance with the prediction of Pippard's detailed model. The absolute values are also discrepant, but since absolute measurements of period are subject to many small corrections, it is not out of the question that some source of systematic error has been overlooked, which might yet change the absolute values by more than the errors suggested in table 1. The source of the discrepancy in the relative values is not yet clear, but it suggests that the detailed form of the departure from sphericity proposed by Pippard may not be unique in accounting for his anomalous skin effect data.

The general topological features of the Pippard model first received confirmation in a study of a gold crystal, which showed a long period, about 31 times that of the belly period, in a range of field directions around [111]. An obvious interpretation is to associate this long period with a cut through the neck in the [111] direction. The geometry of the B.Z. is such that the length of the neck between free electron spheres has to be 0·107 of the sphere diameter; the period shows that the central diameter of the neck for gold is 0·18 that of the sphere. The variation of the neck period with field direction away from [111] suggests (as is very reasonable) that the neck is really more like a hyperboloid of revolution than a cylinder, and a closer study of this variation should provide a detailed picture of the shape of the neck. Following the discovery of the neck period in gold it was looked for more carefully in copper and was eventually shown up in collaboration with Mr. M. G. Priestley who has designed a new magnetic field coil to give $1{\cdot}6\times10^5$ gauss rather than the $1{\cdot}2\times10^5$ gauss available in the standard equipment. The higher

Table 1. Belly Periods (all in units of 10^{-9} G^{-1})

	P_{111}	P_{100}	p_{111}	p_{100}	p_F
Cu	1·608	1·557	±1·00	±0·26	1·637
	(1·681)	(1·698)	(−0·46)	(−0·32)	
Ag	2·00	1·96			2·09
Au	2·05	1·95			2·09

NOTES.—p stands for $(1/P)(d^2P/d\theta^2)$ where θ is a small angle away from a symmetry direction; the sign of the experimental values of p has not been determined and the values are probably accurate to 20%; P_F is the free electron sphere value. The figures in brackets are estimates based on Pippard's model. The experimental values of P, both absolute and relative, have been more carefully determined for Cu than for Ag and Au; the absolute values for Cu should be within 2 or 3% of the true values, while those for Ag and Au may be somewhat more in error.

field revealed long period oscillations in a [111] copper whisker of period about 24 times that of the belly period (i.e. neck diameter 0·20 that of the sphere); the amplitude was feeble and no study of the variation of this period with orientation has yet been attempted. Probably the feebleness of these neck oscillations in copper even in the higher field is associated with the fact that the effective mass of the electrons is higher in copper than in gold (see table 3). The neck diameter in copper is rather larger than that suggested by Pippard (0·16 of sphere diameter) but agrees better with the estimate of Gavenda and Morse (1959) (0·195 of sphere diameter) based on magneto-acoustic resonance. Subsequently the neck period was found also close to the [111] direction in a silver

crystal ; the period was about 51 times that of the belly period, corresponding to a neck diameter of about 0·14 that of the sphere. No study of the variation of this period with orientation has yet been made.

Further confirmation of the topology came from a gold crystal in which the field was close to a [110] direction, when weak but quite definite oscillations were observed with a period about 2·4 times the belly period, though the belly period did not itself occur. For this orientation there can be no extremal closed circuit around the belly with the model under discussion, but if we follow a path round four adjoining cells by way of the necks, there is evidently an extremal closed circuit with a shape rather like a dog's bone. Its area on the simplified assumption of exact cylinders linking exact spheres is just 0·42 or 1/2·4 that of the diametral section of the sphere, which gives very satisfactory quantitative confirmation. This ' dog's bone ' period has been looked for in copper but not yet found, perhaps because of the higher effective mass or of inadequate specimen perfection. No dog's bone period has yet been found in silver either, though it is re-assuring that the belly period in both copper and silver is absent in a range of directions round [110] where no extremal closed circuits round the belly should be possible.

Table 2. Miscellaneous Periods (all in units of 10^{-9} G^{-1})

	Neck [111]	Dog's bone [110]	4-cornered Rosette [100]
Cu	38	—	3·8 (4·1)
Ag	101	—	4·8 (4·9)
Au	62	4·7 (4·7)	—

Notes.—The neck periods were measured absolutely; the others were found by comparison with belly periods using the resonant peak method. The accuracy of the period values is probably of order 3%: the figures in brackets are estimates based on the sphere and cylinders model assuming the diametral area of the sphere to be given by the mean of P_{111} and P_{100} as given in table 1. In Au the variation of the neck period has been studied as H moves away from [111] in a [110] plane; it falls to about 55 at about 13° from [111] (towards [100]) and the oscillations then vanish. A period of about $\frac{1}{2} P_{111}$ has been observed at about 9° from [111] (towards [100]); this period occurs just beyond the angle at which main belly oscillations disappear.

The discovery of the ' neck ' and the ' dog's bone ' stimulated thinking about other possible types of closed circuit and two have in fact shown up. In the [100] direction in both copper and silver a period about 2·4 times the belly period was observed which can probably be associated with a closed circuit alternately above and below a diametral plane and passing around four necks through four adjacent cells ; this has not yet been looked for in gold. Also, in gold, in a direction about 9° off [111] towards [100], where the belly period disappears rather abruptly, a period almost

exactly half that of the belly shows up in a narrow angular range. This can be interpreted as a circuit running through two adjacent cells through the joining neck and just missing the opposite necks on either side. Similar oscillations of $\frac{1}{3}$, $\frac{1}{4}$, etc., of the belly period should in principle also show up but they have not yet been carefully looked for. A summary of all the periods observed so far which support the hypothesis of multiple connectivity is given in table 2.

Some results have also been obtained on the effective electron masses deduced from the temperature variation of the amplitude of the de Haas–van Alphen oscillations, and these are shown in table 3. The results for copper agree reasonably with the cyclotron resonance data, though there are some experimental features which are not yet fully understood ; the results for silver and gold are based on only rough experiments and have no great accuracy. Studies of the variation of amplitude with field, which in principle could give information about relaxation times, have not proved possible because the field variation is considerably modified by slight specimen imperfections (e.g. mosaic structure and bending) which cause complicated interference effects.

Table 3. Effective Masses (in terms of the free electron mass)

	[111] belly	[111] neck	[100] belly	[110] dog's bone
Cu	1·30 (1·30)		1·38 (1·32)	
Ag			0·71	
Au	0·9	0·9	—	1·1

Notes.—The values in brackets are the cyclotron resonance data of Langenberg and Moore (1959). In Cu, where the most thorough observations have been made, a complication arose in that the variation of $\log A/T$ against T for [111] was found to fall into two linear portions of different slope (A is the amplitude); the value 1·30 corresponds to the low temperature portion; above about 1·8°K a value of 1·63 was obtained and it is possible that this is due to eddy current heating effects which falsify the temperatures. The other values were obtained from a more limited range of temperatures (but below 2°K) and the complication was not observed. The values for Au, especially for [110], are very rough and are included only to give some idea of the magnitudes.

No attempt will be made here to discuss the theoretical implications of the results or to relate them to the results of experiments of other kinds. It should however be mentioned that the idea of contact between the Fermi surface and the B.Z. in copper has been suggested not only by the anomalous skin effect results (Pippard 1957) but also by recent results on cyclotron resonance (Langenberg and Moore 1959) and magneto-acoustic

resonance (Gavenda and Morse 1959) while contact for all three metals has been suggested on the basis of magneto-resistance data (Alekseevski and Gaidukov 1959, Gaidukov 1959).

Acknowledgments

In conclusion it is a pleasure to acknowledge the help and advice I have received from many people ; Mr. H. L. Davies constructed most of the equipment, prepared all the silver and gold crystals and assisted in the experiments and I should like to thank him warmly for his willing and patient collaboration. The whole research was started off by the use of copper whiskers and I am very grateful to the General Electric of Schenectady, N.Y., and in particular to Mrs. E. Fontanella, for their generosity in preparing and supplying all the whiskers used in these experiments. I have also benefited greatly from many discussions with Dr. A. B. Pippard, Dr. V. Heine, Mr. M. G. Priestley and Mr. V. M. Morton and I should like to thank them for many valuable suggestions both theoretical and practical. Finally I should like to thank Mr. H. V. Beck, Dr. J. Ashmead, Dr. C. J. Adkins and Mr. F. T. Sadler for help with design and construction of particular items of the measuring equipment.

Note added in proof.—Since this paper was written the dog's bone oscillations have been found along [110] in silver; as in gold, the period was about 2·4 times the belly period.

References

Alekseevski, N. E., and Gaidukov, Yu. P., 1959, *J. exp. theor. Phys.*, **37**, 672.
Gaidukov, Yu. P., 1959, *J. exp. theor. Phys.*, **37**, 1281.
Gavenda, J. D., and Morse, R. W., 1959, *Bull. Amer. phys. Soc.*, **4**, 463.
Langenberg, D. N., and Moore, T. W., 1959, *Phys. Rev. Letters*, **3**, 328.
Pippard, A. B., 1957, *Phil. Trans. roy. Soc.* A, **250**, 325.
Shoenberg, D., 1959, *Nature, Lond.*, **183**, 171.

Magnetoresistance of Copper, Silver and Gold†

By M. G. Priestley
Royal Society Mond Laboratory, Cambridge

[Received January 18, 1960]

Abstract

It is shown that the magnetoresistance measurements of Alekseevskii and Gaidukov on single crystals of copper, silver and gold are consistent with the Fermi surfaces of these metals proposed on the basis of anomalous skin effect and de Haas–van Alphen effect measurements.

The present note discusses the extent to which the magnetoresistance results obtained by Alekseevskii and Gaidukov (1959) and Gaidukov (1959) for copper, silver and gold single crystals are consistent with the Fermi surfaces for these metals proposed as a result of anomalous skin effect and de Haas–van Alphen effect measurements (Pippard 1957, Shoenberg 1960). Each metal has a multiply-connected Fermi surface, which may be thought of roughly as a body-centred lattice of spheres which are extended so as to make contact with each other through 'necks' along the [111] directions. Shoenberg's de Haas–van Alphen experiments show that for silver, gold and copper respectively the areas of contact are 2·1, 3·2 and 4·3% of the relevant free electron sphere extremal area. The discussion will be limited mainly to gold since sufficiently detailed experimental results have been published only for this metal (Gaidukov 1959); such results as are available for silver and copper show the same qualitative features.

The figure shows a stereographic plot of Gaidukov's gold results as a function of magnetic field (H) direction. The essential feature of these results is that the transverse magnetoresistance increases approximately as H^2 over the shaded regions (marked I) and along the lines shown (which are [111] and [110] zones), but saturates over the rest of the stereogram (marked II).

We shall now show that these results can be explained in detail on the basis of the Fermi surface described above by using the theory of Lifshitz and Peschanskii (1958). According to this theory non-saturation is characteristic of the existence of open orbits, which can be of two types.

(1) Those whose axis is a line which can be drawn inside the Fermi surface and which does not intersect it in the extended zone scheme.

---

† Communicated by the Author.

These give rise to a one-dimensional set of field directions. (This type has also been considered by Ziman (1958).)

(2) Those which mark the boundary between hole and electron orbits when a plane is drawn through the extended zone scheme perpendicular to the direction of the magnetic field. These occur over a two-dimensional range of field directions.

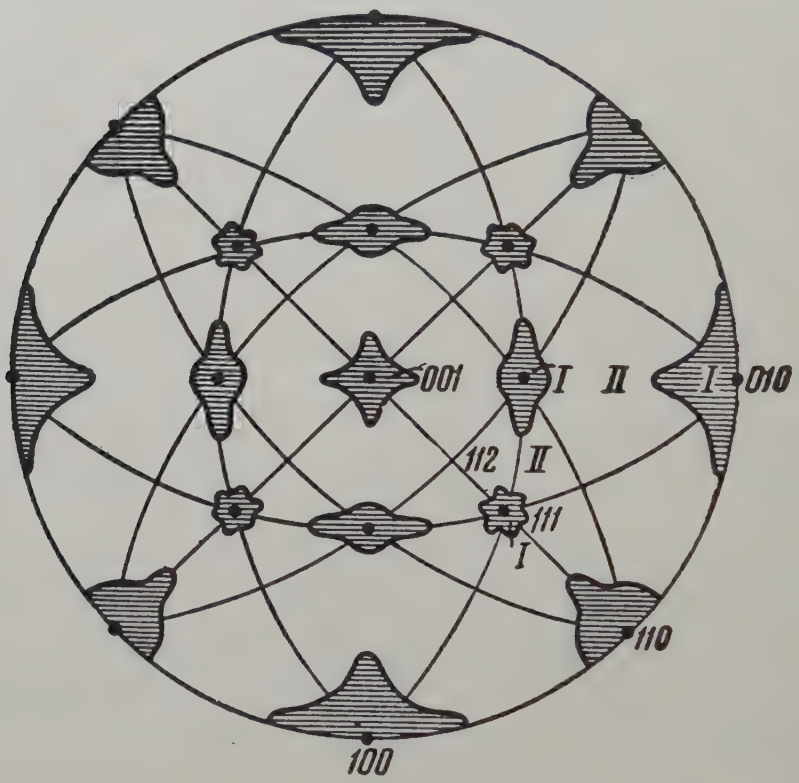

The lines of the stereogram are associated with type (1) open orbits, and the shaded regions with type (2). Since type (2) open orbits mark the boundary between hole orbits and electron orbits, and electron orbits exist for any field direction†, the regions over which the hole orbits and the open orbits exist are identical. Thus the shaded regions should be identical with the regions over which de Haas–van Alphen periods from holes are observed. The boundaries of this region also represent the singular points in the effective mass data from cyclotron resonance experiments‡. As yet such singular points have been observed only in copper (Langenberg and Moore 1959).

† This statement is true in the present case, but would not be true if the necks were too large.

‡ I am indebted to Dr. J. C. Phillips for this observation.

The question of the size and shape of the shaded regions thus reduces to the calculation of the regions over which the hole orbits exist. Since the points at the centre of the necks form a simple cubic lattice and a hole orbit must enter and leave each Brillouin zone via a neck, the central directions for the hole orbits are limited to those zone axes with no index greater than 1, i.e. [100], [110] and [111]. The first two of these have been observed in the de Haas–van Alphen effect (Shoenberg 1960); the [100] 'four cornered rosette' type of orbit in copper and silver, and the [110] 'dog's bone' type in gold. The [111] type of orbit is a large 'rosette' which passes through six necks. Further work may be expected to show up all three types of orbit in each metal.

The angular ranges over which these hole orbits exist can easily be calculated on the assumption that the plane of the limiting hole orbit touches the Fermi surface neck at a negligible distance from the zone boundary. Pippard's proposed surface for copper (1957) suggests that this is a reasonable approximation. The area of the neck is taken from the de Haas–van Alphen results and the contact is assumed to be circular. The results of the calculation are compared with the magnetoresistance data and other available evidence in the table and it can be seen that the agreement is quite satisfactory, bearing in mind the possible errors of the data and the somewhat crude approximation of the calculation. It is likely that much more detailed information on the shape of the neck will soon be available from the de Haas–van Alphen effect, thus providing a basis for a more exact calculation. It can easily be seen that the approximation made above leads to exaggerated estimates of the sizes of the [100] and [111] regions but has little effect on the [110] region. Any departure from the assumption of a circular contact with the (111) zone face would increase the sizes of all the regions.

One other feature of the experimental results calls for comment. Gaidukov states that measurements with H in a (100) plane showed saturation and concludes that this is because there is no open direction along [100], but a detailed examination of his results enables an alternative explanation to be put forward. Only two of his specimens, Au–1 and Au–6, provide evidence on this point since for the others the field directions do not intersect the [100] zone outside the shaded regions. Au–6 is recorded in his table 2 as showing a maximum in the magnetoresistance when the field lies in the [010] zone, and this appears to contradict his statement. Au–1 is recorded as showing saturation, but according to the theory,

$$\Delta\rho_H/\rho_0 \propto H^2 \cos^2\alpha$$

where α is the angle between the current and the axis of the open orbit. Now for Au–1, $\alpha = 84°$, i.e. $\cos^2\alpha \sim 10^{-2}$ and this would probably be sufficiently small to mask any maximum which might be expected. Thus Gaidukov's results provide no clear indication as to whether gold has an open direction along [100]. It should perhaps be pointed out that

Pippard's copper Fermi surface (1957) does have an open direction along [100]. Further magnetoresistance experiments with specimens of suitably chosen orientation should clear up this point.

Region	Measured in plane	'Radius' of region in degrees		
		Gaidukov's gold data		Calculated
		Text	Stereogram	
[100]	(100)	13	15	12·9
	(110)	7·5	9	9·2
[110]	(110)	13	15	15·7
	(100)	7·5	8	11·2
[111]	(110)	6	6	5·3
	(211)	5	5	4·6

Notes.

There are some discrepancies between the experimental results as quoted in the text of Gaidukov's paper and those shown in the detailed stereogram (Gaidukov's fig. 5) and therefore both sets are quoted here.

To obtain the corresponding angles for silver and copper the tangents of the angles in the 'calculated' column should be multiplied by 0·80 and 1·17 respectively.

The few results for silver and copper which are published in Alekseevskii and Gaidukov (1959) show similar qualitative behaviour but it is difficult to estimate the sizes of the angular regions from their diagrams.

The [110] de Haas–van Alphen hole period in gold has been observed up to about 10° from [110] in a plane whose axis is 29° from [100] in a (110) plane: beyond this angle the period disappears abruptly (Shoenberg, private communication). The calculated angle at which the orbit should disappear in this plane is 9·2°.

Langenberg and Moore observed an effective mass singularity in copper at 18° ± 1° from [110] in a (110) plane. The calculated value is 18·2°.

Acknowledgments

I should like to thank Dr. D. Shoenberg for drawing attention to the problem and for discussion of his experimental results and also Dr. A. B. Pippard for a very helpful discussion which clarified several obscure points.

References

Alekseevskii, N. E., and Gaidukov, Yu. P., 1959, *Zh. eksper. i. teor. fiz.*, **37,** 672.
Gaidukov, Yu, P., 1959, *Zh. eksper. i teor. fiz.*, **37,** 1281.
Langenberg, D. N., and Moore, T. W., 1959, *Phys. Rev. Letters*, **3,** 328.
Lifshitz, I. M., and Peschanskii, V. G., 1958, *Zh. eksper. i teor. fiz.*, **35,** 1251.
Pippard, A. B., 1957, *Phil. Trans.* A, **250,** 325.
Shoenberg, D., 1960, *Phil. Mag.*, **5,** 105.
Ziman, J. M., 1958, *Phil. Mag.*, **3,** 1117.

The g-factor and de Haas–van Alphen Effect of Electrons in Bismuth†

By M. H. Cohen‡
Cavendish Laboratory, Cambridge

and E. I. Blount
Westinghouse Research Laboratories, Pittsburgh, Pennsylvania

[Received in revised form June 25, 1959]

Abstract

A theory of the g-factor of conduction electrons is developed which is valid for low symmetry and arbitrary strength of spin–orbit coupling. Application to bismuth shows that $m_s \equiv 2/g \simeq m_0$ for most orientations, where m_0 is the effective mass entering the cyclotron frequency. Thus g is 260 when $\mathbf{H}$ is in the direction of smallest m_0. Further, the lifting of the spin degeneracy by the magnetic field introduces a factor $\cos r\pi m_0/m_s$ into the rth oscillatory term in the susceptibility. This explains the apparent phase shift of $r\pi$ observed in the de Haas–van Alphen oscillations of Bi.

§ 1. Introduction

The g-factor of conduction electrons can differ from the free electron value of 2·0023 because of spin–orbit coupling (Yafet 1952, 1957). Furthermore, the theoretical treatment of Luttinger (1956) demonstrates clearly that the g-factor can greatly exceed 2 when there is a 3-fold orbital degeneracy or when the spin–orbit coupling becomes large compared to the pertinent band gaps. Roth *et al.* (1958) have calculated and measured a value of 50 for the g-factor of electrons in InSb, for which the pertinent band gap is 0·23 ev (Roberts and Quarrington 1955) and the spin–orbit splitting is 0·9 ev (Kane 1957). With a gap of perhaps a few hundredths of an electron volt and an atomic spin–orbit splitting of 1·86 ev (Condon and Shortley 1935, p. 179), electrons in bismuth should have an even larger g-factor. However, the results of Luttinger (1956) and their application to InSb by Roth *et al.* (1958) are not suited to Bi because of the low symmetry of the conduction-electron wave functions in that substance. Further, Yafet's (1957) treatment of g-values pertains too directly to spin-resonance in metals for our present purposes. Accordingly the necessary theory of the magnetic-moment operator and the g-factor are developed in § 2 of this paper. In § 3 it is shown that for

† Communicated by the Authors.

‡ Guggenheim Fellow 1957–1958, on leave from the Institute for the Study of Metals, University of Chicago.

conduction electrons of low symmetry, the splittings of the orbital and spin levels by a magnetic field are practically equal when the band gap is very small. In bismuth, however, the conduction-electron wave numbers lie on reflection planes or 2-fold axes in k-space so that the splittings of orbital and spin levels are equal for most orientations of magnetic field but not all (§ 4). The maximum value of the g-factor is shown to be 260 for electrons in bismuth.

Such large g-factors as are found in InSb and Bi imply that the electron spin can play a significant role in the de Haas–van Alphen effect (Shoenberg 1952, 1957). Electron spin was first introduced into the theory of the de Haas–van Alphen effect Akhieser (1939) for free electrons. He found that the oscillatory term in the susceptibility corresponding to the $(r-1)$th harmonic ($r=1$ for fundamental) obtained without spin is multiplied by

$$\cos r\pi = (-1)^r \quad . \quad . \quad . \quad . \quad . \quad . \quad . \quad . \quad (1)$$

when the lifting of the spin degeneracy by the magnetic field is taken into account. Dingle (1952) and Sondheimer and Wilson (1951) have proved that when the orbital effective mass m_0 of electrons in the crystal differs from the free electron mass m, (1) must be replaced by

$$\cos r\pi m_0/m. \quad . \quad . \quad . \quad . \quad . \quad . \quad . \quad . \quad (2)$$

The work of Lifshitz and Kosevitch (1955) shows that expression (2) holds for an arbitrarily shaped Fermi surface provided that an appropriate redefinition of m_0 is made. For substances like bismuth in which m_0 is much less than m, the electron spin would have little effect according to (2). However, eqn. (2) is derived on the assumption of a g-factor of 2. The generalization of (2) valid for arbitrary g-factor is given in § 3, and it is shown there that the large g-factor of electrons in Bi is responsible for the phase shifts in the de Haas–van Alphen oscillations observed by Shoenberg (1939) and by Dhillon and Shoenberg (1955).

Other implications of the large g-factor in Bi are discussed in § 6.

§ 2. Theory of the g-factor

2.1. *The Magnetic-moment Operator*

We employ a simple one-electron Hamiltonian (Foldy and Wouthuysen 1950) similar to that used by Elliott (1954 a, b), Dresselhaus (1955 a, b) and others:

$$\mathscr{H} = \left(\mathbf{p} + \frac{e}{c}\mathbf{A}\right)^2 \Big/ 2m + V + \frac{1}{8}\lambda^2\nabla^2 V + \left(\mathbf{p} + \frac{e}{c}\mathbf{A}\right) . (\lambda/2mc)\mathbf{s} \times \nabla V. \quad (3)$$

In eqn. (3), V is the crystal potential, $\mathbf{A} = \frac{1}{2}\mathbf{H} \times \mathbf{r}$ is the vector potential for $\mathbf{H}$ a constant magnetic field, and λ is the Compton wavelength over 2π. The eigenfunctions of $\mathscr{H}$ are of the Bloch form

$$\left.\begin{aligned} \mathscr{H}\psi_{\mathbf{k}n\rho} &= E_n(k)\psi_{\mathbf{k}n\rho}, \\ \psi_{\mathbf{k}n\rho} &= (\Delta/(2\pi)^3)^{1/2} \exp(i\mathbf{k}.\mathbf{r})u_{\mathbf{k}n\rho} \end{aligned}\right\} \quad . \quad . \quad . \quad . \quad (4)$$

when $\mathbf{H}=0$, where $u_{\mathbf{k}n\rho}$ is a periodic two-component function normalized to unity over the volume Δ of a unit cell, and $\psi_{\mathbf{k}n\rho}$ is normalized to $\delta(\mathbf{k}-\mathbf{k}')$ over the infinite crystal. The index ρ, $\rho=1$ or 2, distinguishes the two independent eigenfunctions

$$\psi_{\mathbf{k}n1} \quad \text{and} \quad \psi_{\mathbf{k}n2} \quad (=U\psi_{\mathbf{k}n1}) \qquad (5)$$

which belong to a general wave vector $\mathbf{k}$ and energy $E_n(\mathbf{k})$ if the crystal has inversion symmetry. The operator U in (5) is

$$U=(i\sigma_y)CI, \quad U^{-1}=-U, \qquad (6)$$

where I is the inversion operator, $i\sigma_y C$ the time reversal operator, and $C\psi=\psi^*$. We work in the effective-mass approximation for conduction electrons; that is, we consider only states in the neighbourhood of the energy minimum in the conduction band (index o). By measuring $\mathbf{k}$ from the position of the minimum, confining ourselves to small $\mathbf{k}$, and setting $E_0(0)=0$, we get when $\mathbf{H}=0$

$$E_0(\mathbf{k})=\hbar^2\mathbf{k}\,.\,\boldsymbol{\alpha}\,.\,\mathbf{k}/2m. \qquad (7)$$

The components of the inverse effective-mass tensor $\boldsymbol{\alpha}$ are given by the sum rule (Dresselhaus 1955 a, b, Luttinger and Kohn 1955, Luttinger 1956)

$$\alpha_{ij}=\delta_{ij}+m\sum_{n\rho}{}' \frac{\langle o1|v_i|n\rho\rangle\langle n\rho|v_j|o1\rangle+\langle o1|v_j|n\rho\rangle\langle n\rho|v_i|o1\rangle}{(E_0-E_n)}. \qquad (8)$$

The matrix elements

$$\langle o1|\mathbf{v}|n\rho\rangle=(u_{o\sigma 1},\,\mathbf{v}u_{on\rho}) \qquad (9)$$

of the velocity operator

$$\mathbf{v}=\mathbf{p}/m+(\lambda/2mc)\mathbf{s}\times\nabla V. \qquad (10)$$

involve integration only over a unit cell.

The effective mass Hamiltonian becomes

$$\langle o\rho|\mathscr{H}|o\rho'\rangle=\frac{1}{2m}\left(\mathbf{p}_c+\frac{e}{c}\mathbf{A}_c\right).\boldsymbol{\alpha}.\left(\mathbf{p}_c+\frac{e}{c}\mathbf{A}_c\right)\delta_{\rho\rho'} - \langle o\rho|\boldsymbol{\mu}|o\rho'\rangle\,.\,\mathbf{H} \qquad (11)$$

when $\mathbf{H}\neq 0$. The first term in (11) is the usual effective-mass result implying a free-electron like orbital motion from cell to cell (Luttinger and Kohn 1955). In this term, $\mathbf{p}_c=\hbar\mathbf{k}$ is the crystal-momentum operator, and $\mathbf{A}_c$ is obtained by substitution of the crystal-coordinate operator $\mathbf{x}_c=i\hbar\partial/\partial\mathbf{p}_c$ for $\mathbf{r}$ in $\mathbf{A}$ (Adams 1953 a). The second term in (11) shows that an electron carries with it an 'intrinsic' magnetic moment

$$\boldsymbol{\mu}=\boldsymbol{\mu}_l+\boldsymbol{\mu}_s \qquad (12)$$

in this free-electron like motion, partly from the spin

$$\boldsymbol{\mu}_s=-2\beta\mathbf{s} \qquad (13)$$

and partly from unquenched orbital motion

$$\langle o\rho|\boldsymbol{\mu}_l|o\rho'\rangle=-\frac{eh}{2ci}\sum_{n\tau}\frac{\langle o\rho|\mathbf{v}|n\tau\rangle\times\langle n\tau|\mathbf{v}|o\rho'\rangle}{(E_0-E_n)}. \qquad (14)$$

Equation (14) is the result obtained directly from the procedures of Luttinger and Kohn (1955) as generalized by Luttinger (1956); its meaning

is clearer when it is put into the form obtained directly from the procedures of Adams (1952, 1953 a, b), eqn. (18) below. The position operator $\mathbf{r}$ becomes $\mathbf{x}_c+\mathbf{X}$ in the present representation (Adams 1952, 1953 a) where

$$\langle n\rho|\mathbf{X}|n'\rho'\rangle=(u_{\mathbf{k}n\rho},\ i\partial u_{\mathbf{k}n\rho'}/\partial\mathbf{k}), \quad . \quad . \quad . \quad . \quad . \quad . \quad . \quad . \quad (15)$$

$$=\hbar\langle n\rho|\mathbf{v}|n'\rho'\rangle/i(E_n-E_{n'}), \quad n\neq n'. \quad . \quad . \quad (16)$$

We have supposed so far that

$$\langle n\rho|\mathbf{v}|n\rho'\rangle=\hbar^{-1}\partial E_n/\partial k\delta_{\rho\rho'} \quad . \quad . \quad . \quad . \quad . \quad (17)$$

vanishes for n, $\mathbf{k}=0$. Therefore, $\langle o\rho|\boldsymbol{\mu}_i|o\rho'\rangle$ is just

$$\langle o\rho|\boldsymbol{\mu}_i|o\rho'\rangle=-\beta\langle o\rho|\mathbf{l}|o\rho'\rangle, \quad . \quad . \quad . \quad . \quad . \quad (18)$$

where

$$\mathbf{l}=\hbar^{-1}\mathbf{X}\times m\mathbf{v} \quad . \quad . \quad . \quad . \quad . \quad . \quad . \quad . \quad (19)$$

has the nature of an orbital angular momentum. We note that $\langle n\rho|\mathbf{X}|n'\rho'\rangle$ differs from $(u_{\mathbf{k}n\rho},\ \mathbf{r}u_{\mathbf{k}n'\rho'})$ only by an integral over the surface of the unit cell (cf. Kjeldaas and Kohn 1957, Yafet, 1957) so that $\mathbf{l}$ goes over into the ordinary orbital angular momentum in the tight binding limit. Finally, we have from (12), (13) and (18)

$$\boldsymbol{\mu}=-\beta(\mathbf{l}+2\mathbf{s}). \quad . \quad . \quad . \quad . \quad . \quad . \quad . \quad (20)$$

2.2. *The g-factor*

The 2×2 matrix with elements $\langle o\rho|\boldsymbol{\mu}|o\rho'\rangle$ can be expressed as a linear combination of the unit matrix and the three matrices

$$\mathbf{s}_i'=\tfrac{1}{2}\sigma_i, \quad i=x,\ y,\ z \quad . \quad . \quad . \quad . \quad . \quad . \quad . \quad (21)$$

where the σ_i are the three Pauli matrices. The electron spin operator s_i does not have the form (21) in the present representation. From eqns. (5) and (6) it follows that the coefficient of the unit matrix vanishes. We have, then,

$$\langle o\cdot|\mu_i|o\cdot\rangle=-\beta\langle o\cdot|l_i+2s_i|o\cdot\rangle=-\sum_j G_{ij}s_j', \quad . \quad . \quad . \quad (22)$$

$$\left.\begin{aligned}-\beta G_{ix}&=2\,\mathrm{Re}\langle o1|\mu_i|o2\rangle,\\ -\beta G_{iy}&=-2\,\mathrm{Im}\langle o1|\mu_i|o2\rangle,\\ -\beta G_{iz}&=2\langle o1|\mu_i|o1\rangle.\end{aligned}\right\} \quad . \quad . \quad . \quad . \quad . \quad (23)$$

Strictly speaking, the coefficients G_{ij} are not the components of a second-rank tensor; however, the formal structure of eqn. (22) permits them to be so regarded. Even so, G_{ij} is not symmetric and cannot be diagonalized for a point in k-space having symmetry lower than orthorhombic.

The 'spin' Hamiltonian

$$-\langle o\,.\,|\boldsymbol{\mu}|o\,.\,\rangle\,.\,\mathbf{H}=\beta\sum_{ij}G_{ij}H_is_j' \quad . \quad . \quad . \quad . \quad . \quad . \quad (24)$$

has the eigenvalues

$$E_s=\pm\tfrac{1}{2}g\beta H, \quad . \quad . \quad . \quad . \quad . \quad . \quad . \quad . \quad (25)$$

where

$$g=\left[\sum_{ijl}\lambda_i\lambda_jG_{il}G_{jl}\right]^{1/2} \quad . \quad . \quad . \quad . \quad . \quad . \quad . \quad (26)$$

is the usual spectroscopic splitting factor. In (26) the λ_i are the direction cosines of **H** relative to the axes x, y, z. The quantity

$$Q_{ij}=\sum_l G_{il}G_{jl} \quad . \quad . \quad . \quad . \quad . \quad . \quad . \quad . \quad . \quad (27)$$

is a symmetric second-rank tensor and can be diagonalized. We designate the principal components of Q_{ij} as g_1^2, g_2^2 and g_3^2 so that (26) becomes

$$g=[(\lambda_1')^2g_1^2+(\lambda_2')^2g_2^2+(\lambda_3')^2g_3^2]^{1/2}. \quad . \quad . \quad . \quad . \quad . \quad (28)$$

Here the λ_i' are the direction cosines of **H** relative to the principal axes of Q_{ij}. It must be emphasized that despite the simple form of (28), the transformation which diagonalizes the Hamiltonian (24) does not in general diagonalize G_{ij}. This differs from the customary situation in electronic paramagnetism (Bleany and Stevens 1953) because of the low symmetry with which we are concerned here. It is convenient to define a spin effective mass m_s in analogy with the more familiar orbital effective mass,

$$m_s/m=2/g=2[(\lambda_1')^2g_1^2+(\lambda_2')^2g_2^2+(\lambda_3')^2g_3^2]^{-1/2}. \quad . \quad . \quad . \quad (29)$$

The energy levels (25) are then just like those of a free electron except that m_s replaces the free-electron mass in the Bohr magneton. The signs in eqn. (25) derive from the signs of the G_{ij} and hence relate to the effective spin operator s' and not the true spin s. The sense of s_z' is a matter of choice and can be related to that of s_z only when the parentage of the $\psi_{on\rho}$ in terms of orbital and spin functions is particularly simple. Such is the case for conduction electrons in InSb, for which Roth *et al.* (1958) were able to assign a negative value to g itself, but not, e.g. for Bi. For convenience, therefore, we leave the signs unspecified in eqn. (25) and define g as a positive quantity in eqn. (26).

In addition to (25), the energy contains the orbital eigenvalues given by

$$(n+\tfrac{1}{2})\hbar\omega_c+\hbar^2k_z^2/2m_z, \quad n=0, 1, 2, \ldots \quad . \quad . \quad . \quad . \quad (30)$$

when **H** is in the z-direction, where ω_c is the cyclotron frequency,

$$\omega_c=eH/m_0c. \quad . \quad . \quad . \quad . \quad . \quad . \quad . \quad . \quad . \quad (31)$$

If α_i, $i=1, 2, 3$, are the principal components of $\boldsymbol{\alpha}$ and λ_i the direction cosines of **H** relative to its principal axes, we have for m_0 and m_z

$$m_0=m[\lambda_1^2\alpha_2\alpha_3+\lambda_2^2\alpha_3\alpha_1+\lambda_3^2\alpha_1\alpha_2]^{-1/2}, \quad . \quad . \quad . \quad (32)$$

$$m_z=m(\alpha^{-1})_{zz}=m[\lambda_1^2/\alpha_1+\lambda_2^2/\alpha_2+\lambda_3^2/\alpha_3]. \quad . \quad . \quad . \quad (33)$$

Eqns. (29) and (32) provide a convenient basis for the comparison of the splitting of the spin and orbital levels by a magnetic field; the two splittings are equal when the two effective masses are equal.

§ 3. The One-level Case

The expressions for the orbital effective mass, eqn. (32), and the spin effective mass, eqn. (29), are closely related in structure, and related sum rules hold for the quantities entering both, eqns. (8) and (14), respectively.

The condition that m_0 be small is simply that one or more band gaps entering the sum rule (8) be small. The same condition is necessary for m_s to be small (or g large) but is not sufficient. The operator μ_k vanishes in the absence of spin–orbit coupling, as is shown by a simple application of the operator U, eqns. (5) and (6). Thus we must also require the two spin states of given wave number to be completely mixed, for which the spin–orbit coupling must be comparable to or larger than the band gaps. These conditions are met in InSb, for which $m_0 = 0{\cdot}013m$ and $m_s = 3m_0$ (Roth *et al.* 1958) and *a fortiori* in Bi, for which the result $m_s = m_0$ at most orientations of H is obtained in § 4. However, before considering any particular substance, we treat the case of electrons of small effective mass in a crystal whose symmetry operations include inversion.

If the effective-mass components are small, or $\alpha_{ij} > 1$, then at least one level with velocity matrix elements of normal size almost certainly lies within a few tenths of a volt or less of E_0. We restrict ourselves to the *one-level case* in which there is only one such level, E_a, just below E_0. This level dominates the sum rules (8) and (14), and we may neglect the δ_{ij} in (8), the contributions of all other levels to both (8) and (14), and (if spin–orbit coupling is strong) μ_s in (12). Under these circumstances,

$$m_0 = m_s, \quad . \quad . \quad . \quad . \quad . \quad . \quad . \quad . \quad . \quad . \quad (34)$$

which we now proceed to demonstrate.

Take the z-axis along $\mathbf{H}$, and let x and y be arbitrary. Equation (32) then becomes

$$m_0 = m[\alpha_{xx}\alpha_{yy} - (\alpha_{xy})^2]^{-1/2}, \quad . \quad . \quad . \quad . \quad . \quad . \quad (35)$$

and eqn. (29) becomes

$$m_s = 2m[G_{zz}{}^2 + G_{zx}{}^2 + G_{zy}{}^2]^{-1/2}. \quad . \quad . \quad . \quad . \quad . \quad . \quad (36)$$

We define

$$\mathbf{t} = \langle o1|\mathbf{v}|a1\rangle \quad \text{and} \quad \mathbf{u} = \langle o1|\mathbf{v}|a2\rangle. \quad . \quad . \quad . \quad . \quad . \quad . \quad (37)$$

The relations

$$\langle a1|\mathbf{v}|o2\rangle = -\mathbf{u} \quad \text{and} \quad \langle a2|\mathbf{v}|o2\rangle = \mathbf{t} \quad . \quad . \quad . \quad . \quad . \quad (38)$$

are readily established by use of the operator U. With the aid of (37) and (38), we may write the contribution of the level E_a to α_{ij} as

$$\alpha_{ij} = m(t_i t_j{}^* + t_j t_i{}^* + u_i u_j{}^* + u_j u_i{}^*)/(E_0 - E_a) \quad . \quad . \quad . \quad (39)$$

and to G_{ij} as

$$\left.\begin{aligned} G_{iz} &= 2m(t_j t_k{}^* - t_k t_j{}^* + u_j u_k{}^* - u_k u_j{}^*)/i(E_0 - E_a), \\ G_{ix} - iG_{iy} &= 4m(u_j t_k - u_k t_j)/i(E_0 - E_a). \end{aligned}\right\} \quad . \quad (40)$$

Substitutions of (39) into (35) and of (40) into (36) and comparison of the two results leads directly to (34). Thus, we have proved that the splittings of the spin and orbital levels by a magnetic field are equal in the one-level case.

In the absence of spin–orbit coupling, $\mathbf{u}$ vanishes and (38) shows that $\mathbf{t}$ is real. From eqn. (39) we see that the level E_a can then contribute to

only a single component of $\boldsymbol{\alpha}$. The contributions of E_a to the other components of $\boldsymbol{\alpha}$ remain small as long as the spin–orbit splitting is small compared with the band gap $E_0 - E_a$. The above proof of eqn. (34) is valid only if all the components of $\boldsymbol{\alpha}$ are determined by the level E_a. The condition for the equality of m_0 and m_s in the one-level case is therefore that the spin–orbit splitting be comparable to or larger than the band gap $(E_0 - E_a)$.

Further, our considerations do not apply to electrons near points of full cubic or tetrahedral symmetry if one of the two levels is 4-fold degenerate. Specifically, eqn. (34) does not apply to InSb, where the conduction electrons are near $k = 0$ and the lower level is 4-fold degenerate.

§ 4. Bismuth

4.1. *Band Structure*

Electrons in bismuth occupy three or six ellipsoidal energy surfaces according to the de Haas–van Alphen effect (Shoenberg 1939, 1957) and cyclotron resonance (Aubrey and Chambers 1957). One set of ellipsoids is given by

$$E(\mathbf{k}) = (\hbar^2/2m)(\alpha_{xx}k_x^2 + \alpha_{yy}k_y^2 + \alpha_{zz}k_z^2 + 2\alpha_{yz}k_yk_z), \quad . \; . \quad (41)$$

where x and z are chosen along a dyad axis and the triad axis respectively, and $\mathbf{k}$ is measured from the position of the nearest minimum in the conduction band. Two other sets are obtained by rotation of $\pm 120°$ around the triad axis, and the remaining three are obtained from the first three by inversion. The six minima coalesce into three only if they happen to lie at the centres of zone faces. One principal axis of each ellipsoid lies along a dyad axis, but the non-vanishing of α_{yz} implies that neither remaining axis lies along the triad axis. A symmetry argument then shows that the six energy minima lie either in the three reflection planes normal to the dyad axes or on the dyad axes, the two minima in each plane or on each axis being connected by inversion. The best values available for the α_{ij} derive from a combination of de Haas–van Alphen and cyclotron resonance data

$$\alpha_{xx} = 202, \quad \alpha_{yy} = 1{\cdot}67, \quad \alpha_{zz} = 83{\cdot}3, \quad \alpha_{yz} = 8{\cdot}33\dagger, \quad . \; . \quad (42)$$

according to Aubrey (private communication). These lead to the principal values

$$\alpha_1 = 202, \quad \alpha_2 = 0{\cdot}83, \quad \alpha_3 = 84{\cdot}2 \quad . \; . \; . \; . \; . \quad (43)$$

with the principal axis 3 tipped $5{\cdot}80°$ from the triad axis. The Fermi energy is 0·0177 ev at 4°K (Dhillon and Shoenberg 1955).

4.2. *Relation between m_0 and m_s*

We infer from the two large principal values, α_1 and α_3, that at least one level lies just below E_0. Let us assume that we are actually dealing with

† G. Smith (private communication) has pointed out that α_{yz} should be positive in the right-handed coordinate system used here.

a one-level case, that only one band gap is very small and all other contributions to (8) are negligible. A few hundredths of an electron volt is a reasonable guess for this band gap $E_g = E_0 - E_a$ on the basis of eqns. (39) and (32), whereas an appropriate measure of the spin–orbit splitting is 1·86 ev in atomic Bi (Condon and Shortley 1935, p. 179). We can therefore take over the results of the preceding section for bismuth, eqn. (34),

$$m_0 \simeq m_s \quad \text{(Bi)}. \qquad . \quad . \quad . \quad . \quad . \quad . \quad . \quad . \quad . \quad (44)$$

However, eqn. (34) was derived on the assumption that the level E_a determines all the components of α_{ij}. This is clearly not true for Bi where α_2 is small. Thus (44) holds only for orientations of the magnetic field such that α_2 does not contribute appreciably to m_0 in eqn. (32). Substitution of (43) into (32) shows that **H** must not lie within about 5° of the 1, 3 plane for (44) to be valid.

We now explore the implications of the small value of α_2 in more detail. For states at the minimum in the conduction band the group of **k** (Bouckaert *et al.* 1936) contains only the unit operator E and the reflection operator σ or 2-fold rotation C_2. (Addition of inversion does not affect our arguments.) The character table of the double group (Elliott 1954 b) is

	R_1	R_2	R_3	R_4
E	1	1	1	1
$\bar{E}$	1	1	−1	−1
σ or C_2	1	−1	$-i$	i
σ or $\bar{C}_2$	1	−1	i	$-i$

The representations R_3 and R_4 are degenerate by time reversal (Elliott 1954 b). A Bloch function can transform either as R_3 or R_4; we make the arbitrary identification that $\psi_{n\mathbf{k}1}$ transforms as R_3 and $\psi_{n\mathbf{k}2}$ as R_4. The x, y and z components of **v** transform as R_2, R_1 and R_1, respectively. From the multiplications rules $R_1 \times (R_3, R_4) = (R_3, R_4)$ and $R_2 \times (R_3, R_4) = (R_4, R_3)$, we obtain $\langle o1|v_x|n2\rangle$, $\langle o1|v_y|n1\rangle$ and $\langle o1|v_z|n1\rangle$ as the non-vanishing matrix elements of **v** entering (8) and (14). In the one-level case, (8) becomes

$$\left.\begin{aligned} \alpha_{xx} &= 2m|\langle o1|v_x|a2\rangle|^2/E_g, \\ \alpha_{yy} &= 2m|\langle o1|v_y|a1\rangle|^2/E_g, \\ \alpha_{zz} &= 2m|\langle o1|v_z|a1\rangle|^2/E_g, \\ \alpha_{yz} &= 2m\,\mathrm{Re}(\langle o1|v_y|a1\rangle\langle a1|v_z|o1\rangle)/E_g, \\ \alpha_{xy} &= \alpha_{xz} = 0. \end{aligned}\right\} \quad . \quad . \quad . \quad (45)$$

From (45), we see that in general α_1, α_2 and α_3 are all large. The small value of α_2 is thus peculiar to Bi and not a consequence of the reflection or rotation symmetry. We can infer that $\langle o1|v_y|a1\rangle$ vanishes or becomes very small when the y-axis is brought into coincidence with axis 2 by rotation around x. The phases of $\langle o1|v_y|a1\rangle$ and $\langle o1|v_z|a1\rangle$ must therefore differ by nearly 0 or π; in other words, the vector **t** is real apart from

a phase factor. This special circumstance is probably related to the small size of E_g, a qualitative explanation for which has been given by Blount (1956)†.

If we now assume that the phases of $\langle o1|v_y|a1\rangle$ and $\langle o1|v_z|a1\rangle$ differ by precisely 0 or π, then α_2 vanishes in the one-level approximation. Similarly, substitution of the non-vanishing matrix elements of $\mathbf{v}$ into (14), leads to the result

$$g_1=0, \quad g_2{}^2=4\alpha_1\alpha_3, \quad g_3=0; \quad \lambda_2{}'=\lambda_2 \quad . \quad . \quad . \quad . \quad (46)$$

in the one-level approximation, which is equivalent to (44). We can now see clearly that in the complete expressions (28) (or (29)) and (32), instead of (46) we must actually have $\lambda_1{}'=\lambda_1$, $\lambda_2{}'$ and $\lambda_3{}'$ very nearly equal λ_2 and λ_3, $\frac{1}{2}g_1$ and $\frac{1}{2}g_3$ of order unity, and finally $\frac{1}{2}g_2$ very nearly equal to $(\alpha_1\alpha_3)^{1/2}$. Thus, when $\mathbf{H}$ is nearly perpendicular to axis 2, m_s is of order unity and hence $\simeq 10m_0$. On the other hand, eqns. (44) and (46) hold with $\mathbf{H}$ pointing along axis 2, when g takes on the enormous value of *260*.

§ 5. The de Haas–van Alphen Effect

We turn now to consideration of the role played by the electron spin in the de Haas–van Alphen effect. The generalization of (2) required when the spin–orbit coupling is important is simply

$$\cos r\pi m_0/m_s, \quad . \quad . \quad . \quad . \quad . \quad . \quad . \quad . \quad . \quad (47)$$

as is seen immediately upon reviewing the work of Dingle (1952) or of Sondheimer and Wilson (1951). For bismuth, the factor (47) is very nearly equal to $\cos r\pi=(-1)^r$ unless $\mathbf{H}$ comes within 5° of being perpendicular to axis λ, thus recapturing eqn. (1). This is the explanation for the phase shift of π found experimentally by Shoenberg (1939) in the fundamental at a variety of orientations of magnetic field and of the equivalent factor of $(-1)^r$ found by Dhillon and Shoenberg (1955) in the fundamental and the first six harmonics at a single orientation. All orientations of $\mathbf{H}$ at which phases were determined are within the region of validity of eqn. (44).

It would be of interest to study the harmonic content and phases of the de Haas–van Alphen oscillations at an orientation such that (44) does not hold. These can be accurately determined only when a single period is present in the quantity observed (Dhillon and Shoenberg 1955). The periods associated with all six ellipsoids become equal only when $\mathbf{H}$ is along the trigonal axis. For that orientation λ_1 vanishes, $\lambda_2{}^2\alpha_3\alpha_1$ nearly equals $\lambda_3{}^2\alpha_1\alpha_2$, and $(\lambda_3{}')^2(g_3/2)^2$ is negligible relative to $(\lambda_2{}')^2(g_2/2)^2$. It then follows from (29) and (32) that

$$m_s=\sqrt{2}m_0 \quad . \quad . \quad . \quad . \quad . \quad . \quad . \quad . \quad . \quad (48)$$

when $\mathbf{H}$ is along the trigonal axis. Thus (44) is violated and $\cos r\pi m_0/m_s$ $(=\cos r\pi/\sqrt{2})$ differs from $(-1)^r$ for an orientation giving a single period.

† A similar situation occurs in Sb (Shoenberg 1952, Datars and Dexter, private communication).

The phases and amplitudes of successive harmonics should vary in a way quite unlike that expected without the $\cos r\pi m_0/m_s$ factor. Unfortunately the torque vanishes for this orientation, and eqn. (44) holds for those orientations at which a single period is observed by the torque method (Dhillon and Shoenberg 1955). A harmonic analysis of the temperature oscillations recently reported by Kunzler and Boyle (1959) could in principle yield an experimental test of (48). An alternative method would be a direct measurement of the differential susceptibility by the magnetic field modulation scheme commonly applied in nuclear and electron spin resonance studies.

Arsenic and antimony are similar in crystal and electronic structure to Bi and have observable de Haas–van Alphen effects (Shoenberg 1957). One set of carriers in each substance fits into the six ellipsoid scheme holding for electrons in Bi. The analysis developed here for Bi can be taken over unmodified for Sb and As. However, the effective masses and hence the band gaps are larger, while the spin–orbit splittings are smaller than for Bi. Thus, relations like (44) should hold for As and Sb, but with less accuracy than for Bi. A study of the harmonic content and phases of the de Haas–van Alphen oscillations in Sb and As like that of Dhillon and Shoenberg for Bi would therefore be of interest.

Frederikse and Hosler (1957) have observed oscillations in the galvanomagnetic properties of n-type InSb. It is reasonable to suppose that the de Haas–van Alphen effect is also observable (Shoenberg, private communication). The value of m_0 is $0{\cdot}013m$ (Dresselhaus *et al.* 1955) and that of m_s is 0·040 from (29) and $g=50$, or

$$m_s \simeq 3m_0 \text{ (InSb)}. \quad . \quad . \quad . \quad . \quad . \quad . \quad . \quad . \quad (49)$$

Hence the factor (47) is very nearly equal to $\cos r\pi/3$, and the amplitudes and phases of the harmonics of the de Haas–van Alphen oscillations of electrons in InSb should vary in a way inexplicable without (47).

§ 6. Other Implications of the Large g-factor in Bismuth

We have seen in the preceding section how the observed phase shifts in the de Haas–van Alphen oscillations confirm our result $m_0=m_s$ for Bi at most orientations of **H**. An immediate consequence of this is that the Pauli spin paramagnetism is three times larger than the Landau–Peierls diamagnetism when **H** is perpendicular to the trigonal axis, just as for free electrons. Thus Jones' (1934) explanation of the stready diamagnetism of bismuth leads in fact to a net paramagnetism; the correct explanation must lie in the direction suggested by Adams (1953 b).

It would be very amusing to measure a g-factor as large as 260 directly by a spin–resonance experiment. Preliminary calculations indicate that such an experiment is feasible for Bi. Because of the large spin–orbit coupling, the spin relaxation time T_1 is probably comparable to the collision time. Zone-refined Bi should give an $\omega\tau$ of order 100 at 30 000 Mc/s so that line width from collisions should be no problem. Although Dyson's

(1955) theory is not strictly applicable to Bi at 30 000 Mc/s, it suggests that intensity should also be no problem because of the large g-factor.

The spin–orbit coupling is important not only for the magnetic properties of Bi but for the entire band structure. For example, the matrix element $\langle o1|v_x|a2\rangle$, which would vanish without spin–orbit coupling, is 60% larger than $\langle o1|v_z|a1\rangle$, and the spin–orbit splitting itself is two orders of magnitude larger than E_g. It is necessary, therefore, to take explicit cognizance of the spin–orbit coupling in constructing theories of all the electronic properties of bismuth and similar substances.

Thus far we have spoken only of electrons. However, the analysis does not depend on the sign of the effective mass and can immediately be taken over, with all results, to apply to holes.

Finally, certain limitations on our present considerations must be mentioned. A number of terms have been left out of the Hamiltonian of eqn. (11) which *are* obtained by the method of Adams (1953 b). These are of order H^2 and independent of $\mathbf{x}_c$, and so do not affect the de Haas–van Alphen effect. They are of importance only for the steady susceptibility. The multiplicative factor (47) obtains only when energy depends quadratically on wave number at the Fermi surface. In the general case, the g-factor depends on $\mathbf{k}$, which causes the orbital energy levels to depend on spin-direction and thus complicates the de Haas–van Alphen effect. This $\mathbf{k}$-dependence of g also broadens the spin resonance line and may well dominate the breadth in Bi.

Acknowledgments

Part of this work was carried out at the Institute for the Study of Metals of the University of Chicago where it was supported by grant G–4918 from the National Science Foundation. We are grateful to Dr. D. Shoenberg, F.R.S. for helpful and informative discussions and to J. E. Aubrey, also of the Mond Laboratory, for permission to use his effective-mass values prior to publication.

References

Adams, E. N., 1952, *Phys. Rev.*, **85,** 41; 1953 a, *J. chem. Phys.*, **21,** 2013; 1953 b, *Phys. Rev.*, **89,** 633.

Akhieser, A., 1939, *C. R. Acad. Sci. URSS*, **23,** 974.

Aubrey, J. E., and Chambers, R. G., 1957, *J. Phys. Chem. Solids*, **3,** 128.

Bleany, B., and Stevens, K. W. H., 1953, *Rep. Progr. Phys.*, **16,** 108 (London : The Physical Society).

Blount, E. I., 1956, *Bull. Amer. phys. Soc.*, **1,** 143.

Bouckaert, L. P., Smoluchowski, R., and Wigner, E., 1936, *Phys. Rev.*, **50,** 58.

Condon, E. V., and Shortley, G. H., 1935, *The Theory of Atomic Spectra* (Cambridge : University Press), p. 179.

Dhillon, J. S., and Shoenberg, D., 1955, *Phil. Trans.* A, **248,** 1.

Dingle, R. B., 1952, *Proc. roy. Soc.* A, **211,** 500.

Dresselhaus, G., 1955 a, Thesis, University of California, Berkeley (unpublished); 1955 b, *Phys. Rev.*, **100,** 580.

Dresselhaus, G., Kip, A. F., Kittel, C., and Wagoner, G., 1955, *Phys. Rev.*, **98,** 556.
Dyson, F. J., 1955, *Phys. Rev.*, **98,** 349.
Elliott, R. J., 1954 a, *Phys. Rev.*, **96,** 266; 1954 b, *Ibid.*, **96,** 280.
Frederikse, H. P. R., and Hosler, W. R., 1957, *Phys. Rev.*, **108,** 1136.
Foldy, L. L., and Wouthysen, S. A., 1950, *Phys. Rev.*, **78,** 29.
Jones, H., 1934, *Proc. roy. Soc.* A, **147,** 396.
Kane, E. O., 1957, *J. Phys. Chem. Solids*, **1,** 249.
Kjeldaas, T., and Kohn, W., 1957, *Phys. Rev.*, **105,** 806.
Kunzler, J. E., and Boyle, W. S., 1959, *Bull. Amer. phys. Soc.*, **4,** 168.
Lifshitz, I. M., and Kosevitch, A. M., 1955, *J. exp. theor. Phys. U.S.S.R.*, **29,** 730 (Soviet Physics *J.E.T.P.*, **2,** 636 (1956)).
Luttinger, J. M., and Kohn, W., 1955, *Phys. Rev.*, **97,** 869.
Luttinger, J. M., 1956, *Phys. Rev.*, **102,** 1030.
Roberts, V., and Quarrington, J. E., 1955, *J. Electron.*, **1,** 152.
Roth, L. M., Lax, B., and Zwerdling, S., 1958, *Bull. Amer. phys. Soc.*, **3,** 128.
Shoenberg, D., 1939, *Proc. roy. Soc.* A, **170,** 341; 1952, *Phil. Trans.* A, **245,** 1; 1957, *Progress in Low Temperature Physics*, ed. C. J. Gorter (New York: Interscience Publishers, Inc.), **2,** Chap. 8.
Sondheimer, E. H., and Wilson, A. H., 1951, *Proc. roy. Soc.* A, **210,** 173.
Yafet, Y., 1952, *Phys. Rev.*, **85,** 478; 1957, *Ibid.*, **106,** 679.

The Infra-red Absorption of Hot Semiconducting Diamonds†

By C. D. Clark, P. Kemmey and E. W. J. Mitchell
Physics Research Laboratory, The University, Reading
and B. W. Henvis,
Naval Research Laboratory, Washington, D.C.

[Received September 11, 1959]

Abstract

Measurements of the absorption of p-type semiconducting diamonds have been made at temperatures in the range 450 to 600°K and over the wavelength range between 6 and 45 μ. The major effect observed is an absorption, which is present only in hot semiconducting diamonds, which increases with increasing wavelength and temperature. The increase with temperature is similar to that of the increase in carrier concentration as determined from measurements of the Hall effect.

The observed wavelength dependence differs from that predicted by the theory of intervalence band absorption for mass ratios of 1·04, 1·25, 2·5 and 5. It is possible to account for the shape of the spectrum using the single band free carrier theory of Donovan and March. However, the relaxation times deduced are small (*c.* 10^{-14} sec at 563°K) and there is a discrepancy between the calculated and observed magnitude of absorption.

§ 1. Introduction

The semiconducting diamonds which are available at the present time are p-type conductors, as shown by the work of Custers (1952), Austin and Wolfe (1956), Dyer and Wedepohl (1956) and particularly Wedepohl (1957). Measurements of the Hall constant indicate that the hole concentration is *c.* 10^{13} cm^{-3} at room temperature and, consequently, at that temperature, no optical effects are observed which are directly associated with the presence of free carriers.

Wedepohl (1957) described the characteristic infra-red spectrum which semiconducting diamonds have at room temperature. The spectrum comprises sharp lines superposed on a continuum which extends into the red end of the visible spectrum. It was found by Wedepohl that the strength of these features at room temperature was proportional to the concentration of empty acceptor levels as determined from the electrical measurements, that is, to $(N_A - N_D - p)$ where N_A is the acceptor level concentration, N_D the donor level concentration and p the hole concentration. In addition to these features, semiconducting diamonds possess the 3 to 6 μ absorption band which is found in all diamonds, and which, as shown by Stephen (1958) is probably intrinsic vibrational absorption.

† Communicated by Professor R. W. Ditchburn.

A typical spectrum of a semiconducting diamond at room temperature is shown in fig. 1. Beyond $7\,\mu$ there is a small band at about $7{\cdot}8\,\mu$, which will be referred to below, and some evidence of a band at $21\,\mu$, but apart from these we have not detected any absorption for wavelengths out to about $50\,\mu$.

The work described in this paper was carried out to see whether any specifically free carrier effects could be observed in this otherwise transparent region. In order that there should be sufficient free carriers present it is necessary to make measurements with the diamonds at about 300°C when the carrier concentration is *c.* $10^{16}\,\mathrm{cm}^{-3}$.

Fig. 1

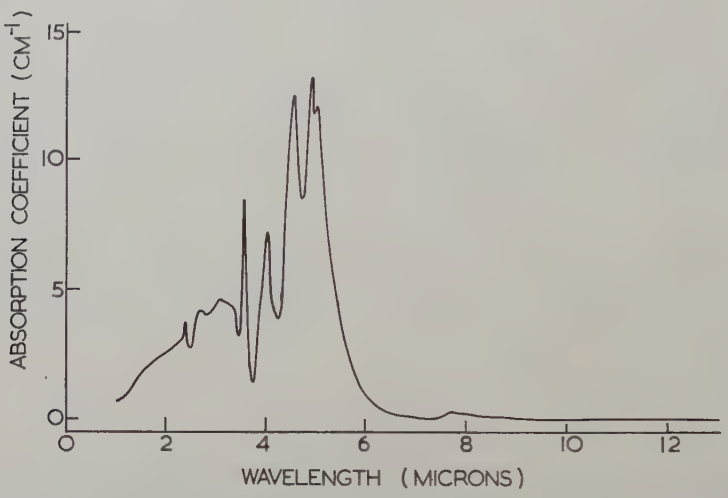

Infra-red spectrum of semiconducting diamond at room temperature.

§ 2. Experimental

The specimens used were natural type IIb diamonds of dimensions about $2 \times 2 \times 5\,\mathrm{mm}$. Resistivity and Hall effect measurements in the temperature range 200 to 700°K were carried out as described by Wedepohl (1957).

Initially the absorption spectra of the specimens were measured for wavelengths up to $15\,\mu$ using the Grubb Parsons double beam spectrometer in the Physics Department of the N.I.R.D., Shinfield, and we are grateful to Dr. J. Goulden of that laboratory for his cooperation in this part of the work. An experimental difficulty was encountered owing to the fact that the radiation emitted by the hot specimen and its holder passed through the chopper and was recorded by the detector. A correction was made for this error by measuring separately the intensity of the emission relative to the reference beam and subtracting it from the apparent transmission curve obtained earlier. The emission was measured by putting an opaque screen on the source side of the crystal.

One specimen was measured between 10 and 24 μ on a single beam instrument using a KBr prism. This was done at the R.A.E., Farnborough, with the kind cooperation of Drs. T. S. Moss and S. D. Smith. In these measurements only the incident light was chopped and the difficulty referred to above was avoided.

The most complete sets of measurements were made at the Naval Research Laboratory, Washington, where C.D.C. and E.W.J.M. spent some time during the summer of 1958. These measurements covered the wavelength range 6 to 45 μ using a single beam Perkin Elmer spectrophotometer with NaCl, KBr, and CsI prisms. Three diamonds were measured of which two were p-type semiconductors (D22 and BP2) and one (D80) a type IIa, which served as a non-conducting control specimen.

Fig. 2

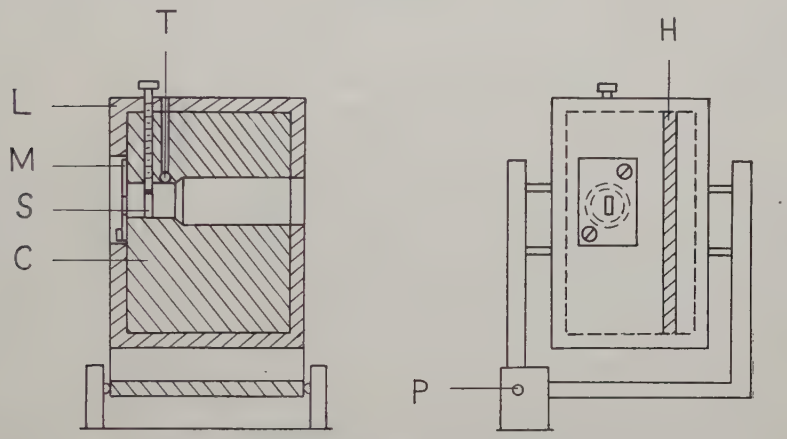

Diagram of furnace used for high temperature spectrum measurements. S : specimen ; M : beam-defining mask ; T : thermocouple ; C : copper block ; H : heating element ; L : thermal insulation ; P : pivot.

A diagram of the furnace used is shown in fig. 2. The crystal was clamped in a hole in a copper block. The block was lagged on the outside and was heated electrically using the element of a small soldering iron. A chromel-alumel thermocouple was used to measure the temperature as close to the diamond as possible. There was a beam defining mask attached to the furnace so that when it was in position the transmitted beam did not reach to the edges of the crystal. The furnace was mounted so that it could be pivoted out of the beam and replaced accurately to its original position. The transmission curves repeated after moving the specimen holder out and putting it back, were reproducible to within $\frac{1}{2}$%.

The measurements were carried out in the following sequence. For a given wavelength range a record was obtained of the intensity transmitted by the specimen at room temperature. Immediately afterwards

the intensity of the incident beam was recorded with the furnace completely removed from the beam. This sequence was repeated until the whole of the wavelength range had been covered.

The series of measurements of incident and transmitted intensity was then carried out with the specimen at 563°K, and later at 484°K. From the records obtained the ratios of the transmitted intensity (I_T) to the beam intensity when the specimen holder was removed (I_B), were calculated for the three temperatures.

The beam apertures in the measurements of I_T and I_B were not the same. Owing to this difference we cannot determine the exact percentage transmission (T) but only a quantity (βT) where β is the aperture ratio. In a given wavelength range β was a constant for the three temperatures of measurement. (Thermal expansion of the mask had a negligible effect.) Consequently we were able to determine for the whole wavelength range T_{563}/T_{293} and T_{484}/T_{293}. In general, referring to a ratio $T_{\text{hot}}/T_{\text{cold}}$ (T_H/T_C) we have:

$$\frac{T_H}{T_C} = \frac{(1-R)^2\exp(-\mu_H t)}{1-R^2\exp(-2\mu_H t)} \frac{1-R^2\exp(-2\mu_C t)}{(1-R)^2\exp(-\mu_C t)}. \quad . \quad . \quad . \quad (1)$$

Here we have assumed that the reflectivity (R) is not significantly dependent on temperature. The change in the bound electron refractive index is likely to be of the order of 0·01 which gives a change in R of 0·001 in 0·170 and this would alter the value of T_H/T_C by less than 0·2%. The extra reflectivity due to the increase in free carrier concentration at the higher temperatures can be neglected for the concentrations encountered in this work.

In eqn. (1) μ_H and μ_C are the absorption coefficients of the specimen hot and cold respectively and t is the specimen thickness. We write $\mu_H = \Delta\mu + \mu_C$ where $+\Delta\mu$ is the additional absorption at the higher temperature. Then (1) may be written:

$$\frac{T_H}{T_C} = \frac{(1-R)^2\exp(-\Delta\mu t)}{1-R^2\exp(-2\Delta\mu t)} \times \frac{1-R^2\exp(-2\mu_C t)}{1-R^2} \times \frac{1-R^2\exp(-2\Delta\mu t)}{[1-R^2\exp(-2\Delta\mu t - 2\mu_C t)]}. \quad . \quad . \quad . \quad . \quad . \quad (2)$$

Measurements on semiconducting diamonds using the double beam instrument showed that between 10 and 15 μ the value of $(\mu_C t)$ was less than 0·1, while the N.R.L. measurements showed that $(\mu_C t)$ did not increase as the wavelength was increased. For $(\mu_C t) = 0{\cdot}1$ the second and third terms of eqn. (2) may be neglected provided that $(\Delta\mu . t) < 2$. For $(\Delta\mu . t) = 2$ the value of T_H/T_C obtained under these conditions is in error by 1%. Our results indicate that $(\Delta\mu . t) \leqslant 2$ so that we have calculated $\Delta\mu$ from:

$$\frac{T_H}{T_C} = \frac{(1-R)^2\exp(-\Delta\mu t)}{1-R^2\exp(-2\Delta\mu t)}. \quad . \quad . \quad . \quad . \quad . \quad . \quad (3)$$

In the experiments using the double beam spectrometer, in order to avoid altering the position of the crystal in the holder, T_C and T_H were not determined absolutely but $\Delta\mu$ was calculated from T_H/T_C using eqn. (3).

§ 3. Results

The observed absorption spectra are shown in fig. 3 where the results for D22 are plotted for temperatures of 563 and 484°K. The experimental points for the non-semiconducting diamond D80 are included. This curve was determined to see whether there were any effects common to IIa and IIb diamonds leading to absorption at the higher temperatures. It will be seen from fig. 3 that the amount of absorption at any wavelength in the semiconducting crystal is much greater than in D80 at the same temperature.

Fig. 3

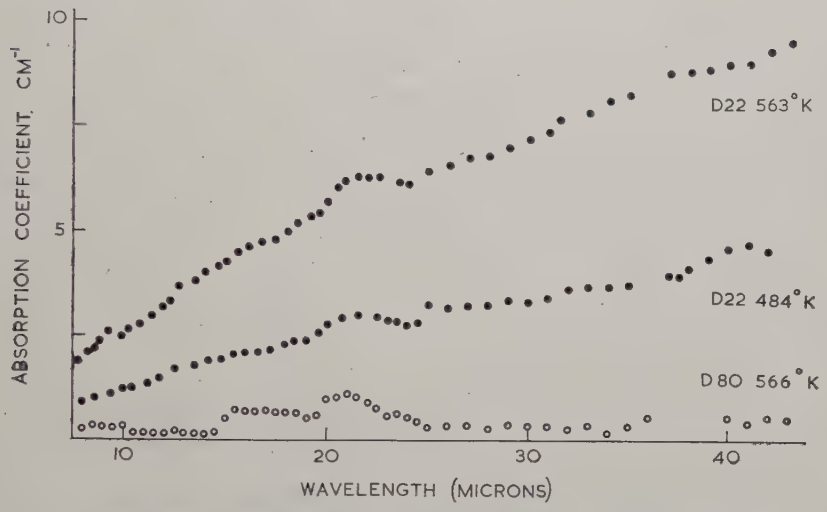

Differential absorption $\Delta\mu$ of semiconducting diamond (D22) and non-semiconducting diamond (D80).

All three spectra have a small peak near 21 μ, indicating that this is not an effect specifically associated with semiconducting diamond. Sutherland *et al.* (1954) reported a band at 20·8 μ at room temperature. Our curves show that there is some absorption in this region which changes with temperature (a band whose position and shape were independent of temperature would not appear on our $\Delta\mu$ curves).

Apart from this 21 μ band, the absorption in the semiconducting diamond increases with wavelength and is still increasing at 45 μ. The rate of increase is smaller at 484 than at 563°K. Similar results over the whole range were obtained on the specimen BP2. This crystal was in the form of a plate and was unsuitable for Hall effect measurements which are required in order to determine the carrier concentration and hence the absorption cross section.

Fig. 4

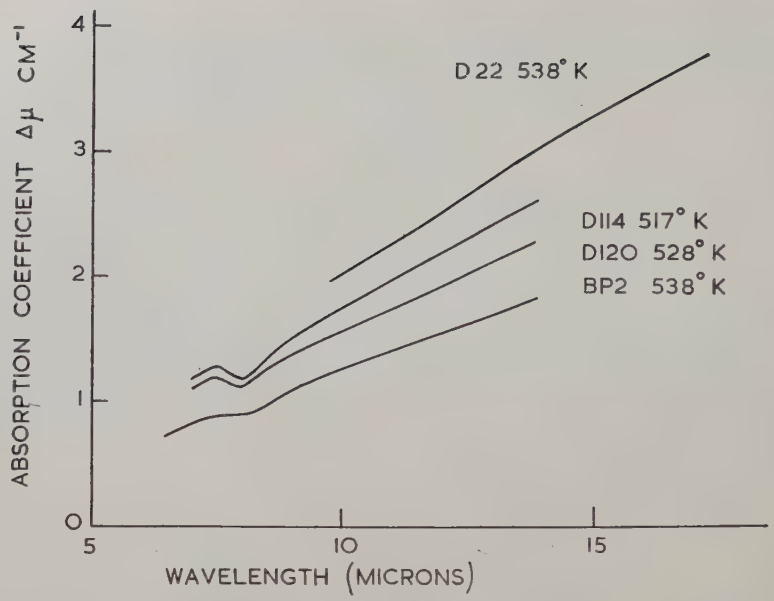

Absorption spectra of four hot semiconducting diamonds in the 5 to 20 μ range.

Fig. 5

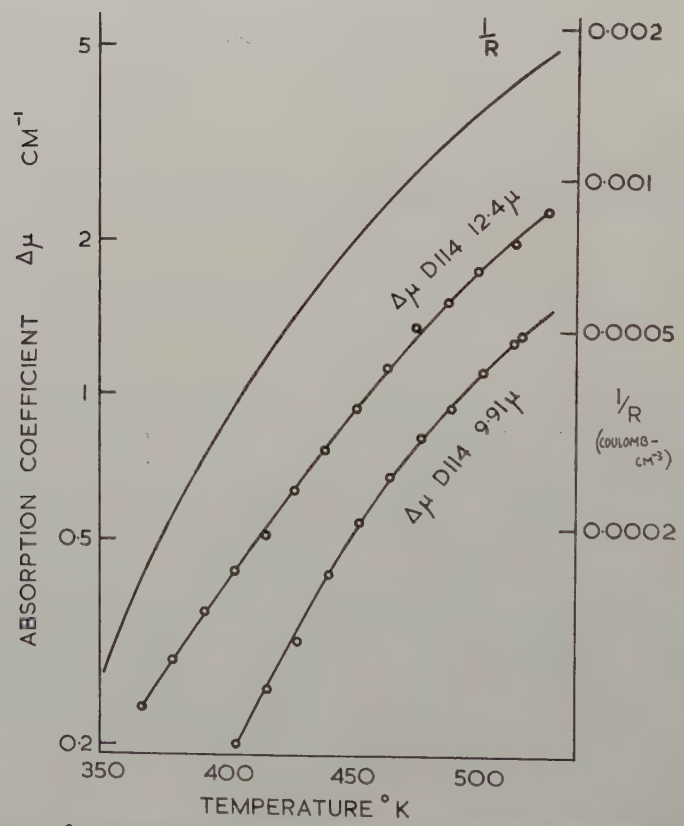

Comparison of temperature dependence of absorption at 12·4 and 9·91 μ with temperature dependence of the inverse Hall coefficient.

The spectra found for other specimens over a narrower wavelength range are shown in fig. 4. These results also indicate an absorption which increases with increasing wavelength.

Fig. 6

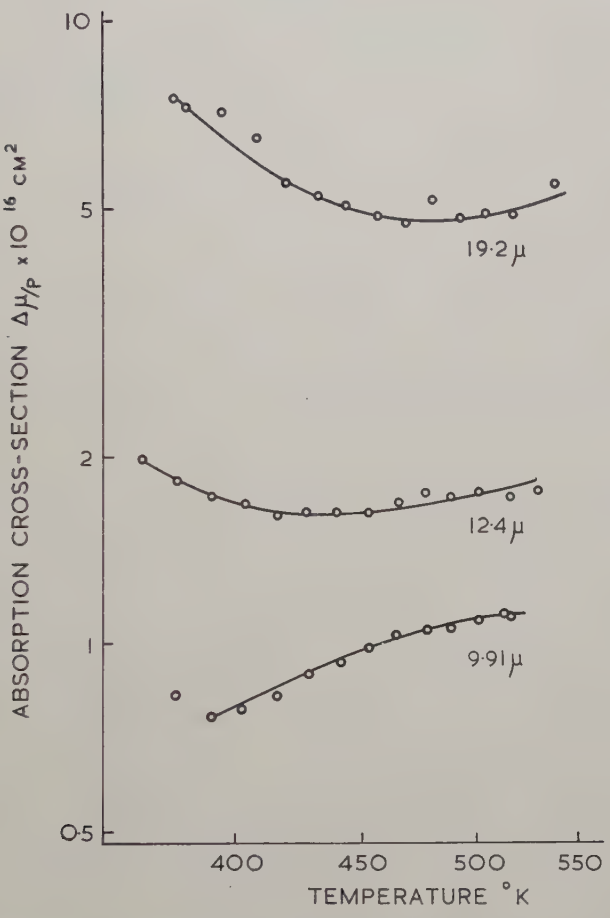

The variation with temperature of the absorption cross section at 19·2, 12·4 and 9·91 μ for specimen D114.

In two cases measurements were made at constant wavelengths as the crystals cooled. Curves of $\Delta\mu$ as a function of temperature for $\lambda = 12{\cdot}4$ and $9{\cdot}91\,\mu$ are plotted in fig. 5, which also contains the reciprocal of the Hall constant (R) as a function of temperature (right-hand ordinate). Using the Hall effect data to find the carrier concentration $[p = (3\pi/8Re)]$ we are able to calculate the absorption cross section $(\Delta\mu/p)$ as a function of temperature and the results are shown in fig. 6.

§ 4. Discussion of Results

The main differences between the absorption spectra in the range 7 to 45 μ of hot and cold semiconducting diamonds are:

(i) The decrease of the absorption at about 7·8 μ with increasing temperature;

(ii) The change in the weak absorption band near 21 μ. This is also found in non-semiconducting diamonds.

(iii) The absorption which increases with increasing wavelength λ. The rate of change of absorption decreases with increasing wavelength but increases with increasing temperature.

Wedepohl (1957) attributed the differences in the electrical properties of hot and cold semiconducting diamonds to:

(*a*) Larger concentration of free holes,

(*b*) Larger concentration of ionized acceptor levels, the concentration of ionized donor levels not changing with temperature.

It is difficult to see how (*b*) could give rise to the continuously increasing absorption with wavelength, although the increase in concentration of ionized acceptor levels may provide the explanation of the feature (i) above.

In an ionized acceptor (i.e. acceptor + an electron) the binding is complete. It would, therefore, be expected that the surrounding atoms would be less disturbed from their normal lattice positions than when the centre is un-ionized and one of the bonds is broken. Hence, a possible explanation of the 7·8 μ absorption is that, in the presence of un-ionized acceptors, the lattice disturbance is sufficient for the normally forbidden 8 μ vibrational absorption to occur. As the temperature increases, the concentration of un-ionized acceptors decreases, and since we suggest that less distortion is produced by the ionized centres, we would expect the absorption to decrease.

The major effect (iii), however, seems to be associated with the presence of the free carriers. Thus for the whole wavelength range of the N.R.L. results on D22 (see fig. 6) $\Delta\mu(563^\circ)/\Delta\mu(484^\circ)$ is equal to $2{\cdot}05 \pm 0{\cdot}10$, compared with the ratio of the reciprocals of the Hall constants, $p(563^\circ)/p(484^\circ) = 2{\cdot}10 \pm 0{\cdot}2$.

There are two effects known from work on other semiconductors which could contribute: single band free carrier absorption and intervalence band transitions of the kind reported by Kahn (1955).

The absorption arising from transitions between two bands, degenerate at $k = 0$, has a maximum value, which like the width and sharpness of the absorption, depends on the effective mass ratio of the two energy bands. In order to obtain anything resembling the observed wavelength dependence it is necessary that our range should be on the high energy side of the peak. The band constants are not known for diamond so that we cannot calculate the magnitude of the absorption. However, the wavelength dependence at any given temperature is determined by the

mass ratio. From eqn. (12) for the absorption coefficient for intervalence band transitions given by Kahn (1955) we have computed the wavelength dependence of the absorption for several mass ratios. Curves of a quantity y proportional to the absorption coefficient are shown in fig. 7, where

$$y = \frac{\nu^{1/2}}{(kT)^{3/2}}\left[\exp - \left(\frac{h\nu}{kT}\frac{m_2^*}{m_1^* - m_2^*}\right) - \exp - \left(\frac{h\nu}{kT}\frac{m_1^*}{m_1^* - m_2^*}\right)\right].$$

In this equation ν is the frequency, T the temperature, m_1^* and m_2^* the effective masses for the two bands.

Fig. 7

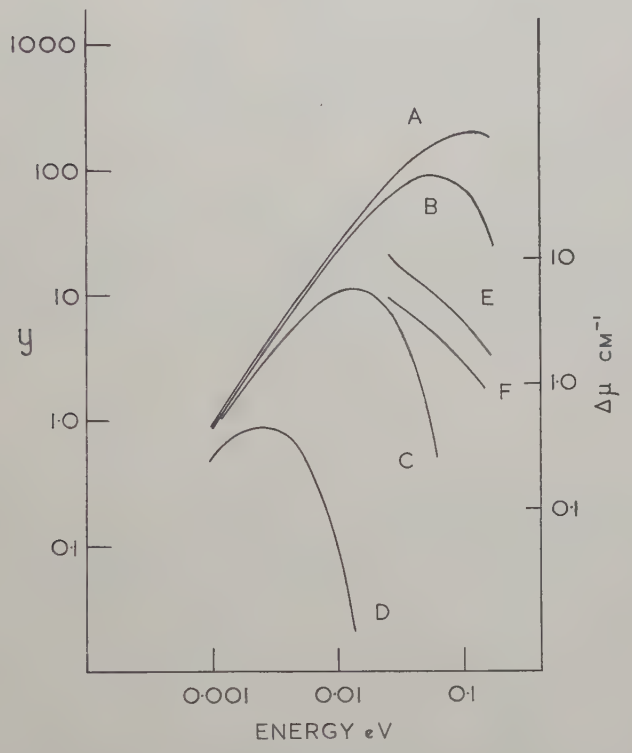

Curves A, B, C and D represent the energy dependence of interband absorption at 525°K for mass ratios 5, 2·5, 1·25 and 1·04 respectively as calculated from Kahn's equation. Curves E and F show measured absorption (right-hand ordinate) of specimen D22 at 563 and 484°K respectively.

The experimental points for D22 at 563 and 484°K are also plotted in fig. 7 and show that the absorption in the range measured increases much less rapidly with increasing wavelength than is predicted. It is, therefore, difficult to see how this type of absorption could account for our results.

4.1. *Single Band Free Carrier Absorption*

Meyer (1958) has given a quantum mechanical treatment of free electron absorption in n-type germanium, taking into account the ellipsodial energy surfaces and various possible scattering mechanisms. While the absolute value of absorption is different from earlier calculations, the wavelength dependence is not drastically altered. Thus Meyer's wavelength dependence, assuming lattice scattering, can be shown numerically to be in the range $\lambda^{1\cdot5}-\lambda^{2\cdot5}$, depending on the particular set of conditions chosen. Since we were working at temperatures between 450 and 600°K lattice scattering should be the predominant scattering mechanism in our crystals.

Under the appropriate conditions, Meyer's theory gives the same wavelength dependence as that given by the Fan *et al.* (1956) theory, in which it had been implicitly assumed that the energy surfaces were spherical. It is concluded therefore that the shape of the energy surfaces is not all important in determining the wavelength dependence of free carrier absorption.

In both theories referred to, the rate of change of absorption with wavelength is increasing with increasing wavelength, contrary to our results. These theories do not apply, however, in the region where $\omega\tau \approx 1$, where ω is the circular frequency ($=2\pi c/\lambda$) and τ the relaxation time†. The observed wavelength dependence may be obtained when $\omega\tau \approx 1$ from the Drude–Zener equation:

$$\mu = \frac{4\pi N e^2}{cm^*} \cdot \frac{\tau}{1+(\omega\tau)^2}. \qquad \ldots\ldots (4)$$

The semiclassical treatment is the only one which gives the wavelength dependence of the absorption when $\omega\tau \approx 1$.

Donovan and March (1956) have performed an improved semi-classical calculation in which an energy dependence of τ is included together with the Maxwell–Boltzmann spread of carrier energies in the band. They find:

$$\alpha = \frac{\mu nc}{4\pi\sigma_0} = 1-u^2+u^4\exp(u^2)\int_{u^2}^{\infty}\frac{\exp(-t)}{t}\,dt. \quad \ldots (5)$$

where

$$u = \tfrac{3}{4}\pi^{1/2}(\omega\tau).$$

In fig. 8 the form of the Donovan and March function is shown, α being plotted against (u) on logarithmic scales. If the experimental curve of $\log \Delta\mu$ vs. $\log\omega$ can be made to coincide with the Donovan and March function by displacements parallel to the ordinate and abscissa, then these displacements can be used to find σ_0 and τ. The points in fig. 8 represent the experimental points for D22 originally plotted on the same log scale but now displaced to fit the theoretical curve. From the

† τ does not enter explicitly into Meyer's theory, but he refers to a condition of this kind.

displacements we find: $\sigma_0 = 0{\cdot}065$ $(\Omega\,\mathrm{cm})^{-1}$ and $\tau = 0{\cdot}91 \times 10^{-14}$ sec. Corresponding to this value of σ_0 obtained from the wavelength dependence we have $\mu_\infty(\mathrm{opt}) = 10{\cdot}1\ \mathrm{cm}^{-1}$, since $\mu_\infty = 156\,\sigma_0$ where μ_∞ is in cm^{-1} if σ_0 is in $(\Omega\,\mathrm{cm})^{-1}$. The value of the d.c. conductivity at 563°K was $0{\cdot}58$ $(\Omega\,\mathrm{cm})^{-1}$ which is equivalent to $\mu_\infty(\mathrm{elec}) = 90\ \mathrm{cm}^{-1}$. These and other values are shown in the table.

Specimen	Spectrometer	Temperature (°K)	Relaxation time τ opt $\times 10^{14}$ sec	μ_∞ (opt) cm^{-1}	μ_∞ (elec) cm^{-1}
D22	N.R.L.	563	0·91	10·1	90
,,	N.R.L.	484	0·89	4·8	66
,,	N.I.R.D.	527	0·58	5·0	80
,,	N.I.R.D.	493	1·00	5·5	69
,,	R.A.E.	538	0·88	7·6	85
D114	N.I.R.D.	547	0·97	8·4	80
D120	N.I.R.D.	528	0·89	6·7	96

The most noticeable features about the parameters determined in this way are the small values of τ, and the discrepancy between the value of μ_∞ obtained from extrapolation of the optical data and the value obtained from the measured d.c. conductivity. In terms of linear frequency

Fig. 8

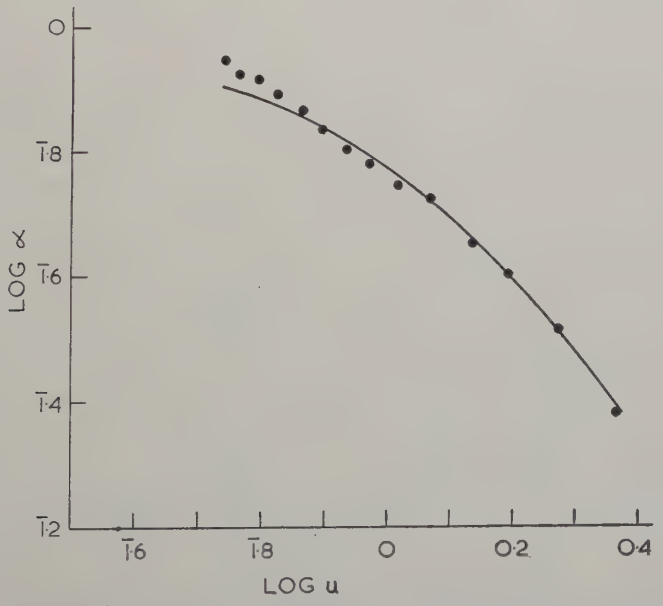

Comparison of wavelength dependence of measured absorption with the theoretical curve due to Donovan and March (1956) (solid line). The experimental points are for specimen D22 at 563°K.

$\tau = 0{\cdot}9 \times 10^{-14}$ sec is equivalent to $1{\cdot}7 \times 10^{13}\,\mathrm{sec}^{-1}$ compared with the maximum vibrational frequency of $3{\cdot}5 \times 10^{13}\,\mathrm{sec}^{-1}$.

It is possible to carry out a similar analysis on the variation of absorption—expressed as $\Delta\mu/\sigma_0(\mathrm{elec})$—with temperature at a constant wavelength. We have from eqn. (5) that

$$\alpha = f(\omega\tau)$$

and if

$$\tau = \tau_0 T^{-x}, \quad \alpha = f(\omega \,.\, \tau_0 T^{-x}).$$

However, in this case we can only determine τ if x is known. The value of τ found will depend critically on the value of x used. In order to make a comparison with the values of τ found above we have assumed that the temperature dependence of τ is the same as the temperature dependence of the Hall mobility ($x = 2{\cdot}8$). Then from the comparison of the Donovan and March function for $\log\alpha$ and $\log(u)$ with the experimental curve of $\log(\Delta\mu/\sigma_0\,\mathrm{elec})$ and $\log(\omega \,.\, T^{-2{\cdot}8})$ we can find values of $(\sigma_0\,\mathrm{elec}/\sigma_0\,\mathrm{opt})$ and τ_0 (and hence τ at any temperature). The values of τ at the appropriate temperature are within a factor of 3 of the values found from the wavelength dependence.

The range of $(\omega\tau)$ covered in the experiments on the variation of absorption with temperature is much less than that covered in the wavelength dependence experiments. We do not attach a great deal of significance, therefore, to the values of τ deduced from the temperature dependence of absorption but note that they are of the same order of magnitude as those deduced from the wavelength dependence.

§ 5. Conclusions

The continuous infra-red absorption in hot semiconducting diamonds is considered to be associated with the presence of free carriers. Even if the valence bands have similar effective masses near $k = 0$, as indicated by the calculations of Hall (1958), it is unlikely that a major part of the absorption can be attributed to intervalence band transitions.

The wavelength dependence of the measured absorption differs from that given by the theories of free carrier absorption of Fan *et al.* (1956) and Meyer (1958). To account for the results in terms of single band free carrier absorption it is necessary that $\omega\tau \approx 1$, where the quantum mechanical treatments referred to are not valid.

Using the semiclassical theory of Donovan and March (1956) we find that the observed wavelength dependence can be obtained for $\tau \approx 1 \times 10^{-14}$ sec. However, there is a discrepancy, ranging from $\times 9$ to $\times 16$, between μ_∞ extrapolated from optical data and μ_∞ determined from the d.c. conductivity. Values of the same order of magnitude are obtained from the less accurate analysis of the temperature dependence data.

Thus we do not yet have an adequate interpretation of the experimental results in terms of free carrier absorption. It will probably not

be possible to obtain a completely unequivocal interpretation until the valence band structure is better known. Meanwhile, an extension of measurements to the microwave region would be desirable.

Acknowledgments

In addition to those people referred to in the paper we should like to thank Professors E. Burstein and R. W. Ditchburn for their interest and encouragement, Drs. G. S. Picus and M. Haas for helpful discussions, Dr. J. F. H. Custers, Director of Research, Diamond Research Laboratory, Johannesburg, for his interest in the work and also for providing the specially cut diamonds which were used, and Industrial Distributors (1946) Ltd. for financial support.

References

Austin, I. G., and Wolfe, R., 1956, *Proc. phys. Soc. Lond.* B, **69,** 329.
Custers, J. F. H., 1952, *Physica*, **18,** 489.
Donovan, B., and March, N. H., 1956, *Proc. phys. Soc. Lond.* B, **69,** 528.
Dyer, H. B., and Wedepohl, P. T., 1956, *Proc. phys. Soc. Lond.* B, **69,** 410.
Fan, H. Y., Spitzer, W., and Collins, R. J., 1956, *Phys. Rev.*, **101,** 566.
Hall, G. G., 1958, *Phil. Mag.*, **3,** 429.
Kahn, A. H., 1955, *Phys. Rev.*, **97,** 1647.
Meyer, H. J. G., 1958, *Phys. Rev.*, **112,** 298.
Stephen, M. J., 1958, *Proc. phys. Soc. Lond.* B, **71,** 485.
Sutherland, G. B. B. M., Blackwell, E. D., and Simeral, W. G., 1954, *Nature, Lond.*, **174,** 901.
Wedepohl, P. T., 1957, *Proc. phys. Soc. Lond.* B, **70,** 117.

The Effect of Internal Oxidation on the Damping Capacity of Copper–Silicon Alloys†

By T. B. Gibbons and S. O'Hara
Royal College of Science and Technology, Glasgow, C.1

[Received October 20, 1959]

Abstract

Damping capacity measurements have been carried out on copper–silicon alloy specimens before and after internal oxidation and the results compared with those for oxygen free, high conductivity copper specimens given the same treatment. High damping values have been noted for the fully internally oxidized copper–silicon material and it is suggested that this is caused, to some extent, by the generation of relatively free dislocations around the silica particles during the growth and subsequent cooling of these inclusions.

§ 1. Introduction

Dissolved impurities are known to lower the damping capacity of metals by pinning the dislocations. Hanstock (1954) has obtained large increases in the damping capacity of aluminium alloys during precipitation. Granato and Lucke (1956) have found increases in damping after internal oxidation and have suggested that the increase in damping in both these cases is due to the removal of the impurities or alloying elements from the lattice by precipitation and the consequent unlocking of pinned dislocations.

In the present work, a copper–silicon alloy, containing about 0·2% silicon, was used to determine the effect of internal oxidation on damping capacity. In all, three effects could be studied, viz. removal of silicon, entry of oxygen to the lattice, and formation of silica particles.

The amplitude dependent damping observed is best described by a static hysteresis mechanism which is frequency independent.

Granato and Lucke (1956) have described this mechanism by suggesting that the dislocation lines bell out under the applied stress and then break away from the pinning points. During the return part of the cycle, the path followed by the dislocation is different from the outgoing path and the resulting hysteresis in the dislocation stress–strain curve. gives rise to an energy loss.

A quantitative treatment of this mechanism gives the following expression for amplitude dependent damping Δ_H

$$\Delta_H = \frac{A}{\epsilon_0} \exp\left(-\frac{B}{\epsilon_0}\right)$$

† Communicated by the Authors.

where ϵ_0 is the measuring strain amplitude

$$A = \frac{2{\cdot}5\Omega\Lambda L_N^3}{\pi^2 L}\frac{K\eta\mathbf{a}}{L\epsilon_0} \text{ and } B = \frac{K\eta\mathbf{a}}{\epsilon_0}$$

where Ω is an orientation factor accounting for difference in resolved shear stress on the slip planes and applied longitudinal stress, Λ is dislocation density, L_N is dislocation network length, L is average dislocation loop length, K is Boltzmann constant, η Cottrell misfit parameter measuring the magnitude of the lattice distortion at a point defect, and $\mathbf{a}$ is a lattice parameter.

Several workers have shown that this law is not complete in itself over large ranges of strain amplitude (Niblett and Wilkes 1959).

§ 2. Experimental

To ensure a uniform grain size, all the specimens were vacuum annealed for 48 hours at 1040°C before internal oxidation. The internal oxidation was carried out by heating the specimens in an enclosed space with equal amounts of cuprous oxide and copper powders. This allowed the silicon to be oxidized to silica without the formation of a cuprous oxide film on the surface. Replicate samples of O.F.H.C. copper and copper–silicon were used so that the effect of oxygen in the copper could be estimated; further, a comparison of the two sets of results gave an indication of the effect of silica particles in the internally oxidized copper-silicon alloy.

Complete internal oxidation was obtained by heating the specimens at 950°C for 100 hours. The partially internally oxidized specimens were held at 900°C for 72 hours. These times were calculated from the formula suggested by Rhines and co-workers (1942), viz.

$$\log\frac{X^2 C_M}{t} = \frac{a'}{T} + b'$$

where X = depth of oxidation in centimetres in time t, C_M = original alloy concentration, T = absolute temperature, a' and b' are constants for the particular alloy.

In the partially oxidized specimens the depth of penetration was, on average, 0·13 cm, which compared favourably with the calculated depth.

The damping capacity of the specimens was measured after the initial vacuum anneal and then after internal oxidation. The apparatus used was designed to measure damping phenomena in the kilocycle range and was initially developed by Förster (1937). The bar vibrates transversely in free-free motion, the damping capacity being measured from the width of the resonant peak at half the resonant amplitude. The specimens were supported a short distance from the nodes by cotton threads which vibrate and detect the vibrations of the bar. Some inaccuracy arises because the support positions and the nodes are not coincident. No correction for this has been applied, hence the individual results are not absolute but may be considered to be comparative.

§ 3. Results

The damping values for the vacuum annealed O.F.H.C. copper are given by curves 2, 3, 4, fig. 1, and curve 1, fig. 1, is typical of a vacuum annealed copper–silicon bar. The very high amplitude dependent damping of curve 2 is the result of having to push the specimen out of its graphite sheath. In general, these results are in agreement with other published work.

Fig. 1

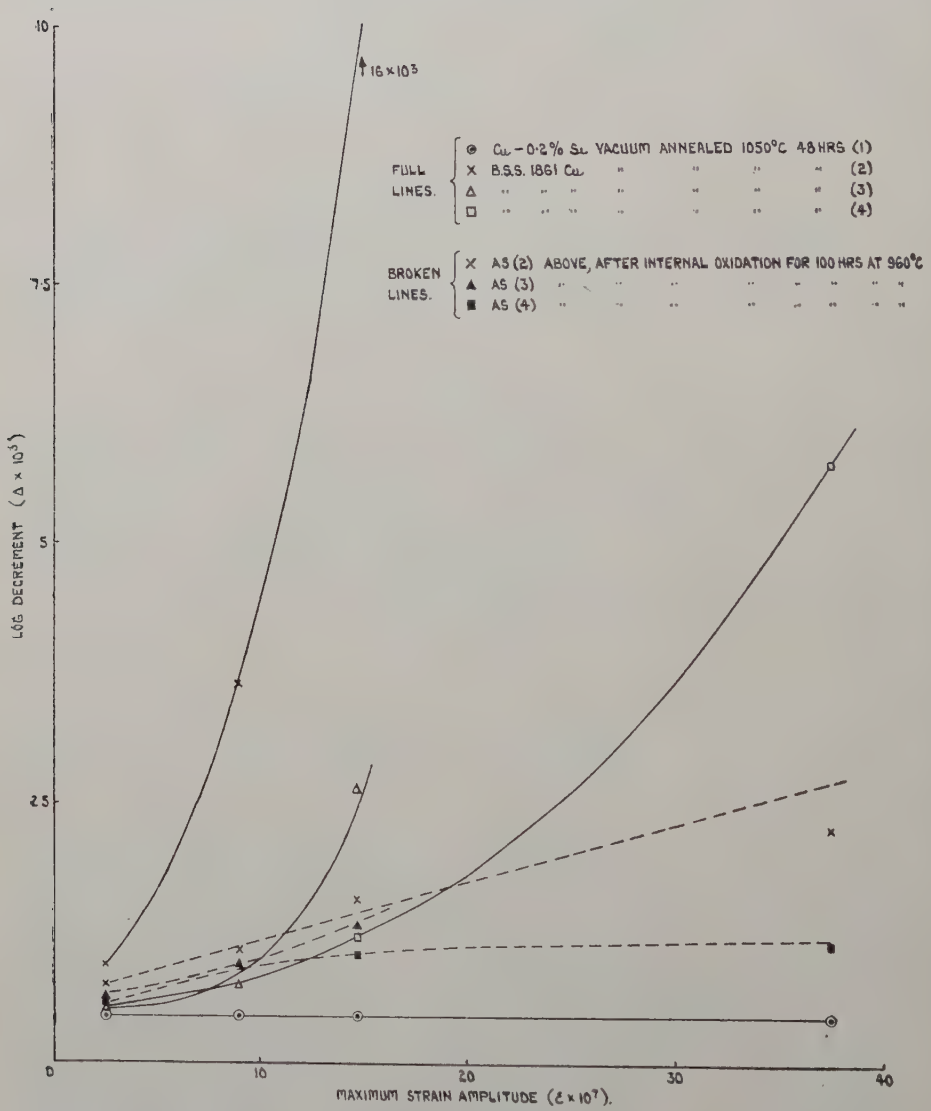

The effect of internal oxidation of these O.F.H.C. copper specimens is quite marked and is particularly noticeable in the case of curve 2. In the three cases amplitude dependent damping has been almost completely removed.

In the copper–silicon specimens, partial internal oxidation has raised the damping from amplitude independence, curve A, fig. 2, to marked amplitude dependence as shown by the broken lines, fig. 2. Complete internal oxidation has raised the curves even further—full lines, fig. 2—and the damping capacity of these specimens is very high. The effect of internal oxidation on the copper–silicon material is therefore opposite to the effect on O.F.H.C. copper.

Fig. 2

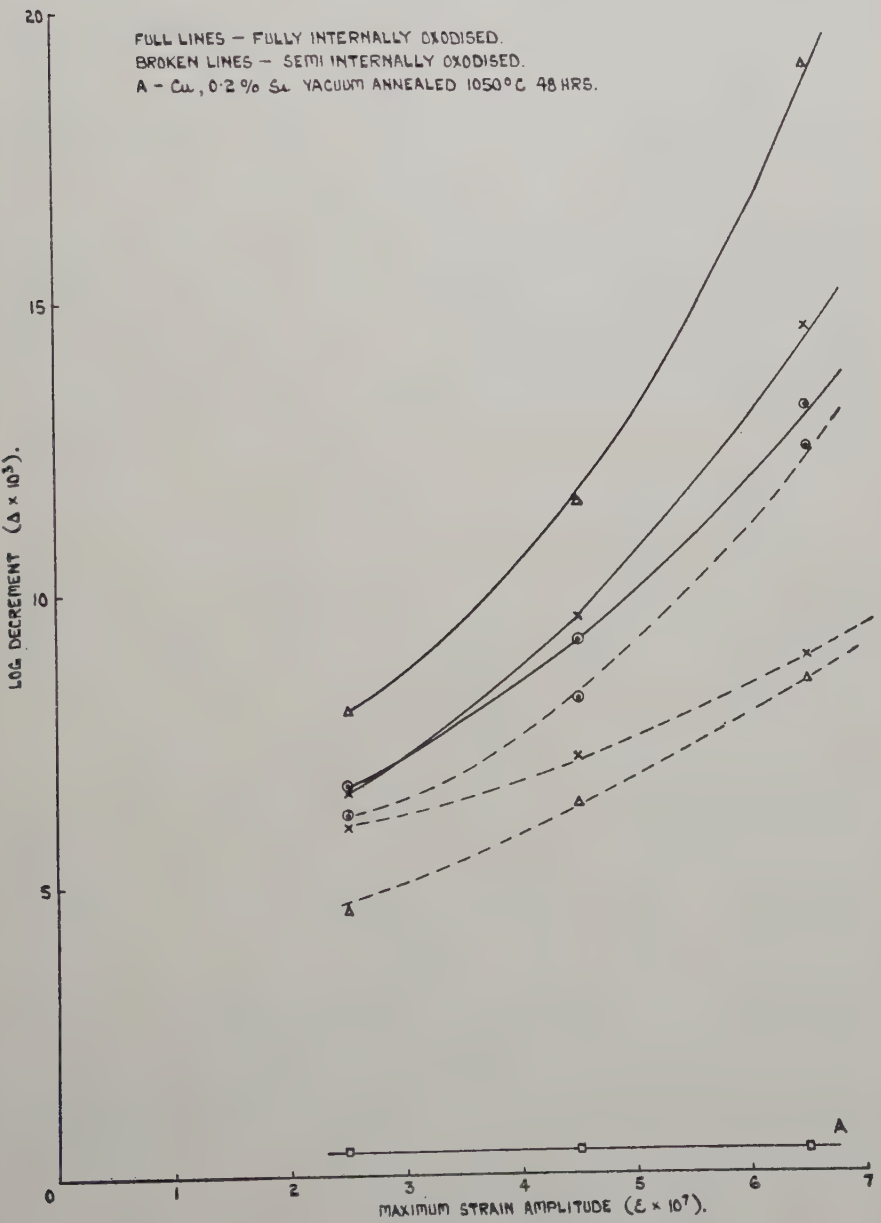

§ 4. Discussion

Perhaps the most significant difference between the fully internally oxidized copper–silicon specimens and the fully internally oxidised O.F.H.C. copper is the presence of silica particles in the former, since no oxide particles were found within the O.F.H.C. copper. The amount of oxygen present in the O.F.H.C. copper specimens, after internal oxidation, will probably be greater than in the internally oxidized copper–silicon alloy since in the latter case the oxidation front advances slowly while precipitation is taking place. It will be observed, however, that the damping values obtained for the internally oxidized copper–silicon alloy are higher than those for the vacuum annealed O.F.H.C. copper. Thus, the different amounts of oxygen present in the two sets of specimens cannot account for the high damping values of fig. 2. The high amplitude dependent damping of the copper–silicon specimens must be a direct result of the presence of silica particles. The decrease in damping capacity, on internal oxidation of annealed O.F.H.C. copper is just as expected due to the pinning effect of oxygen on the dislocation lines.

The amplitude dependent results shown in fig. 2 are characteristic of dislocation damping. It appears, therefore, that in some way, the silica particles are assisting in the creation of many loosely pinned dislocations.

Shear stresses can develop round a particle during growth at high temperature and also during cooling when the particles and matrix have different coefficients of contraction. These stresses can in turn create dislocations.

Parasnis and Mitchell (1959) have observed this effect in crystals of silver chloride. In this case, particles of what is assumed to be silver are surrounded by systems of decorated prismatic dislocation loops and more complex configurations. It is shown that the formation of these dislocations and their subsequent glide can make available the space required for the separation of further silver atoms upon the particles. Jones and Mitchell (1958) have noted systems of prismatic dislocations formed during cooling, round glass spheres in silver chloride crystals.

By direct observation of etch pits, Holden (1959) has noted large numbers of dislocations generated round precipitates formed in an iron–carbon–silicon alloy; these are believed to arise from the shear stresses developed round the particles during cooling of the alloy. Huggins (1959) has calculated the shear stresses which can arise during the formation of a precipitate and also during the anisotropic expansion or contraction of a precipitate in an isotropic matrix. He has shown that these stresses can be of large magnitudes.

In the present work, shear stresses arising during growth of the silica particles and also during cooling, may well create new dislocations around the particles. Also dislocation already in the lattice may be torn away from impurity pinning points and become free. Such a sequence of events would partly explain the high, amplitude dependent, damping results of fig. 2.

The explanation given by Granato and Lucke (1956) to account for the increase in damping after precipitation or internal oxidation is therefore oversimplified. The increased damping caused by precipitation will probably be due to a combination of three mechanisms; namely, a decrease in dissolved impurity or alloying element, the creation of dislocations round precipitates and the freeing of pinned dislocations by the shear stresses in the vicinity of the precipitates.

Acknowledgment

The authors would like to thank Professor Hay for his encouragement while the work was in progress.

References

Förster, F., 1937, *Z. Metallk.*, **29,** 109.
Granato, A., and Lucke, K., 1956, Reported, *Dislocations and Mechanical Properties of Crystals* (Wiley, 1957).
Hanstock, R. F., 1954, *J. Inst. Met.*, **83,** 11.
Holden, J., 1959, *Acta Met.* (to be published).
Huggins, R. G., 1959, *Acta Met.*, **7,** 357.
Jones, D. A., and Mitchell, J. W., 1958, *Phil. Mag.*, **3,** 1.
Martin, J. W., and Smith, G. C., 1954, *J. Inst. Met.*, **83,** 153.
Niblett, D. H., and Wilkes, J., 1959, *Proc. phys. Soc. Lond.*, **73,** 95.
Parasnis, A. S., and Mitchell, J. W., 1959, *Phil. Mag.*, **4,** 171.
Rhines, F. N., Johnson, W. A., and Anderson, W. A., 1942, *Trans. Amer. Inst. min (metall.) Engrs*, **147,** 205.

A 10 in. Diameter Liquid Hydrogen Bubble Chamber†

By Margaret H. Alston‡, D. C. Cundy, W. H. Evans, R. W. Newport, and P. R. Williams

Nuclear Physics Research Laboratory,
University of Liverpool

[Received September 28, 1959]

Abstract

The important design features of a 10 in. hydrogen bubble chamber, its magnet and the associated control circuitry are presented.

§ 1. Introduction

A liquid hydrogen bubble chamber of 10 in. diameter and 4 in. depth has been constructed for use with the 383 mev synchrocyclotron. The dynamic heat input is kept to a minimum by using metal bellows to provide liquid phase expansion. It has been operated in the π-meson beams of the synchrocyclotron with a repetition period of 4 sec, in a magnetic field of 8000 oersted.

§ 2. General Arrangement (fig. 1 (*a*), 1 (*b*))

The vacuum tank of 1 in. thick stainless steel (grade EN 58 B) is in the form of a cross. The vertical member contains the chamber, the liquid hydrogen reservoirs, most of the copper radiation shield and its liquid nitrogen reservoirs. The cylindrical arms of the cross, $13\frac{1}{8}$ in. diameter and 24 in. long, house extensions bolted on to the main radiation shield which reduce the solid angle subtended at the chamber by areas at room temperature to about $\frac{1}{5}$ steradian.

Illumination is provided by a high-speed flash tube which gives a spherical source less than $\frac{3}{8}$ in. diameter (GE FT 230 or A.E.I. FA 5), and a plano-convex lens placed close to the chamber. This system produces a convergent beam of light which comes to a focus along the axis of the chamber and in the plane of the two camera lenses. The lenses are 10 in. apart, 45 in. from the centre of the chamber and lie symmetrically on either side of the cone of light. This arrangement ensures an essentially constant light scattering angle equal to half the stereo angle for all points photographed in the chamber. The two stereo views are taken on one frame of 35 mm film for ease of measurement and handling.

† Communicated by Professor H. W. B. Skinner, F.R.S.

‡ Now at the Lawrence Radiation Laboratory, University of California.

Fig. 1 (*a*)

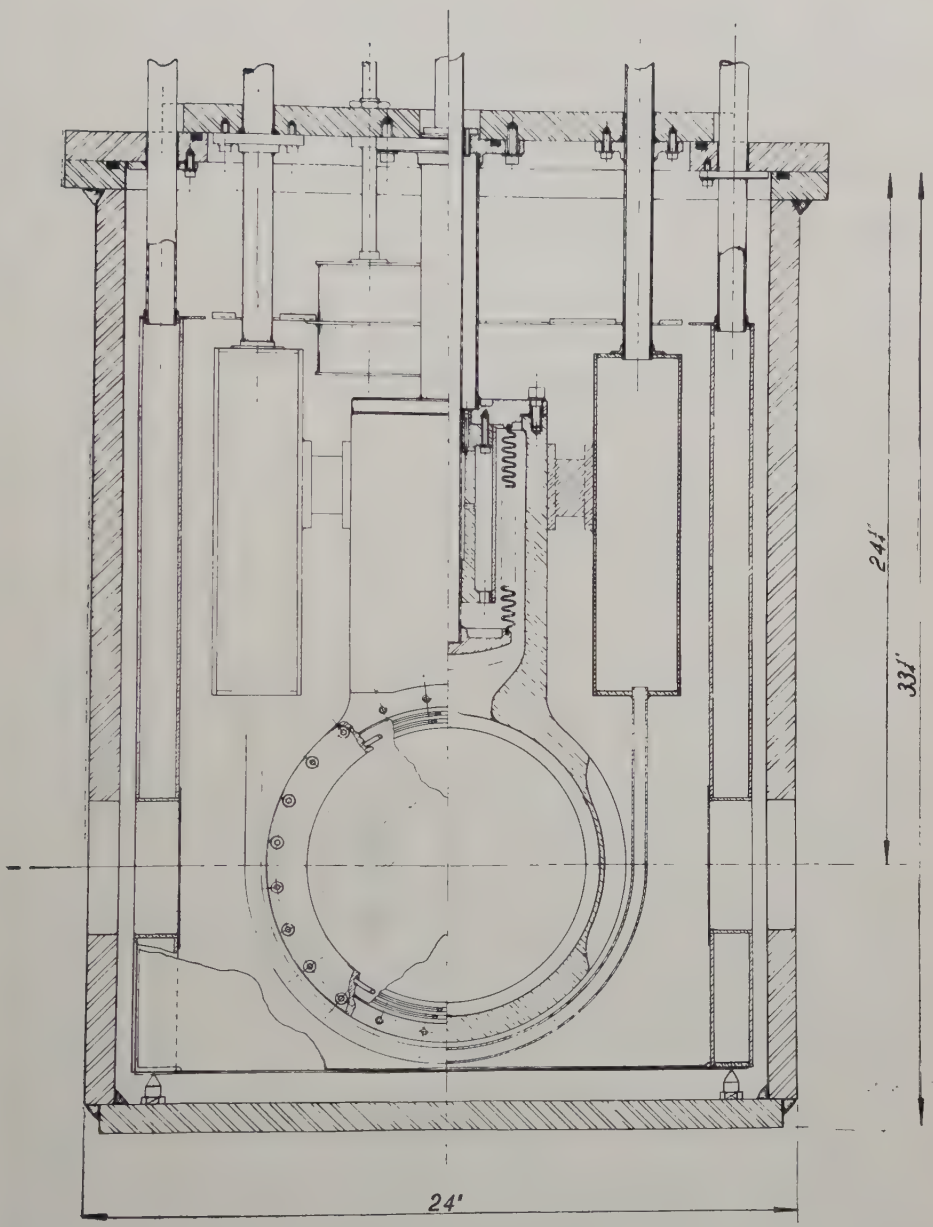

(*a*) General arrangements showing the mounting of the bubble chamber and the hydrogen reservoirs in the vacuum tank. (*b*) General arrangement showing the bubble chamber, liquid nitrogen radiation shield, the optical system and the expansion system.

Fig. 1 (*b*)

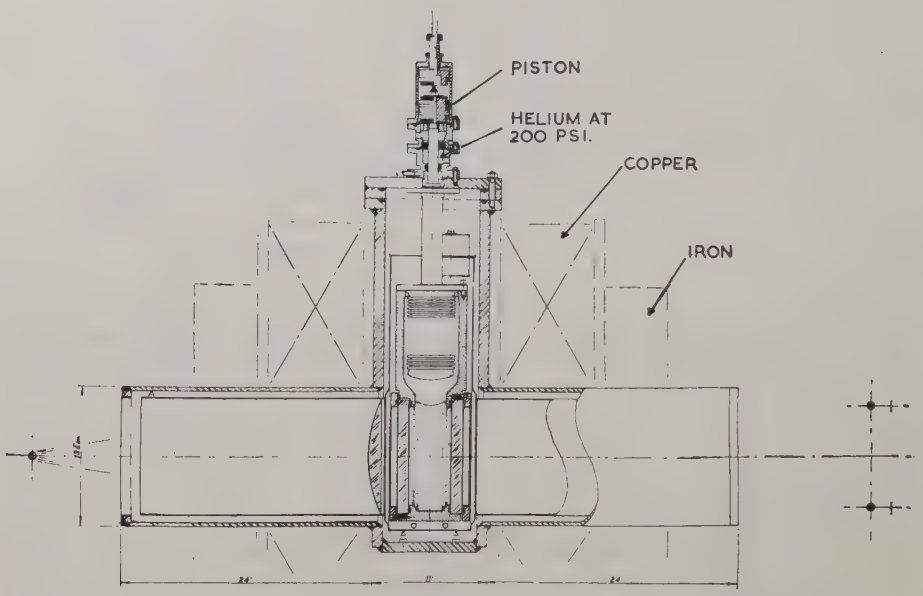

§ 3. Chamber Body (fig. 2, Pl. 19)

This was machined from a single forging of phosphorized de-oxidized copper and consists of a cylinder 10 in. in diameter 4 in. deep intersecting at right angles a second 5 in. in diameter and 10 in. deep. This second cylinder houses the bellows used for expansion. The orientation of the chamber, i.e. windows vertical with the expansion cylinder above the observed volume, was chosen so that bubbles formed during expansion rise to a position where the heat of re-compression can easily be removed (cooling takes place at the top of the expansion cylinder). Stable temperature gradients giving variable sensitivity with height are thus eliminated. This procedure also ensures that solid impurities do not collect in positions where they can obscure the field of view. It is by no means the only solution to these problems but appears to be the simplest method in practice.

The sealing of flanges and windows is achieved by using double lead ' 0 ' rings with pump-outs. The whole unit and the 1 in. thick toughened-glass windows were designed to withstand 200 p.s.i.

The wall thickness is partly determined by mechanical considerations and partly by the need to keep temperature gradients in the metal to a minimum. The average thickness is 1 in. and it only departs appreciably from this in the regions of beam entry and exit where it is $\frac{1}{8}$ in. thick.

The chamber is supported by a 2 in. diameter, 0·048 in. wall stainless-steel tube welded to a flange which is in turn bolted on to the expansion cylinder.

§ 4. Expansion System

This consists of a 4-ply stainless steel bellows, each ply of 0·011 in. thickness, hard soldered to the support flange on the expansion cylinder. The bellows projects downwards into the expansion cylinder and is driven by a 1 in. diameter 0·048 in. wall stainless steel tube connected to a dished end cap on its lower end. The other end of the tube is connected to a 3-in. diameter air-driven aluminium-alloy piston at room temperature. Heat conducted along the drive tube is introduced at the bottom of the bellows and is easily removed by convective motion of the liquid hydrogen in the space between the bellows and the expansion cylinder. Helium gas is maintained in the space above the bellows to assist in the initial cooling by convection and is used to control the speed of expansion by altering the pressure. This method of control has the advantage that the expansion speed can be altered without affecting the speed of re-compression.

The drive tube is used in compression and, to reduce the tendency to buckle, cylindrical guides are provided to restrict the maximum free length to 8 in.

Failure of the bellows would result in hydrogen gas at the operating pressure entering the space above the bellows. To prevent this gas from entering the cylinder containing the air-driven piston and forming an explosive mixture with air, the drive rod passes through a small compartment containing helium gas at 200 p.s.i. and sealed by Gaco distributor seals. This pressurized helium compartment also prevents leakage of air into the bellows.

Expansion and re-compression are achieved by release of the air behind the piston and its subsequent re-introduction by means of a three-way valve. For a typical setting the cycle consists of a 8 ms expansion, a 15 ms expanded phase and an 9 ms re-compression. The system is reproducible in time to better than 0·5 ms and the particle beam traverses the bubble chamber under accurately reproducible conditions.

Under normal operating conditions the hydrogen vapour pressure is 67 p.s.i.g. and the pre-expansion pressure is 78 p.s.i.g. The expanded pressure is not accurately known but the variation of chamber pressure is displayed on one trace of a double beam oscilloscope by using a condenser gauge and the FM detector circuit described previously (Alston *et al.* 1957). The entry of the beam of particles and the position of the light flash is displayed on the second trace.

The expansion system has satisfactorily performed 10 000 cycles at room temperature and 50 000 at liquid hydrogen temperatures with a stroke of 0·7 in. corresponding to a volume expansion of $2\frac{1}{4}\%$.

§ 5. Temperature Control

The chamber is kept at the operating temperature by connecting the upper portion of the expansion cylinder to the liquid hydrogen reservoirs through two metal straps whose size is determined by the total heat

input to the chamber at the operating temperature. Since the cool-down to 78°K is achieved by filling the liquid hydrogen reservoirs with liquid nitrogen and the thermal capacity of the chamber increases with temperature, the conductivity of the straps should increase correspondingly with temperature if the cool-down is to be achieved in a reasonable time. Phosphorized de-oxidized copper was chosen for the material of the straps since it has the required characteristics.

In practice the chamber is slightly over-cooled and small heaters embedded in the wall of the expansion cylinder are used in conjunction with a contact pressure-gauge connected to a vapour pressure thermometer to provide temperature control. This system regulates the vapour pressure of the hydrogen filling to 1 p.s.i.

Liquid hydrogen consumption is 1·6 litres per hour total and is constant if the chamber temperature is kept constant. The dynamic load for the chamber at 15 cycles per minute is equivalent to about 0·5 litres/hour of liquid hydrogen. This figure was calculated from the difference in the power supplied by the control heaters in the cycled and uncycled chamber. It is essential to isolate the chamber from the filling line during expansion and this is achieved by using a helium-gas operated bellows-valve placed close to the chamber.

§ 6. Magnet

A cross section of the magnet is shown in fig. 1 (*a*). It consists of two coils, each 14½ in. ID and 44½ in. OD by 8·5 in. deep, surrounded by an iron return path but no poles. The iron end pieces are bored 14½ in. diameter to permit illumination and photography. The magnet weighs 6 tons and the gap between the coils is 14 in. Each set consists of eight double pancakes electrically in series with the cooling water in parallel. The two coils in each double pancake are joined at the centre so that the inlet and outlet water connections are on the outside. Water at 500 p.s.i. is used for cooling. Typical operating conditions are 800 amps at 240 volts giving a field of 8000 oersted with a variation of $\pm 2\%$ over the illuminated volume.

§ 7. Safety Arrangements

The utmost care is taken to ensure the safety of the personnel operating the chamber. The procedure adopted follows closely that employed at the UCRL. Failure of the toughened glass windows would result in the release of 6 litres of liquid hydrogen into the vacuum tank and a rapid rise in the tank pressure to about 70 p.s.i. Subsequent heat transfer from the tank to the cold hydrogen would cause a slower rise to a final pressure of around 40 atmospheres.

The tank is connected to a ' rupture disc ' and a 4 in. diameter vent line. The rupture disc is constructed so that during normal operation, with the tank at high vacuum, it rests on a concave perforated plate. Should the tank pressure rise one or two pounds above atmospheric

pressure the disc is forced against a sharp cutting edge and is fractured. This method of construction ensures that the performance is not strongly dependent on the unsupported strength of the disc.

The vacuum tank and all units connected to the vacuum system will withstand 150 p.s.i. High-vacuum gauges are housed in protecting brass cylinders. All hydrogen gas released is vented into the atmosphere outside the building. This applies to gas escaping from relief valves and the boil-off from the two reservoirs.

A power failure or a fault in the magnet stabilizer circuit can cause the current in the magnet to decay with a time constant of around 1·5 sec. The subsequent mechanical impulse to the chamber can be considerable (Gow, private communication). The maximum rate of current decay is reduced by using the stored rotational energy of the motor generator set. The generator is excited by means of a d.c. amplifier and a high gain amplidyne set. The output from the generator is coupled in anti-phase via a condenser to subsidiary windings in the amplidyne unit. By this means the current decay is made approximately linear and extended to 10 sec.

§ 8. Cool-down Procedure

The vacuum tank is first evacuated to below 10^{-5} mm mercury and the chamber is pumped through a liquid nitrogen trap to remove condensable vapours. The chamber is then filled with pure hydrogen gas which is maintained at 78 p.s.i.g. and assists in cooling the inner faces of the glass windows by convection. This gas, obtained by passing commercial hydrogen through the purifying circuit of a hydrogen liquefying plant, can be liquefied in the chamber without further cleaning.

The liquid nitrogen radiation shield is cooled at least 2 hours before the chamber. This precuation is taken to avoid condensation on the outer faces of the glass windows. No trouble due to this cause has been experienced in several days' operation.

Hydrogen condensing in the chamber is pre-cooled to 27°K through two heat exchangers at 78°K and 20°K respectively. Before cycling the chamber it is important to make sure that it is completely full of liquid hydrogen. The top of the expansion cylinder is the coldest point in the system and there is no danger that a large bubble of gaseous hydrogen be left at this point.

§ 9. Operating Procedure with the Synchrocyclotron

In normal operation the synchrocyclotron gives one pulse of particles every 10 ms. To ensure that the particles traverse the chamber in an accurately reproducible manner the circuit shown schematically in fig. 3 is used. The pulsed-arc ion source of the synchrocyclotron is not pulsed until required. Synchronizing pulses from the accelerator appear at 10 ms intervals. These are fed into an electronic gate which is opened by the sequence unit. The next synchronizing pulse is transmitted through

the gating circuit and operates a delay unit which controls the current pulse to the 3-way solenoid operated air valve. The bubble chamber is expanded after an interval governed by the setting of the delay unit and the mechanical inertia of the valves. Synchronizing pulses are also fed through the electronic gate into a 0 to 10 variable scaler, the output of which generates a pulse to trigger the synchrocyclotron pulsed-arc source. The scaler is initially set at some arbitrary figure and the dynamic pressure change in the chamber and the beam traversal time (detected by a 2-fold scintillation counter) are observed on the double beam oscilloscope. The variable delay and the scaler are then set so that the particles traverse the chamber at the correct time. A typical trace obtained is shown in fig. 4 (Pl. 20).

Fig. 3

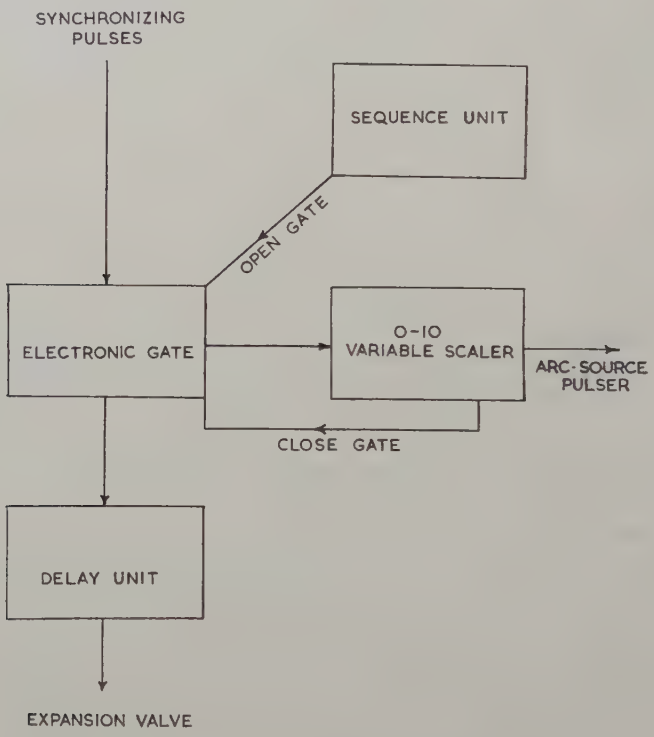

Schematic diagram of the electronic control unit.

The intensity of the circulating beam in the synchrocyclotron is recorded pulse by pulse on a commercial pen recorder, thus enabling the operator to correct for long period drifts.

Particles entering the chamber are deflected by the magnetic field around the chamber and some allowance must be made for this if the particles are to traverse the chamber symmetrically. In bubble chambers employing a vertical magnetic field the whole equipment can be rotated

about a vertical axis. Bubble chambers with a horizontal field cannot in general be tilted and some other solution must be sought. A reasonably successful solution is to raise the whole equipment some inches above beam height. Any reduction necessary in the energy of the particles should be carried out as close to the chamber as possible.

An example of the pictures taken is shown in fig. 5 (Pl. 21) and a photograph of the apparatus is shown in fig. 6 (Pl. 22).

Acknowledgments

We are grateful to Professor H. W. B. Skinner and Professor J. M. Cassels for their interest and encouragement ; to Professor L. W. Alvarez and his colleagues for sending us technical information on hydrogen bubble chambers ; to Mr. J. H. Craig and his staff for constructing the equipment, to Mr. A. Amery who made all the engineering drawings, to Dr. B. C. Collinge and his staff who designed and built some of the electronic equipment, to B. Halliday and Metropolitan Vickers for work on the magnet power supplies and to the synchrocyclotron and liquefier crews for their co-operation.

One of us (D.C.C.) is indebted to D.S.I.R. for a studentship ; M.H.A. and P.R.W. to the I.C.I. for Fellowships.

Reference

Alston, Margaret H., Collinge, B., Evans, W. H., Newport, R. W., and Williams, P. R., 1957, *Phil. Mag.*, **2**, 820.

Systematic Track Distortion in a 10 in. Diameter Liquid Hydrogen Bubble Chamber†

By D. C. Cundy, W. H. Evans, D. W. Hadley, P. Mason, R. W. Newport, J. R. Smith and P. R. Williams
Nuclear Physics Research Laboratory, University of Liverpool

[Received September 28, 1959]

Abstract

An investigation has been made of the dependence of systematic track distortion in a 10 in. diameter liquid hydrogen bubble chamber upon track position in the chamber, beam entry time and flash delay.

It is seen that provided photography occurs before recompression the distortions are small compared with the multiple scattering curvature, and are not significantly different from zero except at the extreme top and bottom of the chamber.

§ 1. Introduction

The bubble chamber described in the preceding paper has been placed in the pion beam of the Liverpool 156 in. synchrocyclotron, the energy of the beam traversing the chamber being 85 mev.

It is essential that distortions produced in the chamber be small, and it is useful to determine if these can be minimized by letting the beam enter the chamber at one particular instant of the sensitive time.

To detect and measure any such distortions the magnetic field was switched off, and deviations from linearity of the meson tracks were calculated in a manner very similar to that used earlier for a propane bubble chamber (Evans *et al.* 1959).

Three earlier reports of distortion measurements in hydrogen bubble chambers have been published. The first of these (Cresti) deals with the Berkeley 25 cm chamber, which had horizontal windows, and gas-phase expansion through a small diameter expansion line. Systematic general distortions were reported, these being greatest near the expansion line. Maps were plotted showing the distortion at different points in the chamber, and also the variation of curvature with flash delay.

Recently the distortion pattern in the C.E.R.N. 10 cm chamber has been investigated (Budde *et al.* 1959), the technique employed being somewhat different from that used at Liverpool, the statistics being poorer. This chamber is of similar shape to the Liverpool instrument, although of smaller size and with a different system of cooling. The results did show some systematic distortion at certain flash delays, but

† Communicated by Professor H. W. B. Skinner, F.R.S.

these were small compared with the effects of multiple scattering. At the top and bottom of the chamber radii of curvature of both signs and widely differing values were observed. It was thought that these were due to local turbulences in the liquid, which would be of diminished importance in a larger chamber.

A full measurement of distortion in the 72 in. chamber at Berkeley, an instrument of completely different design from any of the above, has not yet been carried out. However, in a preliminary report (Alston 1959) the induced curvatures do not appear to differ significantly from zero.

§ 2. Sources of Distortion

In addition to distortion arising from mass motions of the liquid hydrogen, spurious curvatures will be caused also by defects of the optical system and by multiple coulomb scattering.

Optical distortions arise from defects both of the camera lens and its associated optical system, and the armour plate glass windows on the chamber body and the vacuum tank, the window closest to the camera having the greatest effect.

The average curvature expected from multiple scattering can be calculated (Blackett 1954), being $3{\cdot}34\sqrt{L}$ for pions of momentum 175 Mev/c, where L is the track length in centimetres. This gives a radius of curvature of 13·3 metres for the majority of tracks measured, the extreme values being 14·9 and 11·5 metres for the longest and shortest tracks respectively.

§ 3. Method

Particles entered the chamber at points A, B and C on the pressure–time curve, fig. 1, at each setting the bubble growth time being varied between 1·5 and 5 msecs, although the intermediate values are not considered here.

The chamber took 8 msec to expand. Point A, occurring 4 msec later, being the earliest instant at which sensitivity was attained. Consequently such tracks consisted of widely spaced bubbles and were difficult to observe, accurate measurements being possible only on tracks with a flash delay of 5 msec. Point B occurred 14 msec after the commencement of expansion, the tracks then being of much higher quality, enabling measurements to be made at the 1·5 msec flash delay.

The time at which recompression is applied varies by about one millisecond, and photographs taken at C (21 msec after beginning of the expansion cycle) with a delay of 1·5 msec occurred sometimes before and sometimes after the application of recompression. Photographs taken with long delays occurred always after recompression.

It can be seen from fig. 1 that the pressure slowly falls during the whole of the expanded state. This is due to slight flexibility of the piston back-stop, which prevents overstressing of the drive rod.

Fig. 1

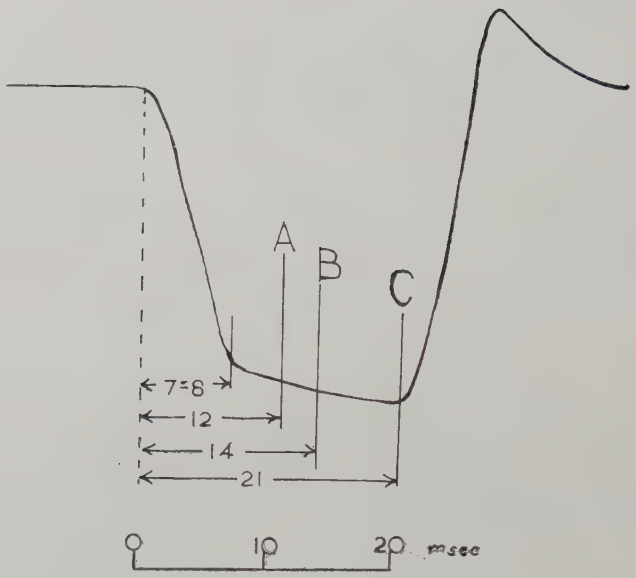

The pressure–time curve for the expansion cycle, showing time of beam entry.

Fig. 2

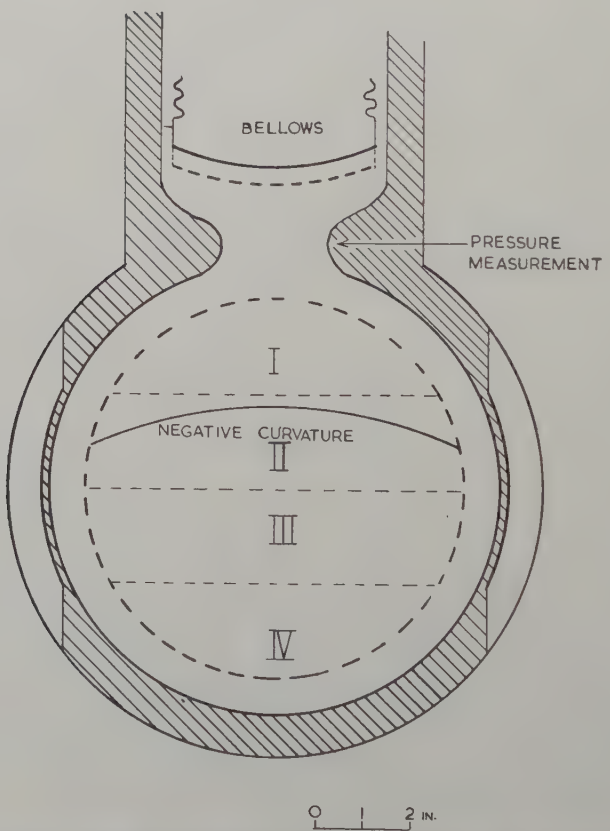

Schematic section through chamber showing division into zones and position of bellows vertically above the illuminated region.

The random effects of multiple scattering may be eliminated statistically by measuring a large number of tracks traversing the same zone of the chamber, leaving only the systematic distortion caused by liquid motions.

Fig. 3

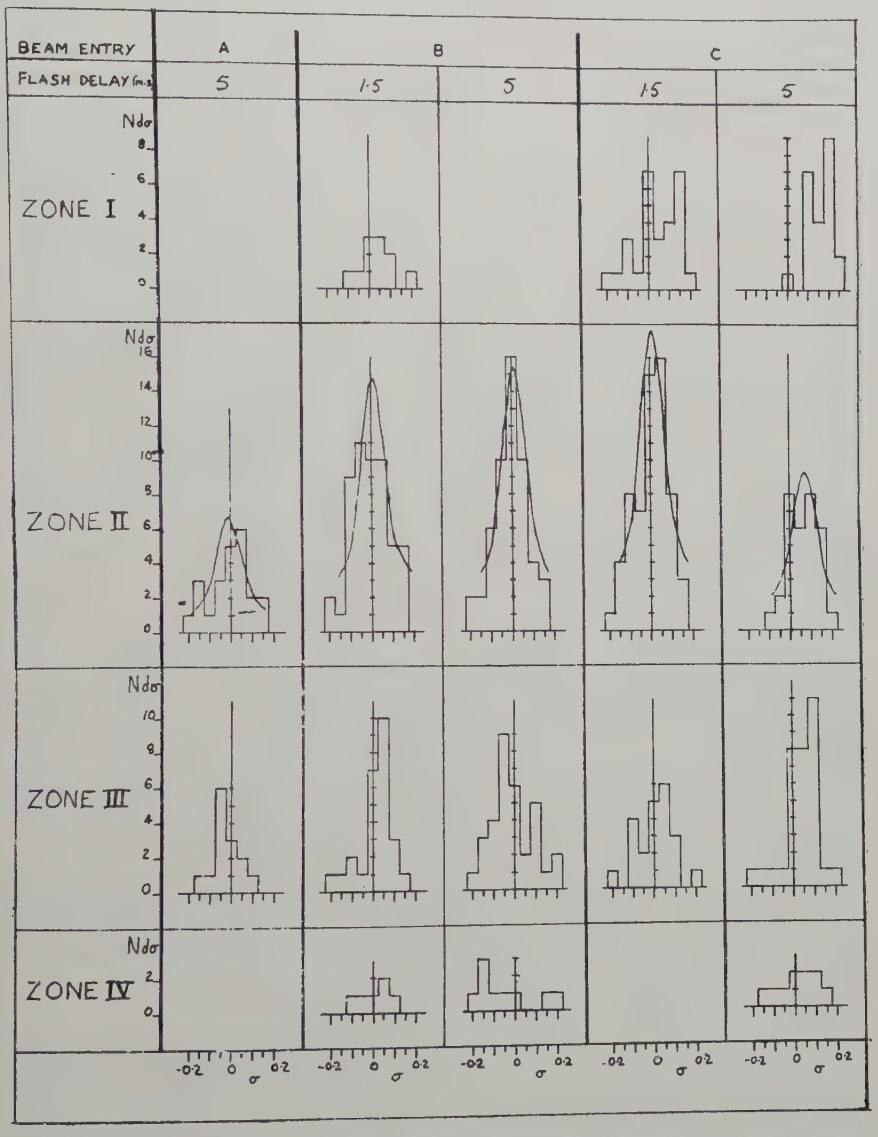

Distribution of systematic curvatures. Ordinate is number of tracks per unit range of curvature. Abscissa (σ) is curvature in reciprocal metres.

The Gaussian distribution plotted in zone II has a half-width given by the multiple scattering, the mean value being that obtained from the individual readings and not from the block histogram.

The illuminated region of the chamber consisted of a circle 20 cm in diameter, which at a magnification of 1/20 gave a circular image approximately 1 cm diameter on the film. For the purpose of the analysis the chamber was divided into four horizontal zones of equal height the majority of tracks passing through the two central zones, with only a very small number within 2 cm of the top or bottom of the illuminated region.

The stereo-camera took two photographs of each expansion, with an angle of 13° between the camera axes. Initially about 60 tracks were measured on both views, the distance of each track from the chamber windows then being calculated. It was found that in all but three of these cases the tracks were at least 1 in. from the windows. Since any variations in distortion across the width of the chamber would be most significant close to the windows it was thus considered sufficiently accurate to assume the distortions to be uniform across the chamber width. Hence the remaining measurements were carried out on only one photograph of each stereo pair. Such a procedure assumed that all the tracks were parallel to the plane of the windows, but it was shown that this assumption introduced a negligible error into the final result, as did the angle of $6\frac{1}{2}°$ between the camera and bubble chamber axes (the camera used in this analysis was an earlier model than that described in the preceding paper).

Only tracks within 10° of the horizontal were measured, readings being spaced 1 mm apart on the film, except for short tracks close to the upper or lower boundaries, where readings were taken every 0·5 mm. The image width was generally 18–20 μ, readings being reproducible to within 2 μ.

Curvatures were calculated by a least squares method, negative curvature implying an upward, and positive a downward, movement of the track centre with respect to the ends. The curvatures for each zone at each expansion condition were then calculated, and are shown plotted in histogram form (fig. 3). Any curvatures (σ) having a value on the film of $|\sigma| > 5{\cdot}5\ \mathrm{m}^{-1}$ were neglected, since it was obvious from the form of the plotted distribution that these were due to single scatters which had not been detected visually.

Optical distortions were measured in the chamber position by suspending a frame carrying a grid of stretched nylon fibres. Measurement of photographs taken with this arrangement gave curvatures which were negligible compared with the errors on the main analysis.

§ 4. Discussion of Results

The results of the analysis are given in the table, and illustrated graphically in fig. 3. From the histograms it can be seen that except possibly in the lowest zone (IV) where there are too few tracks, the half width of the distribution is approximately equal to the curvature arising from multiple scattering. This exception is probably caused by poor statistics, but there may possibly be an increased spread due to local vortices or turbulences in the liquid, which may not be constant from expansion to expansion.

The Variations of Track Curvature

Beam entry	A	B				C			
Flash delay	5 msec	1·5 msec		5 msec		1·5 msec		5 msec	
Zone	Curvature (m^{-1}) / No. of tracks	(N)	(m^{-1})	N	(m^{-1})	N	(m^{-1})	N	(m^{-1}) / N
I		—	0·018	—	−0·031	—	0·046	—	0·148
		—	±0·020	10	±0·047	4	±0·011	28	±0·005 / 21
II	−0·0045	—	0·045	—	−0·0065	—	0·004	—	0·068
	±0·020 / 23	—	±0·013	51	±0·011	53	±0·011	61	±0·006 / 32
III	−0·032	—	0·022	—	−0·008	—	0·009	—	0·042
	±0·017 / 14	—	±0·014	25	±0·017	33	±0·018	20	±0·011 / 33
IV		—	0·011	—	−0·050	—	—	—	0·012
		—	±0·021	6	±0·048	9	—	—	±0·032 / 10

At the earliest setting (A) statistically significant results could be obtained only for the two central zones of the chamber and then only with the 5 msec flash delay. Although the errors are large there is a tendency for the tracks to be slightly affected by the upward movement of the bellows at expansion, i.e. negative curvature. Photographs taken at B with 5 msec delay are not in disagreement with this possibility, although those taken at 1·5 msec delay show a slight tendency towards positive curvature. In all cases the residual curvatures are much smaller than those caused by multiple scattering, and it is not impossible that they are all zero, since the quoted errors are merely those calculated from the statistical spread of the individual points.

Tracks entering the chamber at C do, however, show an entirely different, and consistent, form of distortion. In all cases the curvature is positive, being greatest near the top of the chamber. This is consistent with the rapid downward movement of the bellows at recompression, the curvature being more pronounced at the longer delay times, when photography takes place always after the commencement of this movement. With the delay of 1·5 msec, for which recompression has sometimes not yet begun, the curvatures are still not significantly different from zero in the central zones of the chamber, and it is only close to the bellows cavity that distortion becomes appreciable. It is interesting to note that in the Saclay propane bubble chamber the particle beam enters always after the application of recompression (Bloch 1959). Distortion measurements in this chamber have not, however, yet been published.

It is seen that provided photography occurs always before the commencement of recompression the systematic distortions introduced by liquid movement are small compared with the effects of multiple scattering.

For work at high energies it would be essential to repeat the above measurements in a high energy proton beam, multiple scattering then being reduced, so that the final accuracy of the result would depend largely upon the accuracy of measurement.

Acknowledgments

We wish to thank all those associated in operating the bubble chamber, the cyclotron crew for provision of beam facilities and R. Martin and S. Austin for maintaining a supply of liquid hydrogen. Miss M. Stynes assisted in the work of track measurement. D. C. C. and J. R. S. wish to thank D.S.I.R. for the receipt of research grants.

References

Alston, M. H., 1959, U.C.R.L. Eng. Note 4313–03/M26.

Blackett, P. M. S., 1954, *Nuovo Cim. Sup.* **2**, 264.

Bloch, M., C.E.R.N. 59–24 Pg. 15.

Budde, R., Burger, A., Filthuth, H., Goldschmidt-Clermont, Y., Mayer, H. M., Morrison, D. R. O., Peyrou, C., and Trembley, J., 1959, *Nuovo Cim.*, **14**, 778.

Cresti, M., U.C.R.L. Eng. Note 4312–07/M37.1.

Evans, W. H., Hadley, D. W., Morgan, T. D. N., Williams, P. R., and Kirk, A., 1959, *J. sci. Instrum.*, **36**, 365.

The Angular Dislocation†

By Elizabeth H. Yoffe
Cavendish Laboratory, Cambridge

[Received September 22, 1959]

Abstract

The stress field of a sharply angular dislocation is calculated by Burgers' method. It is shown that more complicated configurations may be composed of angular dislocations, and the corresponding stress fields deduced by adding the fields of the components. Some examples are given, including the triangle, hexagon and tetrahedron.

§ 1. Introduction

Recent theories of work hardening depend on the elastic interaction of many dislocations. These may lie in different planes and interact with one another to form a complicated three-dimensional network of dislocation lines.

Since the equations of elasticity are linear it is possible to find the stress field due to each small part of the network, and add the results to find that of the whole. It might be thought that a straight line segment of the network would be a suitable element to consider, and this would be true if the field of such an element could be calculated. Unfortunately this is not so, since a dislocation cannot begin nor end in the interior of a perfect elastic medium, although some approximative theories have been based on the assumption that the field is similar to that of an infinite straight dislocation.

A more suitable element is the closed circuit of dislocation line, finite in extent and polygonal in shape, with a constant Burgers vector. It is found that the general network can be built up of such elements combined, where necessary, with infinite straight dislocations.

The stress field of a polygonal dislocation may be derived from the formulae of J. M. Burgers (1939) by integrating certain functions over a surface bounded by the polygon. In order to show the significance of the various terms a simple angular dislocation is considered first; that is, a dislocation composed of two semi-infinite straight arms meeting at the origin.

The stress field of the angular dislocation is derived in § 2, the triangle and hexagon are solved in detail in § 3 and § 4 and other applications are discussed in § 5.

† Communicated by the Author.

§ 2. The Elastic Field of the Angular Dislocation

Burgers (1939) has derived the displacements for a dislocation of arbitrary shape. His method is followed here for a dislocation line ζOZ as shown in fig. 1. The x axis is taken normal to the paper and cartesian coordinates (x, y, z) or (x, η, ζ) are used, where

$$\eta = y\cos\alpha - z\sin\alpha,$$

$$\zeta = y\sin\alpha + z\cos\alpha.$$

Also:

$$r^2 = x^2 + y^2 + z^2 = x^2 + \eta^2 + \zeta^2.$$

Fig. 1

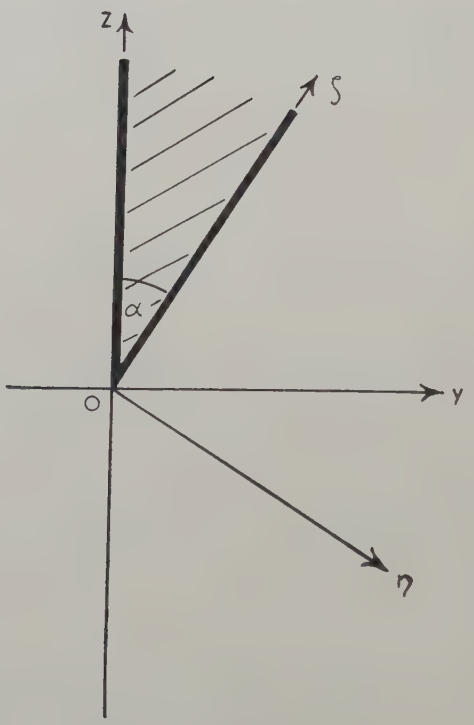

The multivalued terms in the displacements come from Burgers' function ϕ, which in this case must have a surface of discontinuity bounded by the positive z and ζ axes. In particular the surface may be the plane region shown shaded in fig. 1 and extending to infinity. At any point $P(x, y, z)$ the function ϕ has a value proportional to the solid angle subtended at P by this shaded area:

$$\phi = \frac{1}{4\pi}\int\int \frac{x}{R^3}\,dy'\,dz'$$

$$= \frac{1}{4\pi}\left(\tan^{-1}\frac{y}{x} - \tan^{-1}\frac{\eta}{x} + \tan^{-1}\frac{xr\sin\alpha}{x^2\cos\alpha + y\eta}\right) \quad . \; . \; . \quad (1)$$

where $$R^2 = x^2 + (y-y')^2 + (z-z')^2.$$

The term $\tan^{-1} y/x$ corresponds to an infinite straight dislocation along the entire z axis, and the term $\tan^{-1} \eta/x$ to one on the ζ axis. The last term on the right-hand side corresponds to a junction of dislocations, as shown in fig. 2, since it is equal to half the solid angle subtended by the shaded areas in that figure. On adding these terms it is found that ϕ remains single valued on circling the negative z and ζ axes, but increases by unity when its circuit passes once into the paper between the positive axes.

Fig. 2

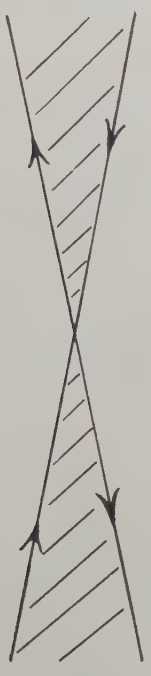

If the Burgers vector of the angular dislocation is b in the direction of x, the other terms used by Burgers are:

$$u^{**} = 0,$$

$$v^{**} = \frac{b}{4\pi}(\cos\alpha \log(r-\zeta) - \log(r-z)),$$

$$\omega^{**} = -\frac{b}{4\pi}\sin\alpha \log(r-\zeta),$$

$$\psi = \frac{b}{8\pi(1-\sigma)}(y\log(r-z) - \eta\log(r-\zeta))$$

where σ is Poisson's ratio. The complete displacements are:

$$u = b\phi + \frac{b}{8\pi(1-\sigma)}\left(\frac{xy}{r(r-z)} - \frac{x\eta}{r(r-\zeta)}\right),$$

$$v = \frac{b}{8\pi(1-\sigma)}\left(\frac{\eta \sin\alpha}{r-\zeta} - \frac{y\eta}{r(r-\zeta)} + \frac{y^2}{r(r-z)} + (1-2\sigma)(\cos\alpha \log(r-\zeta) - \log(r-z))\right),$$

$$\omega = \frac{b}{8\pi(1-\sigma)}\left(\frac{\eta\cos\alpha}{r-\zeta} - \frac{y}{r} - \frac{\eta z}{r(r-\zeta)} + (1-2\sigma)\sin\alpha \log(r-\zeta)\right). \quad (2)$$

From these expressions the components of strain and stress may be calculated in the usual way. The derivatives of the function ϕ reduce to simple forms:

$$\frac{\partial\phi}{\partial x} = \frac{1}{4\pi}\left(\frac{\eta}{r(r-\zeta)} - \frac{y}{r(r-z)}\right),$$

$$\frac{\partial\phi}{\partial y} = \frac{1}{4\pi}\left(\frac{x}{r(r-z)} - \frac{x\cos\alpha}{r(r-\zeta)}\right),$$

$$\frac{\partial\phi}{\partial z} = \frac{1}{4\pi}\frac{x\sin\alpha}{r(r-\zeta)},$$

so that the stress components are easily calculated. They consist of sums of elementary functions, and singularities on the positive z and ζ axes only. For example

$$\widehat{xx} = \frac{\mu b}{4\pi(1-\sigma)}\left(\frac{\eta}{r(r-\zeta)} - \frac{y}{r(r-z)} - \frac{x^2 y}{r^3(r-z)} - \frac{x^2 y}{r^2(r-z)^2} + \frac{x^2\eta}{r^3(r-\zeta)} + \frac{x^2\eta}{r^2(r-\zeta)^2}\right),$$

$$\widehat{xz} = \frac{\mu b x}{4\pi(1-\sigma)}\left(\frac{y}{r^3} + \frac{\sin\alpha}{r(r-\zeta)} - \frac{\eta\cos\alpha}{r(r-\zeta)^2} + \frac{\eta z}{r^3(r-\zeta)} + \frac{\eta z}{r^2(r-\zeta)^2}\right), \quad (3)$$

$$\widehat{zz} = \frac{\mu b}{4\pi(1-\sigma)}\left(\frac{yz}{r^3} - \frac{\eta}{r(r-\zeta)} + \frac{\eta z^2}{r^3(r-\zeta)} + \frac{\eta z^2}{r^2(r-\zeta)^2} - \frac{2\eta z\cos\alpha}{r(r-\zeta)^2} + \frac{\eta\cos^2\alpha}{(r-\zeta)^2} + 2\sigma\left[\frac{y\cos\alpha}{r(r-\zeta)} - \frac{\sin\alpha\cos\alpha}{r-\zeta} - \frac{y}{r(r-z)}\right]\right).$$

If the angular dislocation has Burgers vector b in the y direction the corresponding functions are:

$$u^* = 0 = \omega^* = v^{**} = w^{**},$$

$$v^* = b\phi,$$

$$u^{**} = \frac{b}{4\pi}(\log(r-z) - \cos\alpha \log(r-\zeta)),$$

$$\psi = \frac{bx}{8\pi(1-\sigma)}(\cos\alpha \log(r-\zeta) - \log(r-z)).$$

The stress components are again readily calculated from the complete displacements:

$$\left.\begin{aligned} u &= \frac{b}{8\pi(1-\sigma)}\left(\frac{x^2\cos\alpha}{r(r-\zeta)} - \frac{x^2}{r(r-z)} - (1-2\sigma)(\cos\alpha\log(r-\zeta) - \log(r-z))\right), \\ v &= b\phi + \frac{bx}{8\pi(1-\sigma)}\left(\frac{y\cos\alpha}{r(r-\zeta)} - \frac{\sin\alpha\cos\alpha}{r-\zeta} - \frac{y}{r(r-z)}\right), \\ w &= \frac{bx}{8\pi(1-\sigma)}\left(\frac{z\cos\alpha}{r(r-\zeta)} - \frac{\cos^2\alpha}{r-\zeta} + \frac{1}{r}\right). \end{aligned}\right\} \quad . \; . \; . \quad (4)$$

Similarly if the Burgers vector is in the z direction the following expressions are obtained:

$$\left.\begin{aligned} u^{**} &= \frac{b\sin\alpha}{4\pi}\log(r-\zeta) = -\frac{2(1-\sigma)\psi}{x}, \\ u &= \frac{b\sin\alpha}{8\pi(1-\sigma)}\left((1-2\sigma)\log(r-\zeta) - \frac{x^2}{r(r-\zeta)}\right), \\ v &= \frac{bx\sin\alpha}{8\pi(1-\sigma)}\left(\frac{\sin\alpha}{r-\zeta} - \frac{y}{r(r-\zeta)}\right), \\ w &= b\phi + \frac{bx\sin\alpha}{8\pi(1-\sigma)}\left(\frac{\cos\alpha}{r-\zeta} - \frac{z}{r(r-\zeta)}\right). \end{aligned}\right\} \quad . \; . \; . \quad (5)$$

The stress field of an angular dislocation of arbitrary Burgers vector is fully described by its components from eqns. (3), (4) and (5) in suitable proportion. A constant term may be added to ϕ or to any displacement without affecting the stress field.

§ 3. The Triangle

A triangular dislocation of constant Burgers vector is readily composed of three angular dislocations. These form exterior angles to the triangle, as indicated by shading in fig. 3, with the infinite segments cancelling one another.

As a particular case consider the dislocation in the form of an equilateral triangle with Burgers vector normal to its plane, in the sense that u increases by b on circling the line so as to emerge upwards from the paper inside the triangle.

Let the vertices A, B and C have coordinates $(0, 0, h)$, $(0, -\sqrt{3}h/2, -h/2)$ and $(0, \sqrt{3}h/2, -h/2)$ respectively and let

$$\eta_1 = -z - \frac{h}{2}, \qquad \zeta_1 = y,$$

$$\eta_2 = \frac{\sqrt{3}y + z - h}{2}, \qquad \zeta_2 = -\frac{(y - \sqrt{3}z)}{2},$$

$$\eta_3 = -\frac{(\sqrt{3}y - z + h)}{2}, \qquad \zeta_3 = -\frac{(y + \sqrt{3}z)}{2}.$$

Then the function ϕ of the angular dislocation at A is given by

$$\phi_A = \frac{1}{4\pi}\left[\tan^{-1}\frac{\eta_3}{x} - \tan^{-1}\frac{\eta_2}{x} + \tan^{-1}\left(\frac{\sqrt{3}xr_A}{2\eta_2\eta_3 - x^2}\right)\right]$$

where

$$r_A{}^2 = x^2 + y^2 + (z-h)^2.$$

Fig. 3

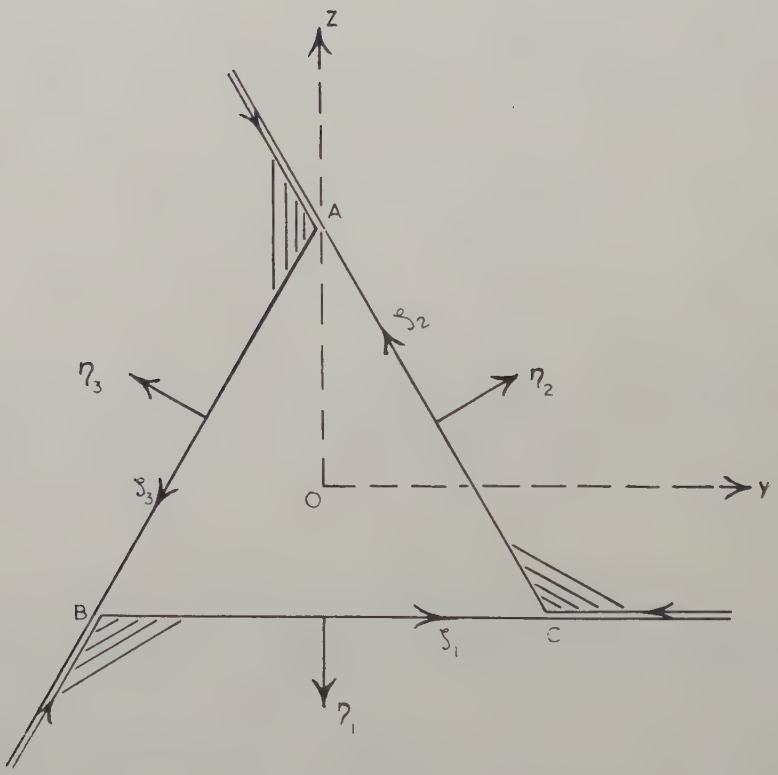

On adding similar expressions for the angular dislocations at B and C, the following function is obtained for the whole triangle:

$$\phi = \phi_A + \phi_B + \phi_C$$
$$= \frac{1}{4\pi}\left[\tan^{-1}\frac{\sqrt{3}xr_A}{2\eta_2\eta_3 - x^2} + \tan^{-1}\frac{\sqrt{3}xr_B}{2\eta_3\eta_1 - x^2} + \tan^{-1}\frac{\sqrt{3}xr_C}{2\eta_1\eta_2 - x^2}\right].$$

The same result may be obtained directly by integration over the triangle, or by composing the triangle of three dislocation junctions at the vertices. It is a matter of taste whether junctions or angular dislocations are used as the primitive component of a network.

Using the results derived for angular dislocations, the normal displacement for the triangle is given by:

$$u = b\phi + \frac{bx}{8\pi(1-\sigma)}\left(\frac{\eta_3}{r_A(r_A - {}_A\zeta_3)} - \frac{\eta_2}{r_A(r_A - {}_A\zeta_2)} + \frac{\eta_1}{r_B(r_B - {}_B\zeta_1)}\right.$$
$$\left. - \frac{\eta_3}{r_B(r_B - {}_B\zeta_3)} + \frac{\eta_2}{r_C(r_C - {}_C\zeta_2)} - \frac{\eta_1}{r_C(r_C - {}_C\zeta_1)}\right)$$

where the prefix indicates the origin of the coordinate in each case,

$${}_A\zeta_2 = \zeta_2 - \sqrt{3}h/2,$$
$${}_B\zeta_1 = \zeta_1 + \sqrt{3}h/2, \quad \text{etc.}$$

The other displacements may be written down in a similar manner, but to save space will not be given here. The stress components may then be calculated as required.

From eqns. (3) it is seen that the normal stress $\widehat{xx}$ on the plane $x=0$ reduces to the simple form:

$$\widehat{xx} = \frac{\mu b}{4\pi(1-\sigma)}\left(\frac{\eta_2}{r_A(r_A - {}_A\zeta_2)} - \frac{\eta_3}{r_A(r_A - {}_A\zeta_3)} + \frac{\eta_3}{r_B(r_B - {}_B\zeta_3)}\right.$$
$$\left. - \frac{\eta_1}{r_B(r_B - {}_B\zeta_1)} + \frac{\eta_1}{r_C(r_C - {}_C\zeta_1)} - \frac{\eta_2}{r_C(r_C - {}_C\zeta_2)}\right).$$

The calculation of the elastic strain energy is therefore a simple matter in this case. If the triangle is situated in an infinite elastic body unstressed at infinity, the strain energy may be expressed as the work done against the normal stress on increasing the relative displacement from 0 to b over the surface of the triangle. That is, if the normal stress is given by

$$\widehat{xx} = bX \text{ on } x=0,$$

then

$$E = \tfrac{1}{2}b^2 \int\int X\, dy\, dz.$$

The integral is to be evaluated over the interior of the triangle, and may be reduced to the form

$$E = \frac{3\mu b^2}{4\pi(1-\sigma)} \int_0^{3h/2} dy \int_{y/\sqrt{3}}^{\sqrt{3}h - y/\sqrt{3}} \frac{z}{y\sqrt{(y^2+z^2)}}\, dz$$
$$= \frac{3\mu b^2}{4\pi(1-\sigma)} \cdot \sqrt{3}h(\log 2/\sqrt{3} - 1 + \log h/\delta)$$
$$= \frac{C\mu b^2}{4\pi(1-\sigma)} \log \frac{0{\cdot}85R}{\delta} \qquad \ldots\ldots\ldots\ldots \quad (6)$$

where C is the circumference of the triangle, R the radius of the inscribed circle and δ the core radius (of the order of b).

Corresponding results are readily obtained for Burgers vectors in other directions.

§ 4. The Hexagon

Six angular dislocations of angle $\pi/3$ and the same Burgers vector may be arranged to form a finite hexagonal dislocation in the plane $x=0$, with all the infinite segments cancelling, as shown in fig. 4.

The stress components may be calculated by adding the stresses due to the six angular dislocations, changing the origin of coordinates in each case and taking care to choose the correct Burgers vector. For instance if the Burgers vector is in the direction y at all points of the hexagon, then the stresses due to the angular dislocations at O and C are derived from eqns. (4) only, while those from A, B, D and E will include terms from both (4) and (5). The resulting expressions are long, and will not be given here, but the strain energy will be calculated for two cases of practical interest.

Fig. 4

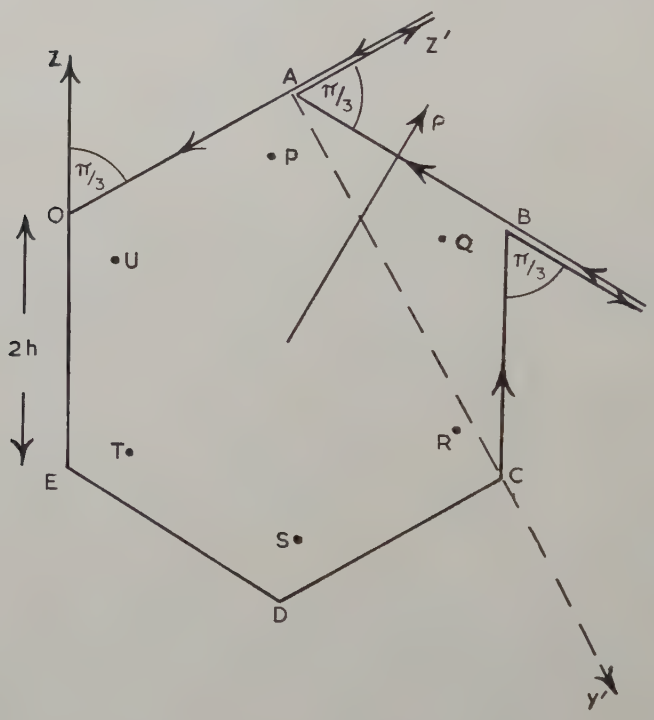

4.1. *Burgers Vector b_1 Normal to the Hexagon*

The strain energy in this case is equal to the work done against the normal stress $\widehat{xx}$ on the plane $x=0$ in forming the dislocation. From eqns. (3) this may be written

$$E=\frac{3\mu b_1^2}{4\pi(1-\sigma)}\int\int\left(\frac{\eta}{r(r-\zeta)}-\frac{y}{r(r-z)}\right)dy\,dz \quad . \quad . \quad (7)$$

where the factor $b_1^2/2$, obtained on integrating from 0 to b_1, has been multiplied by six for the six angular dislocations. The integral is to be taken over the interior of the hexagon, and readily simplifies to the form:

$$E = \frac{-3\mu b_1^2}{4\pi(1-\sigma)}\left\{\int_0^{\sqrt{3}h}\left[\frac{2\sqrt{(y^2+z^2)}}{y}\right]_{-2h-y/\sqrt{3}}^{y/\sqrt{3}} dy + \int_{\sqrt{3}h}^{2\sqrt{3}h}\left[\frac{2\sqrt{(y^2+z^2)}}{y}\right]_{-4h+y/\sqrt{3}}^{2h-y/\sqrt{3}} dy\right\}$$
$$= \frac{3\mu b_1^2}{4\pi(1-\sigma)} 4h(\log\sqrt{3}h/\delta + 1 - \sqrt{3} + 2\log 2(2+\sqrt{3})/3\sqrt{3})$$

where $2h$ is the length of a side of the hexagon, and δ is the core radius (of the order of b_1). This energy may also be written

$$E = \frac{C\mu b_1^2}{4\pi(1-\sigma)}\log\frac{0{\cdot}99R}{\delta}, \qquad \ldots\ldots\ldots \quad (8)$$

where C is the circumference of the hexagon and R the radius of the inscribed circle.

4.2. *Burgers Vector b_2 at an Angle to the Plane of the Hexagon*

Let the vector $\mathbf{b}_2$ have components

$$\left.\begin{aligned} b_x &= \sqrt{2}b_2/\sqrt{3}, \\ b_y &= b_2/2\sqrt{3}, \\ b_z &= b_2/2, \end{aligned}\right\} \qquad \ldots\ldots\ldots \quad (9)$$

in the directions of the x, y, z axes respectively. This corresponds to the case of a face centred cubic metal with the Burgers vector $\frac{1}{2}$ [110] not in the (111) plane of the hexagon, and the sides of the hexagon lying along [110] type directions in this plane. In calculating the strain energy in this case there are contributions from the stress component $\widehat{x\rho}$ as well as $\widehat{xx}$, where ρ lies along the projection of the Burgers vector in the y, z plane (see fig. 4).

An angular dislocation of Burgers vector b_x only has zero shear stresses $\widehat{xy}$, $\widehat{xz}$ in the plane $x=0$, while b_y and b_z give zero $\widehat{xx}$ on that plane. For this reason the terms in the strain energy separate and it may be written in the form

$$E = \frac{3\mu b_x^2}{4\pi(1-\sigma)}\int\int\left(\frac{\eta}{r(r-\zeta)} - \frac{y}{r(r-z)}\right)dy\,dz + \int\int\left\{\int_0^{b/\sqrt{3}}\sum\widehat{x\rho}\,db_\rho\right\}dy\,dz \qquad \ldots\ldots \quad (10)$$

where $\sum\widehat{x\rho}$ indicates the sum of six terms from the six angular dislocations. The first term of (10) is similar to eqn. (7) with b_1 replaced by $b_x = \sqrt{2}b_2/\sqrt{3}$ and therefore its value is readily obtained from (8).

To evaluate the second term of (9) consider the shear stresses across the (yz) plane at some arbitrary point P inside the hexagon due to the angular dislocation at O. The shear stresses $\widehat{xy}$, $\widehat{xz}$ may be written in the form

$$\left.\begin{aligned} \widehat{xy} &= b_y Y_2 + b_z Y_3, \\ \widehat{xz} &= b_y Z_2 + b_z Z_3 \end{aligned}\right\} \qquad \ldots\ldots\ldots \quad (11)$$

where Y_2 and Z_2 are derived from eqns. (4) and Y_3, Z_3 from (5). Resolving in the direction of ρ

$$\begin{aligned}\widehat{x\rho}_0 &= \widehat{xy}/2 + \widehat{xz}\sqrt{3}/2 \\ &= b_2(Y_2/4\sqrt{3} + Y_3/4 + Z_2/4 + \sqrt{3}Z_3/4). \quad . \; . \; . \quad (12)\end{aligned}$$

By symmetry it is found that the stresses at a corresponding point S due to the angular dislocation at C are equal to those at P due to the dislocation at O:

$$\widehat{x\rho}_C(\text{at point S}) = \widehat{x\rho}_0 \text{ (at point P)}. \quad . \; . \; . \; . \quad (13)$$

For the angular dislocation at A take new axes y', z' as indicated and consider the stresses at a point Q corresponding to P and S. Then

$$\begin{aligned}\widehat{xy}' &= -b_2 Y_2/2\sqrt{3} + b_2 Y_3/2, \\ \widehat{xz}' &= -b_2 Z_2/2\sqrt{3} + b_2 Z_3/2,\end{aligned}$$

and the shear stress $x\rho$ at Q is given by

$$\begin{aligned}\widehat{x\rho}_A &= -\widehat{xy}'/2 + \sqrt{3}\widehat{xz}'/2 \\ &= b_2(Y_2/4\sqrt{3} - Y_3/4 - Z_2/4 + \sqrt{3}Z_3/4). \quad . \; . \; . \quad (14)\end{aligned}$$

The dislocation at D is found to contribute the same value of $\widehat{x\rho}$ at the corresponding point T.

Finally the angular dislocations at B and E each contribute the shear stress

$$\widehat{x\rho}_B = b_2 Y_2/\sqrt{3} \quad . \; . \; . \; . \; . \; . \; . \; . \quad (15)$$

at the corresponding points R and U respectively.

On changing the order of integration in the second term of (10) it becomes possible to sum the terms of $\widehat{x\rho}$ from (12), (14) and (15). It is found that Y_3 and Z_2 disappear and the integral simplifies:

$$\begin{aligned}\int_0^{b_2/\sqrt{3}} \left\{ \iint \widehat{x\rho}\, dy\, dz \right\} db &= \int_0^{b_2/\sqrt{3}} \left\{ \iint \sqrt{3} b (Y_2 + Z_3)\, dy\, dz \right\} db \\ &= \frac{{b_2}^2}{2} \iint (Y_2 + Z_3)\, dy\, dz \\ &= \frac{(2-\sigma)\mu {b_2}^2}{8\pi(1-\sigma)} \iint \left(\frac{\eta}{r(r-\zeta)} - \frac{y}{r(r-z)} \right) dy\, dz. \\ & \qquad . \; . \; . \quad (16)\end{aligned}$$

Substituing this in eqn. (10) and comparing with (8), the strain energy of the hexagonal dislocation with $\mathbf{b}_2$ in a [110] direction is given by

$$E = (1 - \sigma/6) \frac{C\mu {b_2}^2}{4\pi(1-\sigma)} \log \frac{0{\cdot}99R}{\delta} \quad . \; . \; . \; . \; . \quad (17)$$

where C is the circumference of the hexagon and R the radius of the inscribed circle.

§ 5. Other Applications

The angular dislocation may be used as a unit in constructing other figures of practical interest.

5.1. *Kinked Dislocation*

A simple example is the kinked dislocation shown in fig. 5, such as may arise from cross slip or prismatic slip. It may be formed by the superposition of one straight and two angular dislocations, in either of the two ways indicated in the figure.

Fig. 5

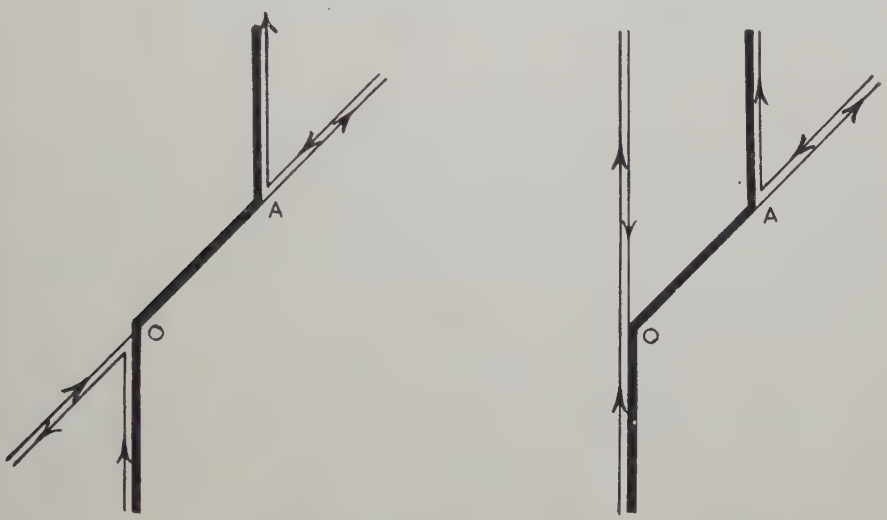

The displacements due to each angular dislocation are obtained from eqns. (2), (4) and (5) according to the Burgers vector. For example if $b_z = b$ so that the infinite segments are pure screw dislocations, and if A is the point $(0, Y, Z)$ so that $Y/Z = \tan\alpha$, the displacements have the form

$$u = \frac{b\sin\alpha}{8\pi(1-\sigma)}\left(\frac{x^2}{r(r-\zeta)} - \frac{x^2}{r_A(r_A-\zeta_A)} + (1-2\sigma)\log\frac{r_A-\zeta_A}{r-\zeta}\right),$$

$$v = \frac{b\sin\alpha x}{8\pi(1-\sigma)}\left(\frac{y}{r(r-\zeta)} - \frac{y-Y}{r_A(r_A-\zeta_A)} - \frac{\sin\alpha}{r-\zeta} + \frac{\sin\alpha}{r_A-\zeta_A}\right),$$

$$w = b(\phi-\phi_A) + \frac{bx\sin\alpha}{8\pi(1-\sigma)}\left(\frac{z}{r(r-\zeta)} - \frac{z-Z}{r_A(r_A-\zeta_A)} - \frac{\cos\alpha}{r-\zeta} + \frac{\cos\alpha}{r_A-\zeta_A}\right)$$

where ϕ is given by eqn. (1), ϕ_A is the corresponding expression referred to the point A, and

$$r_A^2 = x^2 + (y-Y)^2 + (z-Z)^2,$$

$$\zeta_A = \zeta - Y\sin\alpha - Z\cos\alpha.$$

It may be of interest to examine the stress components in the case where the distance OA is small, to see by how much they differ from the stresses of a straight screw dislocation. For instance the component $\widehat{zz}$ is zero for the straight dislocation, but here it has the value

$$\widehat{zz} = \frac{\mu b x \sin\alpha}{4\pi(1-\sigma)}\left(\frac{1}{r_A(r_A-\zeta_A)} + \frac{\cos^2\alpha}{(r_A-\zeta_A)^2} - \frac{1}{r(r-\zeta)} - \frac{\cos^2\alpha}{(r-\zeta)^2}\right).$$

At points on a line normal to the paper midway between O and A this reduces to

$$\widehat{zz} = -\frac{\mu b \sin\alpha}{2\pi(1-\sigma)}\left(\frac{\zeta}{rx} + \frac{\zeta r}{x^3}\right)$$

showing that there is noticeable tension and compression on opposite sides of the kink at points adjacent to it.

5.2. *Plane Polygons*

It was shown in § 3 and § 4 that a finite dislocation in the form of a triangle or hexagon may be built up of angular dislocations. The same is true of an arbitrary plane polygon, which may be obtained by varying the magnitude of the angles as shown in fig. 6. The case of the square has been worked out in detail, but will not be described here for reasons of space. The strain energy however may be compared with that of the triangle or hexagon:

$$E = \frac{C\mu b^2}{4\pi(1-\sigma)}\log\frac{0{\cdot}92R}{\delta} \quad . \quad . \quad . \quad . \quad . \quad . \quad (18)$$

where C is the circumference of the square and R the radius of the inscribed circle.

5.3. *Non-planar Figures*

Angular dislocations may also be used to determine the stress field near a junction of three dislocation lines, not necessarily coplanar, and of arbitrary Burgers vectors $\mathbf{b}_1$, $\mathbf{b}_2$, $\mathbf{b}_3$. It is only necessary to rotate one angular dislocation about the z axis through a suitable angle, and then assemble the components as indicated in fig. 7. Here one of the side arms is supposed inclined to the plane of the paper. The three vertical segments cancel one another since the vector $\mathbf{b}_1 - \mathbf{b}_2 - \mathbf{b}_3$ must be zero.

In this manner a three dimensional network of dislocations may be built up of angular dislocations, although the labour of calculation of stress components increases steeply with the number of nodes. In certain cases however the problem simplifies to that of an assembly of plane figures each of constant Burgers vector. One example is the tetrahedron recently observed in quenched gold (Silcox and Hirsch 1959).

5.4. *The Tetrahedron*

This configuration may be composed of four equal triangular dislocations each of Burgers vector b_4 normal to its plane. The stress field is simply that obtained by adding the fields of the separate triangles as calculated in § 3.

Fig. 6

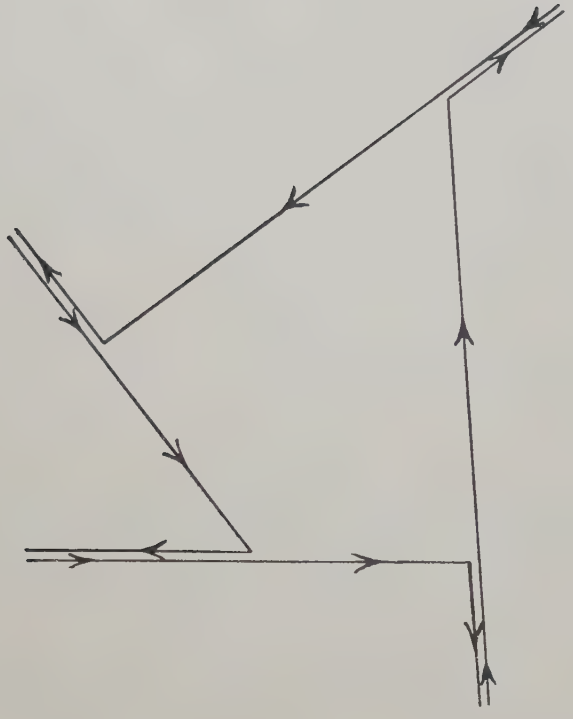

Fig. 7

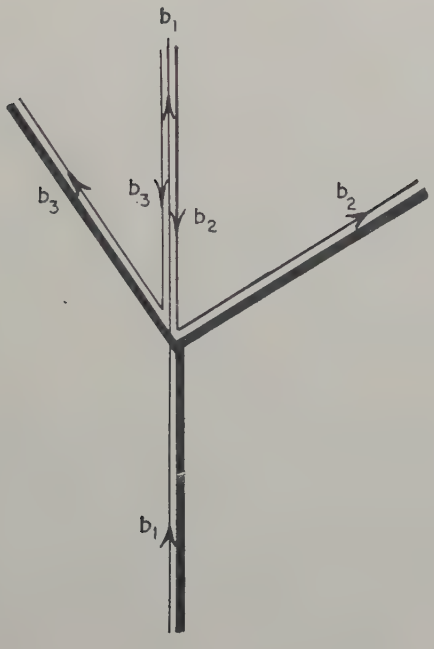

The strain energy of this tetrahedron may also be calculated. It is composed of four times the self energy of one triangle as calculated in § 3, together with twelve times the work done in forming one triangle against the normal stress due to any other triangle. That is

$$E = 4\left(\tfrac{1}{2}b_4 \int\int \widehat{xx}\, dy\, dz\right) + 12\left(\tfrac{1}{2}b_4 \int\int \widehat{nn}\, dS\right)$$

where S is the area of a side face of outward normal n, the base triangle being that of inward normal x. The calculation of the second integral is greatly simplified by the use of Stokes' theorem and the symmetry of the problem, whereby terms of the form

$$\int\int \frac{\partial \phi}{\partial n}\, dS$$

where ϕ is harmonic, may be replaced by

$$\frac{1}{3}\int\int \frac{\partial \phi}{\partial x}\, dy\, dz.$$

The second integral of the strain energy finally yields one term equal to a third of the first integral and also a term independent of the core radius δ. Using the same notation as for the triangle the strain energy of the tetrahedron is given by:

$$E = \frac{C\mu b_4}{4\pi(1-\sigma)}\left(\frac{16}{3}\log\frac{0{\cdot}85R}{\delta} - (1-2\sigma)\,3{\cdot}6\right) \quad . \quad . \quad (19)$$

where C is the circumference of a triangle, and R the radius of its inscribed circle.

According to Silcox and Hirsch (1959) such a tetrahedron can be formed in quenched Au by dissociation of a triangular Frank sessile dislocation (Burgers vector type $\frac{1}{3}[111]$). The tetrahedron consists of stair-rod edge dislocations (Burgers vector type $\frac{1}{6}$ [110]) along the [110] edges of the tetrahedron bounding the stacking faults on the (111) faces. An approximate calculation by Silcox and Hirsch indicates that this dissociation reduces the dislocation energy to one-third of that of the triangular configuration. The calculation in the present paper is based on the fact that the tetrahedron can also be considered as consisting of four triangles whose Burgers vector is one quarter that of a Frank sessile dislocation, and also normal to the plane of the triangle. The stair-rod dislocations are then formed by reactions of the type

$$\tfrac{1}{12}[111] + \tfrac{1}{12}[11\bar{1}] = \tfrac{1}{6}[110];$$

thus, to compare the energies of the triangle and tetrahedron we put $b_4 = \frac{1}{4}b$, where b is the Burgers vector of the Frank sessile dislocation. Comparing eqns. (6) and (9) it is clear that the energy of the term involving the logarithm is reduced to one-third its previous value, in agreement with the result of the simple calculation, but that there is a further reduction in energy which depends on R only through C.

§ 6. Conclusion

In order to simplify the calculation of the stress field due to two or three dimensional networks of dislocations, Burgers' method has been used to derive formulae appropriate to an elementary component of such networks. It has been shown that any network of dislocations consisting of straight line segments may be built up of such components, so that the calculation of the stress field is tedious rather than difficult.

A network of curved segments requires further investigation, as does the extension to anisotropic media.

Acknowledgments

The author wishes to thank Dr. P. B. Hirsch for very helpful discussions, advice and encouragement, Dr. J. D. Eshelby for reading the manuscript and the Atomic Energy Research Establishment, Harwell, for a grant.

References

Burgers, J. M., 1939, *Proc. Acad. Sci., Amst.*, **42**, 293.
Silcox, J., and Hirsch, P. B., 1959, *Phil. Mag.*, **4**, 72.

The Kinetics of the Growth of Precipitates from Solid Solutions†

By J. Burke
Department of Metallurgy, University of Liverpool

[Received October 2, 1959]

Abstract

Equations are derived for the rate of precipitation from an initially homogeneous solid solution on the assumptions that the process involves growth of existing nuclei and that the rate of growth is controlled by diffusion. Various forms of precipitate are considered. Impingement of the zones of the parent solution depleted in solute is allowed for by multiplying the diffusion potential by $(1-y)$ where y is the fraction of the total precipitation which has occurred. The results are appreciably different from the equations currently used to analyse kinetic data.

§ 1. Introduction

Theoretical treatments of the kinetics of the growth of precipitates from supersaturated solid solutions have been given by a number of authors—see the review by Hardy and Heal (1954). The results can usually be reduced to the general form

$$y = 1 - \exp -(t/k)^n \quad . \quad . \quad . \quad . \quad . \quad . \quad . \quad (1)$$

where y is the fraction precipitated at the time t, k is the time constant, the value of which is determined by the parameters of the system considered and n is a constant. In deriving equations of this type the procedure has been to calculate the rate of growth of one particle of the new phase as a function of time, sum over all the particles present in unit volume of the solid solution and then allow for the reduction in reaction rate consequent upon the impingement of the zones of the parent phase depleted of solute. Following Johnson and Mehl (1939), the impingement allowance usually has consisted of multiplying the overall rate of reaction by $(1-y)$. If, as is frequently the case, the growth of the new phase is determined by the rate of diffusion of the solute in the matrix, impingement will modify the diffusion potential and hence the rate of growth. Thus it would appear more satisfactory to include the impingement factor in the growth equation for each particle. Doremus (1957) employed this procedure for a limited number of precipitate shapes and his results indicate that the rate equations so derived are sufficiently different from those obtained by the former method as to completely alter the interpretation of experimental results. This has prompted a re-derivation of the rate equations for the isothermal

† Communicated by the Author.

precipitation of a solute from a supersaturated solid solution proceeding by the diffusion limited growth of existing nuclei. The same problem was discussed by Wert (1949) and by Zener (1949) using the latter method of allowing for impingement.

Fig. 1

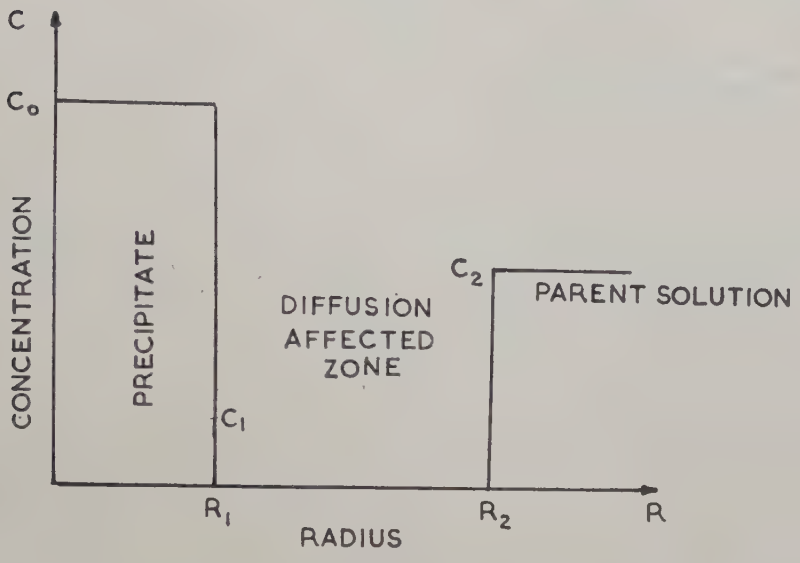

Concentration conditions around a growing particle of precipitate.

Because the rate of reaction varies with the shape of the precipitate, the following cases are considered: (*a*) spherical particles, (*b*) cylindrical particles growing in one, two or three dimensions and (*c*) discs growing in one, two or three dimensions. The following assumptions are made throughout:

(1) The reaction proceeds by the growth of a fixed number of nuclei, all of which formed at $t=0$.

(2) The supersaturated matrix is initially homogeneous.

(3) The distribution of nuclei is random.

(4) The rate of growth is determined by the rate of diffusion of solute in the matrix and the diffusion coefficient, D, is independent of concentration.

(5) The influence of the size and shape of the particles on the equilibrium matrix concentration is negligible.

§ 2. The Growth of Spherical Particles

Consider the conditions shown in fig. 1. An isolated particle of precipitate, radius R_1, solute concentration c_0, is in equilibrium with a solid solution, concentration c_1. Solute is being drawn from a sphere, radius R_2;

the initial concentration of the matrix is c_2. The relation between R_1 and R_2 is

$$R_1^2\,dR_1(c_0-c_1)=R_2^2\,dR_2c_2 \qquad (2)$$

and thus

$$R_2=\alpha R_1 \qquad (3)$$

where

$$\alpha=\sqrt[3]{\left(\frac{c_0-c_1}{c_2}\right)}. \qquad (4)$$

The rate of radial growth is given by

$$4\pi R_1^2\frac{dR_1}{dt}(c_0-c_1)=4\pi R_1^2D\left(\frac{\partial c}{\partial R}\right)_{R=R_1} \qquad (5)$$

where D is the diffusion coefficient for the solute in the matrix. It is assumed that after a short time a quasi-stationary state is established. The solution of Fick's equation, as given by Barrer (1941) is then

$$\frac{\partial c}{\partial R}=\frac{c_2-c_1}{(1/R_1-1/R_2)R^2}. \qquad (6)$$

Putting (6) and (3) into (5) gives

$$R_1\left(\frac{dR_1}{dt}\right)=D\frac{(c_2-c_1)}{(c_0-c_1)}\cdot\frac{\alpha}{(\alpha-1)} \qquad (7)$$

which can be written

$$R_1\left(\frac{dR_1}{dt}\right)=\beta. \qquad (8)$$

Thus for a single, isolated particle

$$R_1^2=2\beta t. \qquad (9)$$

This is of the same form as obtained by Zener (1949), but differs in the formulation of the constant β. Birchenall and Mead (1956), using a method differing slightly from the present one, obtained an expression for the radius of a graphite nodule growing in an austenite-cementite mixture which is equivalent to eqn. (7) except for the additional terms arising from the solution of the cementite.

For non-isolated particles impingement of the zones surrounding each particle results in a lowering of the rate of growth. To allow for this the right-hand side of eqns. (7) and (8) is multiplied by $(1-y)$, where y is the fraction of the total precipitation which has occurred at time t. The impingement allowance is discussed in § 9. Thus

$$R_1\left(\frac{dR_1}{dt}\right)=\beta(1-y). \qquad (10)$$

Assuming that all particles commence to grow at time $t=0$ and that there are N particles per unit volume of sample,

$$y=\tfrac{4}{3}\pi R_1^3\,.\,N\,.\left(\frac{c_0}{c_2-c_1}\right)=\gamma R_1^3 \quad \text{(say)}. \qquad (11)$$

Putting the values of R_1 and dR_1/dt from eqn. (11) into eqn. (10) gives

$$\int \frac{dy}{y^{1/3}(1-y)} = \int 3\beta\gamma^{2/3}\,dt \quad . \quad . \quad . \quad . \quad . \quad . \quad (12)$$

which on integration yields

$$\tfrac{1}{2}\ln\left[\frac{1+y^{1/3}+y^{2/3}}{(y^{1/3}-1)^2}\right]+\sqrt{3}\left[\tan^{-1}-\left(\frac{2y^{1/3}+1}{\sqrt{3}}\right)-\frac{5\pi}{6}\right]=3\beta\gamma^{2/3}t\dagger. \quad (13)$$

This is the rate equation for this particular model. Values of the function on the left-hand side of eqn. (13) are tabulated in table 1 to permit comparison with experimental data.

Table 1

Values of the function $f(y)=\frac{1}{2}\ln\left[\frac{1+y^{1/3}+y^{2/3}}{(y^{1/3}-1)^2}\right]+\sqrt{3}\left[\tan^{-1}-\left(\frac{2y^{1/3}+1}{\sqrt{3}}\right)-\frac{5\pi}{6}\right]$

y	0·1	0·2	0·3	0·4	0·5	0·6	0·7	0·8	0·9	0·95
$f(y)$	0·3371	0·5601	0·7723	0·9918	1·2297	1·5018	1·8341	2·2787	3·0040	3·7223

To illustrate the difference between this and previous methods the corresponding equation is derived using the impingement allowance employed by Johnson and Mehl (1939).

For an isolated particle

$$R_1^2 = 2\beta t$$

and the fraction precipitated, $y=\gamma R_1^3$

then

$$\frac{dy}{dt} = 3\gamma R_1^2 \cdot \frac{dR_1}{dt}(1-y). \quad . \quad . \quad . \quad . \quad . \quad . \quad (14)$$

In this case the impingement factor $(1-y)$ is placed in the overall rate equation. Substitution for R_1 and integration yields

$$\ln(1-y) = -(2\gamma^{2/3}\beta t)^{3/2}. \quad . \quad . \quad . \quad . \quad . \quad (15)$$

This is identical to eqn. (1) with $n=3/2$.

The rate curves derived from eqns. (13) and (15) are compared in fig. 2. These are approximately the same at early stages of precipitation but diverge appreciably towards the end.

§ 3. Cylindrical Particles Growing Radially Only

Proceeding as before and using the steady state solution of Fick's Law for cylindrical symmetry gives the usual parabolic law for an isolated particle

$$R_c^2 = 2\beta_{cr} \cdot t \quad . \quad . \quad . \quad . \quad . \quad . \quad . \quad . \quad (16)$$

where

$$\beta_{cr} = D\left(\frac{c_1-c_2}{c_0-c_1}\right) \cdot \frac{1}{\ln\sqrt{\left(\frac{c_2}{c_0-c_1}\right)}} \cdot \quad . \quad . \quad . \quad . \quad (17)$$

† $\sqrt{3}(5\pi/6)$ is the integration constant.

Fig. 2

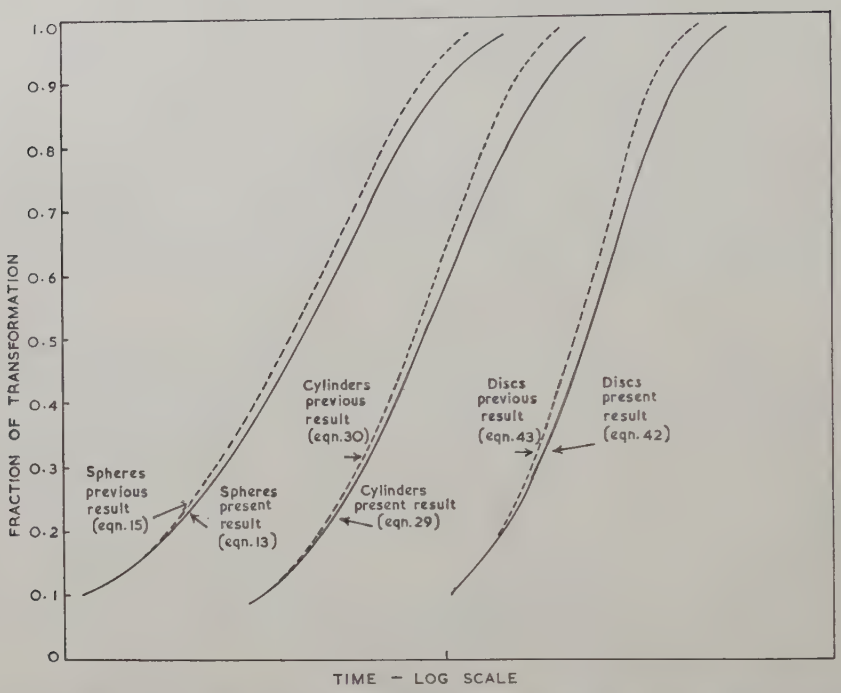

A comparison of the rate curves obtained using the Johnson–Mehl impingement factor (broken curves) and the present equations for various shapes of precipitate. The positions on the time axis are arbitrary.

Allowing for impingement

$$R_c \frac{dR_c}{dt} = \beta_{cr}(1-y); \qquad \ldots\ldots (18)$$

y is the fraction of the total precipitation which has occurred at time t and is given by

$$y = 2\pi R_c^2 L . N\left(\frac{c_0}{c_2 - c_1}\right) = \gamma_{cr} . R_c^2 \qquad \ldots\ldots (19)$$

in which $2L$ is the length of the particle, assumed constant. Putting eqn. (19) into eqn. (18) gives

$$\frac{dy}{(1-y)} = 2\gamma_{cr} . \beta_{cr} . dt$$

and integrating

$$\ln\left(\frac{1}{1-y}\right) = 2\gamma_{cr} . \beta_{cr} . t\dagger. \qquad \ldots\ldots (20)$$

The applicability of this equation in any case can be checked by plotting $\ln(1/1-y)$ as a function of time.

† The integration constant is zero.

§ 4. Cylindrical Particles Growing Axially Only

As pointed out by Wert the concentration conditions around the ends of a cylindrical particle growing axially remain unchanged. Thus the axial rate of growth is constant and it is possible to write

$$L=\beta_{ca}.t. \qquad \ldots\ldots\ldots \quad (21)$$

For non-isolated particles

$$\frac{dL}{dt}=\beta_{ca}(1-y) \qquad \ldots\ldots\ldots \quad (22)$$

which gives a rate equation

$$\ln\left(\frac{1}{1-y}\right)=\gamma_{ca}.\beta_{ca}.t, \qquad \ldots\ldots\ldots \quad (23)$$

where

$$\gamma_{ca}=2\pi R_c^2.N\left(\frac{c_0}{c_2-c_1}\right) \qquad \ldots\ldots\ldots \quad (24)$$

and R_c is the radius, assumed constant.

§ 5. Cylindrical Particles Growing in All Directions

The volume of such a particle growing from negligible initial dimensions is $2\pi R_c^2 L$ and the fraction precipitated y is

$$2\pi N\left(\frac{c_0}{c_2-c_1}\right).R_c^2 L, \quad \text{say} \quad \gamma_c.R_c^2.L.$$

The rate of reaction is given by

$$\frac{dy}{dt}=\left(\frac{\partial y}{\partial R_c}\right)_L.\frac{\partial R_c}{\partial t}+\left(\frac{\partial y}{\partial L}\right)_{R_c}.\frac{\partial L}{\partial t}. \qquad \ldots\ldots \quad (25)$$

Noting that eqns. (18) and (22) can be put into the integral forms

$$R_c^2=2\beta_{cr}\int_0^t(1-y)\,dt, \qquad \ldots\ldots\ldots \quad (26)$$

$$L=\beta_{ca}\int_0^t(1-y)\,dt, \qquad \ldots\ldots\ldots \quad (27)$$

and carrying out the operations indicated by the right-hand side of (25) gives an integral equation

$$\frac{dy}{dt}=4\beta_{cr}.\beta_{ca}\gamma_c(1-y)\int_0^t(1-y)\,dt. \qquad \ldots\ldots \quad (28)$$

The solution is

$$y=\tanh^2\sqrt{[2\beta_{cr}.\beta_{ca}.\gamma_c]}.t. \qquad \ldots\ldots \quad (29)$$

Using the previous method of allowing for impingement gives for this form of precipitate

$$y=1-\exp-(2\beta_{cr}.\beta_{ca}.\gamma_c).t^2. \qquad \ldots\ldots \quad (30)$$

Graphs of eqns. (29) and (30) are plotted in fig. 2 from which it can be seen that there is again an appreciable difference in the two results, especially during the later stages of the process.

§ 6. Discs Growing Only on its Faces

If X is the half-thickness of the disc

$$X\left(\frac{dX}{dt}\right)=\beta_{df}(1-y) \quad . \quad . \quad . \quad . \quad . \quad . \quad . \quad (31)$$

where

$$\beta_{df}=D\left(\frac{c_2-c_1}{c_0-c_1}\right)\frac{1}{\left\{\frac{c_0-c_1}{c_2}-1\right\}}. \quad . \quad . \quad . \quad . \quad (32)$$

Volume of disc is $2\pi R_d{}^2X$ where R_d is the radius, assumed constant.

$$y=2\pi R_d{}^2.X.N\left(\frac{c_0}{c_2-c_1}\right)=\gamma_{df}.X. \quad . \quad . \quad . \quad (33)$$

This yields a rate equation

$$y+\ln(1-y)=-\beta_{df}.\gamma_{df}{}^2.t. \quad . \quad . \quad . \quad . \quad . \quad (34)$$

§ 7. Discs Growing Radially Only

Again following Zener and Wert it is assumed that the rate of radial growth is constant. For non-isolated particles

$$\frac{dR_d}{dt}=\beta_{dr}(1-y) \quad . \quad . \quad . \quad . \quad . \quad . \quad . \quad (35)$$

and

$$y=2\pi R_d{}^2X.N.\left(\frac{c_0}{c_2-c_1}\right)=\gamma_{dr}.R_d{}^2. \quad . \quad . \quad . \quad (36)$$

This gives

$$\frac{dy}{\sqrt{y.(1-y)}}=2\sqrt{(\gamma_{dr})}.\beta_{dr}.dt.$$

Integrating

$$y=\tanh^2\sqrt{(\gamma_{dr})}.\beta_{dr}.t. \quad . \quad . \quad . \quad . \quad . \quad (37)$$

§ 8. Discs Growing in Three Dimensions

Following the same procedure as used for cylinders growing in three dimensions leads to

$$\frac{dy}{dt}=\frac{5}{\sqrt{2}}\gamma_d.\beta_{dr}{}^2\sqrt{\beta_{df}}(1-y)\left[\int_0^t(1-y)\,dt\right]^{3/2} \quad . \quad . \quad (38)$$

where

$$\gamma_d=2\pi N.\left(\frac{c_0}{c_2-c_1}\right).$$

This equation can be solved by writing $x=(1-y)$ and differentiating to remove the integral. The result is

$$x\frac{d^2x}{dt^2}-\left(\frac{dx}{dt}\right)^2+\tfrac{3}{2}A^{2/3}.x^{8/3}.\left(-\frac{dx}{dt}\right)^{1/3}=0 \quad . \quad . \quad . \quad (39)$$

where

$$A=\frac{5}{\sqrt{2}}.\gamma_d.\beta_{dr}{}^2.\sqrt{\beta_{df}}.$$

Substitution of $z^{3/5}=(-dx/dt)$ yields a linear, first-order equation, the solution of which is

$$z=5/2A^{2/3}.x^{5/3}(1-x). \quad . \quad . \quad . \quad . \quad . \quad . \quad (40)$$

Thus

$$\frac{dy}{(1-y)y^{3/5}}=\int(5/2A^{2/3})^{3/5}.dt. \quad . \quad . \quad . \quad . \quad . \quad (41)$$

This equation has not been integrated analytically. It can be solved numerically or by expanding $(1-y)^{-1}$ and integrating term by term which gives

$$y^{2/5}\left(1+\frac{2}{7}y+\frac{1}{6}y^2+\ldots+\frac{2}{5n-3}y^{n-1}+\ldots\right)=[\sqrt{(2\beta_{df})}\beta_{dr}{}^2.\gamma_d]^{2/5}t\dagger$$

. . . (42)

which is the rate equation for this particular model. The series converges rapidly at low values of y; at $y=0{\cdot}9$ ten terms gives an accuracy better than 1%. A table of values of this series is given in table 2.

Table 2

Value of the series $f(y)=y^{2/5}\left(1+\frac{2}{7}y+\frac{1}{6}y^2+\ldots+\frac{2}{5n-3}y^{n-1}+\ldots\right)$									
y	0·1	0·2	0·3	0·4	0·5	0·6	0·7	0·8	0·9	0·95
$f(y)$	0·4101	0·5588	0·6819	0·7960	0·9132	1·0348	1·1759	1·3651	1·6177	1·8128

Values accurate to within 1%.

It can be simply shown that the corresponding equation using the previous impingement factor is

$$y=1-\exp-[\sqrt{(2\beta_{df})}.\beta_{dr}{}^2.\gamma_d].t^{5/2}. \quad . \quad . \quad . \quad . \quad (43)$$

Graphs of eqns. (42) and (43) are shown in fig. 2.

§ 9. Discussion

The results of widest interest are the equations giving the fraction transformed as a function of time for the spherical, disc-like and cylindrical particles growing in three dimensions. The results are grouped in fig. 2 together with the corresponding rate curves derived on the basis of the Johnson–Mehl impingement factor. It is clear from the derivation of the equations that the values of the various constants do not affect the shape of the curves, only the position on the time axis; the shape of the curve is determined by the shape of the precipitate. The present results indicate a slower rate of reaction in all cases; the divergence becomes marked for y greater than 0·5.

Although the present method of allowing for impingment is considered to be more satisfactory than previous methods in which a correction is

† The constant of integration is zero in this equation.

applied to the integrated rate of transformation, the use of $(1-y)$ as the impingement factor is quite arbitrary. It is difficult to conceive an analytical method which is not dependent upon equally arbitrary assumptions concerning the distribution of precipitate and the behaviour of the surfaces of the diffusion zones after impingement. Indeed, the treatment of the simplest idealized model would be formidable since non-radial diffusion is inevitable after contact of the diffusion zones. In the absence of an analytical treatment a factor is required which expresses the fact that the rate of growth decreases as the matrix is consumed; the growth rate is thus some function of $(1-y)$. The exact function will possibly vary from system to system. Here it was decided to use the simplest possible function viz. $(1-y)$. It is reasonable because it allows for immediate impingement which must occur in a random distribution of nuclei; and because it allows for the fact that impingement dominates towards the end of the reaction. Other factors have been suggested e.g. $(1-y)^2$, Mishima (1951). Doremus (1957) used both $(1-y)$ and $(1-y)^2$. The effect of the latter on the present equations is being examined.

Another consequence of the present method of allowing for impingement is important in connection with experimental measurement of rates of growth of precipitates. Such results are normally intepreted in terms of the parabolic law eqn. (9). However, eqn. (10) is more appropriate. Substituting the value of y from eqn. (11) into eqn. (10) gives

$$\int \frac{R_1 dR_1}{(1-\gamma R_1^3)} = \int \beta \, dt, \quad . \quad . \quad . \quad . \quad . \quad . \quad . \quad (44)$$

integration gives

$$-\frac{1}{3\gamma A}\left[\frac{1}{2}\ln\left\{\frac{A^2-AR_1-R_1^2}{(A+R_1)^2}\right\}+\sqrt{3}\left\{\tan^{-1}\left(\frac{2R_1-A}{A\sqrt{3}}\right)-\frac{5\pi}{6}\right\}\right]$$
$$=\beta\gamma^{2/3}t, \quad A^3=-1/\gamma. \quad . \quad . \quad . \quad . \quad . \quad . \quad (45)$$

A simple and more revealing way of integrating (44) is by series expansion of the denominator. The result is

$$R_1^2\left(1+\frac{2}{5}\gamma R_1^3+\frac{1}{4}\gamma^2 R_1^6+\ldots+\frac{2}{3n-1}\gamma^{3(n-1)}+\ldots\right)=2\beta t. \quad . \quad (46)$$

Thus the law differs from the usual parabolic law by the second and subsequent terms of the series. The two forms of growth curve are compared in fig. 3 using values of R_1, γ and β which would permit microscopic (optical) measurement of growth rates in a typical metal system. The curves are almost identical at small R but diverge considerably as the size of the particle increases. Thus the fitting of growth data to parabolic curves with the subsequent conclusion that the rate of growth is governed by diffusion is open to considerable criticism.

In the cases of eutectoid transformations and re-crystallization the Johnson-Mehl equation will probably give a better representation of experimental data than the present equations. In these reactions only short range diffusion is involved, the re-distribution of the components

Fig. 7

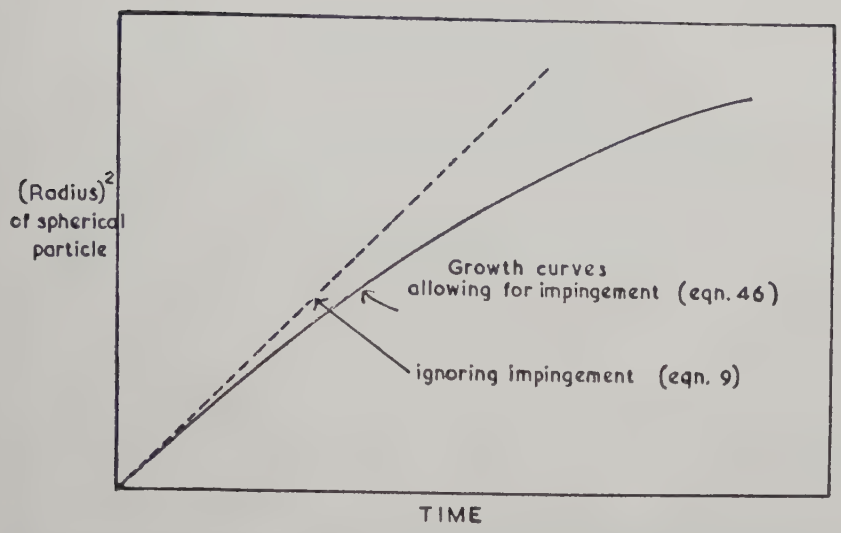

Hypothetical growth curves, (*a*) ignoring impingement (broken curve) and (*b*) considering impingement (eqn. (46)).

occurring in the parent solution adjacent to the interface. Impingement consists of direct contact between grains of the new phase and the diffusion potential is not affected.

Acknowledgments

The author is grateful to Mr. A. Young of the Department of Applied Mathematics for help with the solutions of eqns. (28) and (38).

References

Barrer, R. M., 1941, *Diffusion in and through Solids* (Cambridge : University Press).

Birchenall, C. E., and Mead, H. W., 1956, *Trans. A.I.M.M.E.*, **206** (*J. Metals*, **8**, 1004).

Doremus, R. H., 1957, *Acta Met.*, **5**, 293.

Hardy, H. T., and Heal, T. J., 1954, *Progress in Metal Physics*, **5**, 143.

Johnson, W. A., and Mehl, R. F., 1939, *A.I.M.M.E.*, **135**, 416.

Mishima, T., 1951, *Proc. First World Met. Congress* 1950, *Cleveland*, (American Society of Metals), p. 668.

Wert, C., 1949, *J. appl. Phys.*, **20**, 943.

Zener, C., 1949, *J. appl. Phys.*, **20**, 950.

CORRESPONDENCE

Density and Expansivity of Solid Krypton

By B. F. Figgins and B. L. Smith
Department of Physics, Queen Mary College (University of London), London, E.1

[Received January 11, 1960]

The theoretical study of ideal crystal lattices is considerably strengthened when use can be made of experimental values for the thermodynamic properties of the solidified inert gases (Dobbs and Jones 1957) and in an earlier paper (Dobbs *et al*, 1956) experimental values of the density and expansivity of solid argon were reported. In the present note we give the corresponding figures for krypton.

The same two methods were used as in the earlier work. Debye–Scherrer powder photographs were taken between 20°K and 90°K and a bulk density method gave results between 70°K and the melting point ($T_m = 116$°K) where the large grain size made the x-ray method inaccurate. Using krypton supplied by the British Oxygen Company and stated to contain up to $\frac{1}{2}\%$ xenon and of the order $0{\cdot}001\%$ of other impurities, good agreement was not obtained where the two methods overlapped. However, when krypton supplied by the Air Reduction Sales Company and stated to be $99{\cdot}98\%$ pure was used for the bulk density method agreement was complete within the experimental accuracy ($\pm 0{\cdot}001$ A at 20°K rising to $\pm 0{\cdot}003$ A at 90°K for the lattice parameter from x-ray measurements and $\pm 0{\cdot}0025$ A as deduced from bulk density measurements).

The present results are shown in the figure, together with the results of earlier workers at isolated temperatures or over narrow ranges of temperatures. It will be seen that large discrepancies occur between the various sets of results but, as already stated, there is good agreement between our results obtained by the two methods. The following table shows our values for the density and derived values of the expansivity and Gruneisen parameter $\gamma = \alpha V/\kappa_s C_v$.

T°K	20	40	60	80	90
(g cm^{-3})	3·078	3·040	2·988	2·926	2·893
$\alpha \times 10^4$ (deg^{-1} c)	4·8	7·7	9·7	11·0	11·2
γ	2·1	2·2	2·5	2·5	2·1

In order to calculate γ we have used the specific heat values of Clusius (1936) and the value of compressibility obtained by Stewart at 77°K

(1955). The latter value was corrected for temperature variation by a comparison with the results of Barker and Dobbs (1955) for argon, using a reduced temperature T/T_m.

An estimate of the density at absolute zero made by an extrapolation of our curve leads to a value of 3·09 g cm^{-3} which is to be compared with the best previous estimate (see for example Dobbs and Jones 1957) of 3·01 g cm^{-3}. The average value of the Gruneisen parameter is about 2·3 and it appears to have a maximum value of about 2·6. It is interesting to note that roughly the same variation of γ with reduced temperature was observed for argon.

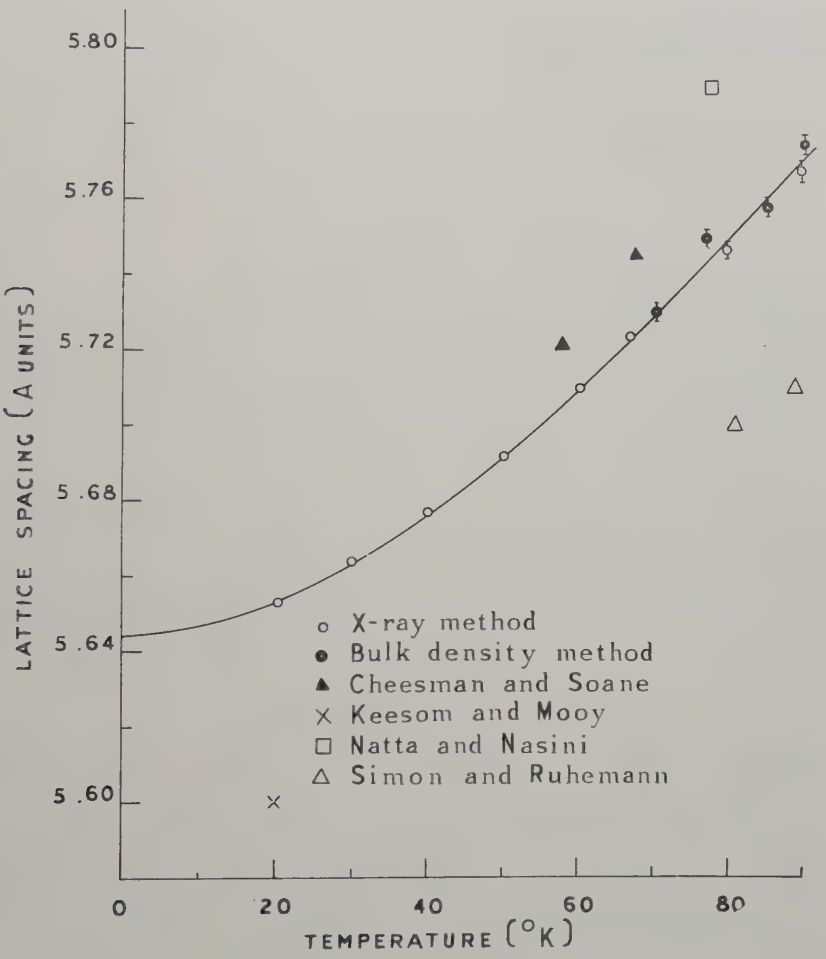

Acknowledgments

We wish to acknowledge the valuable help and advice of Dr. E. R. Dobbs and of Professor G. O. Jones. We are indebted to the British Oxygen Company for a Research Fellowship (to B.F.F.) and to the D.S.I.R. for a maintenance grant (to B.L.S.)

References

Barker, J. R., and Dobbs, E. R., 1955, *Phil. Mag.*, **46,** 1069.
Cheesman, G. H., and Soane, C. M., 1957, *Proc. phys. Soc., Lond.* B, **70,** 700.
Clusius, K., 1936, *Z. phys. Chem.* B, **31,** 459.
Dobbs, E. R., Figgins, B. F., Jones, G. O., Piercey, D. C., and Riley, D. P., 1956, *Nature, Lond.*, **178,** 483.
Dobbs, E. R., and Jones, G. O., 1957, *Rep. Prog. Phys.*, **20,** 516.
Keesom, W. H., and Mooy, H. H., 1931, *Leiden Commun.* 2096.
Natta, G., and Nasini, A., 1930, *Accad. Lincei. Atti.*, **12,** 141.
Simon, F., and Ruhemann, B., 1932, *Z. phys. Chem.* B, **15,** 389.
Stewart, J. W., 1955, *Phys. Rev.*, **97,** 578.

An Anomaly in the Heat Capacity of Chromium at 38·5°C

By R. H. Beaumont†, H. Chihara† and J. A. Morrison

Division of Pure Chemistry, National Research Council, Ottawa, Canada

[Received December 28, 1959]

Several properties of pure chromium metal show an anomalous temperature dependence in a broad temperature region below 50°C (Sully 1954); the temperature coefficients of some (e.g. Young's modulus, expansivity) undergo an abrupt reversal of sign at about 38°C. Different interpretations of the phenomena have been discussed (Pursey 1958, Neumann and Stevens 1959), but none seems to have been fully substantiated.

Although the general trend of the heat capacity curve of chromium is known between 56° and 1100°K (Anderson 1937, Armstrong and Grayson-Smith 1950), no detailed results are available for the region where an anomaly, corresponding to the anomalies in other properties, would be expected to occur. In view of the possibility that the heat capacity could yield useful additional information, we have made closely spaced measurements in the region $-5°$ to 51°C; the results are described in this note. Clear evidence has been obtained of a lambda type anomaly, the maximum occurring at $38{\cdot}5 \pm 0{\cdot}3$°C.

The specimen of ductile chromium (99·998% pure) used was part of that employed by Rayne and Kemp (1956) in heat capacity measurements below 4·2°K‡. It was in the form of a cylinder, diameter 2·5 cm and height 3·8 cm, and weighed 135·2 g. A copper holder was attached by means of a copper screw which passed through the holder and into a hole tapped in the base of the specimen. A platinum thermometer (T–4, Los and Morrison 1951) and a manganin heater were cast with Woods metal

† National Research Council Postdoctorate Research Fellow.

‡ This specimen was originally produced by the Aeronautics Research Laboratory, Melbourne and its mode of preparation has been described (Wain *et al.* 1954–55).

into a well in the holder at one side of the chromium cylinder. The holder and specimen were suspended by three nylon threads within the adiabatic shield of an assembly used previously for heat capacity measurements (calorimeter II: Flubacher *et al.* 1959). Thermal contact between the holder and the specimen was satisfactory throughout. During input of energy, the temperature difference between the heating element and its surroundings was not greater than 0·2°C. Also, the half life for the process of distribution of energy after heating was only 1 to 2 min.

The experimental results are shown in fig. 1, and are compared with results of measurements on other specimens in fig. 2. In estimating the absolute accuracy, only the comparison with the work of Anderson (1937) is useful. In the region where the two sets of measurements overlap there is a small systematic difference of 0·5 to 1%. This may reflect a variation from specimen to specimen but the difference is within the accuracy quoted by Anderson (1930) for his method. For our present purposes the precision of the measurements is more important. Below 38·5°C, the root mean square deviation of our results from a smooth curve (fig. 1) is 0·13%.

The general shape of the heat capacity curve displayed in fig. 1, is clearly that of a lambda type anomaly. Within the precision available in the measurements, the heat capacity remains finite throughout the transition region. If, as seems reasonable, the contribution of the undisturbed state can be represented by the light dashed curve in fig. 1, estimates of the enthalpy and entropy associated with the transition can be made. These are small; the change in enthalpy amounts to 1·4 cal/g atom and the change in entropy to 0·0044 cal/g atom deg.

It is important to establish whether the magnitude of the excess heat capacity is consistent with the changes in the expansivity and compressibility of chromium which have been observed previously. The three quantities are related (Prigogine and Defay 1954) and at the lambda point the relationship takes the form

$$\Delta C_p = \frac{V_\lambda T_\lambda (\Delta\alpha)^2}{\Delta\chi}, \qquad (1)$$

where ΔC_p, $\Delta\alpha$ and $\Delta\chi$ refer to differences between the observed heat capacity, expansivity and compressibility and the values attributable to the undisturbed state. V_λ is the atomic volume at the transition temperature T_λ.

Two of the three quantities required for the estimation of ΔC_p from eqn. (1) are directly accessible. With adequate accuracy the density can be taken as 7·18 g/cm^3 (Sully 1954). The expansivity of chromium (99·8% pure) has been measured by Fine *et al.* (1951) and a value of $\Delta\alpha$ can be obtained from their graph.

In order to compute $\Delta\chi$, a knowledge of both Poisson's ratio (μ) and Young's modulus (E) is required, since

$$\chi = \frac{3(1-2\mu)}{E}. \qquad (2)$$

Fig. 1

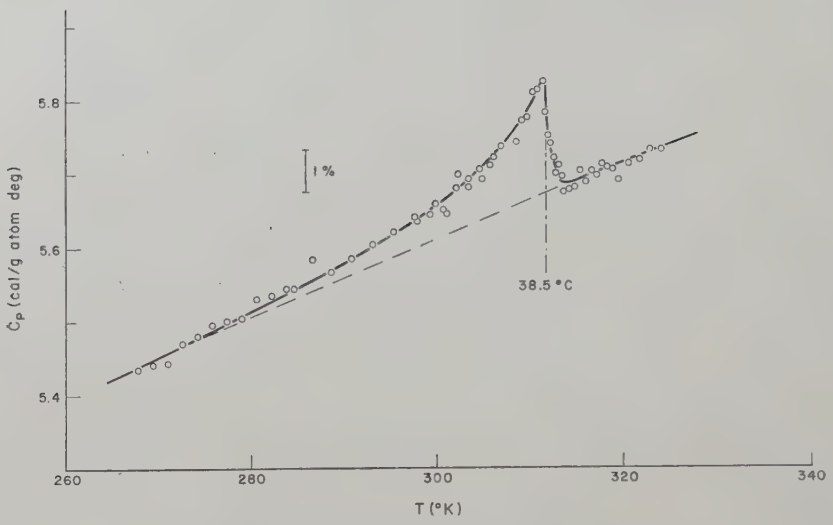

Measured heat capacities of chromium.

Fig. 2

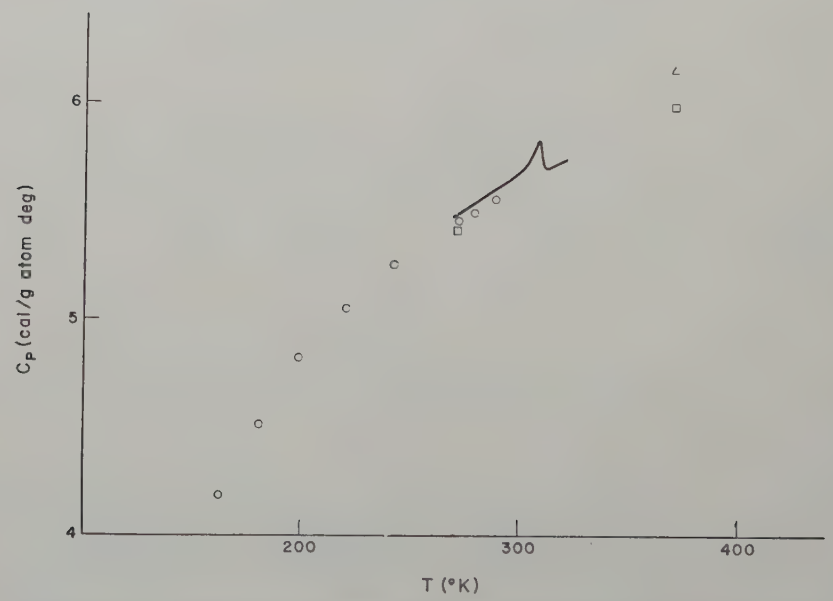

A comparison of different measurements of the heat capacity of chromium.
——Present results.
⊡ Armstrong and Grayson-Smith (1950).
○ Anderson (1937).
△ Umino (1926).

E has been determined by Fine *et al.* (1951) and by Pursey (1958), and the two sets of results are in substantial agreement. There is therefore no difficulty in making an estimate of the change in E at the lambda point. μ for pure chromium outside the transition region appears to be about one-third but its actual value at 38°C has not been measured. However, Pursey (1958) has established that the change in μ for the transition in chromium containing metallic impurities is about 0·2. There is evidence (Neumann and Stevens 1959) that such impurities enhance the anomaly. Therefore, it seems reasonable to suppose that μ for pure chromium at 38°C lies between 0·13 and 0·33. These values lead to lower and upper bounds on ΔC_p of 0·05 and 0·30 cal/g atom deg. respectively; direct experiment gives $\Delta C_p = 0{\cdot}15$ cal/g atom deg.

This excellent agreement between the experimental and calculated values of ΔC_p shows that the different bulk measurements on relatively pure chromium are consistent. Furthermore, since the measurements have been made on different specimens, the agreement indicates that the anomaly in chromium at 38·5°C is not to be ascribed to the presence of small amounts of impurities such as oxygen or nitrogen in the lattice. Instead, the anomaly must be the reflection of a change in the chromium lattice itself. Neutron diffraction studies by Dr. G. E. Bacon of Harwell (private communication) have recently confirmed that high purity chromium becomes weakly antiferromagnetic below about 40°C (see also, Corliss *et al.* 1959). The shape and position of the heat capacity anomaly are consistent with an antiferromagnetic transition.

Acknowledgment

We should like to thank Dr. G. K. White for suggesting the problem and for helpful correspondence.

References

Anderson, C. T., 1930, *J. Amer. chem. Soc.*, **52,** 2712; 1937, *Ibid.*, **59,** 488.
Armstrong, L. D., and Grayson-Smith, H., 1950, *Canad. J. Res.*, A, **28,** 51.
Corliss, L. M., Hastings, J. M., and Weiss, R. J., 1959, *Phys. Rev. Letters*, **3,** 211.
Fine, M. E., Greiner, E. S., and Ellis, W. C., 1951, *J. Metals* (*Trans. A.I.M.E.*, **191**), 56.
Flubacher, P., Leadbetter, A. J., and Morrison, J. A., 1959, *Phil. Mag.*, **4,** 273.
Los, J. M., and Morrison, J. A., 1951, *Canad. J. Phys.*, **29,** 142.
Neumann, M. M., and Stevens, K. W. H., 1959, *Proc. phys. Soc. Lond.*, **74,** 290.
Prigogine, I., and Defay, R. 1954 *Chemical Thermodynamics* (Translated by D. H. Everett) (London: Longmans Green and Co.), p. 296 et seq.
Pursey, H., 1958, *J. Inst. Met.*, **86,** 362.
Rayne, J. A., and Kemp, W. R. G., 1956, *Phil. Mag.*, **1,** 918.
Sully, A. H., 1954, *Chromium* (London: Butterworths Scientific Publications), chap. 3.
Umino, S., 1926, *Sci. Rep. Tôhoku Univ.*, **15,** 597.
Wain, H. L., Henderson, F., and Johnstone, S. T. M., 1954–55, *J. Inst. Met.*, **83,** 133.

Direct Observation of Dislocations in Magnesium Oxide

By J. Washburn†, A. Kelly and G. K. Williamson‡
Department of Metallurgy, University of Cambridge

[Received February 9, 1960]

Dislocations have been observed in thin metal foils by electron transmission microscopy for a number of years. We have recently observed directly the motion of dislocations in thin crystals of magnesium oxide, a ceramic material of high melting point. Large crystals, supplied by the Norton Company, were prepared by cleavage followed by chemical polishing, to produce a thin specimen. From the measured separations of the traces of (110) slip planes on the two surfaces of the specimen the thickness was found to be 3000 to 5000 Å.

Direct evidence for the double cross-slip of individual screw dislocations from a given (101) slip plane into nearby parallel glide planes is shown in fig. 1 (*a*), (*b*), (*c*) (Pls. 23 and 24). The beam current was momentarily increased between exposures to move the dislocations. Multiplication of dislocations took place at the tip of a short crack near one edge of the specimen. The thermal stresses due to local heating of the crystal by the beam tended to drive screw dislocations along the (101) plane into the crystal. The paths taken by individual moving dislocations were clearly delineated at the surface by a contrast effect similar to that seen in metal foils (Hirsch *et al.* 1956). It has been suggested for metals that this effect is associated with the presence of an oxide film. This cannot be the case for magnesium oxide but films of magnesium hydroxide or deposited carbon may have been present. The paths taken by some of the dislocations show that motion was not confined to a single (101) slip plane. The band spread sideways as the dislocations moved away from the edge by frequent cross-slip, probably into (010) and then back into (101). The double cross-slip took place on a very fine scale resulting in what appeared to be noncrystallographic glide paths. All the dislocations were retarded at their intersections with the surfaces and many were also held back at one or two interior points along their length. They were bowed out between these locking points which may have been jogs consisting of short segments of edge dislocation connecting a length of dislocation in the original slip plane with another part which had undergone double cross-slip into a parallel plane. They could also have been formed by cutting of an intersecting screw dislocation by the moving dislocation.

† National Science Foundation fellow on leave from University of California.
‡ On secondment from C.E.G.B., Berkeley Nuclear Laboratories.

Plastic deformation associated with the propagation of cracks was also observed. Figure 2 (Pl. 24) shows a crack on a (100) plane at right angles to the plane of the foil. A row of dislocations extending from the crack surface to either the top or bottom surface of the foil can be seen on both sides of the crack.

Dislocation pile-ups consisting of a large number of dislocations lying on a single slip plane held up behind an immobile dislocation have not been observed and perhaps would not be expected in this material due to the manifest ease of cross-slip.

One particularly encouraging aspect of this work is that it has been possible to study imperfections in a refractory ceramic material using electron transmission microscopy in the same way as with metal specimens.

Reference

Hirsch, P. B., Horne, R. W., and Whelan, M. J., 1956, *Phil. Mag.*, **1**, 677.

REVIEWS OF BOOKS

Concepts of Classical Optics. By JOHN STRONG. (San Francisco: W. H. Freeman; London: Bailey Bros. and Swinfern, 1958.) [Pp. xxii+692.] 80*s*.

THIS excellent textbook deals with the subject in an agreeably matter of fact way. The necessary mathematics is there, but the emphasis is on physical insight; laboratory work is kept constantly before the reader's mind by Roger Hayward's illuminating diagrams. The book could provide an ideal refresher course for technologists who found optics dull in their undergraduate days.

The first three chapters deal with light as wave motion, with superposition of wave motions and with electromagnetic waves; the next four with the interaction of light and matter. Then follow accounts, all very well written, of interference, diffraction and coherence. Chapter 12 discusses reflection-reducing overcoats on optical surfaces, interference filters, and multiple beam interferometry. Chapters 13–16 deal with the simpler properties of optical systems, and with the testing of optical surfaces. They keep closely in touch with practical problems and give an excellent introduction to optical design.

The book ends with seventeen appendices contributed by (or quoted by permission of) various authors. Although the presentation in some of the appendices is below the high standard of the main text, they bring the reader into closer touch with the growing edge of the subject and add to the vitality and interest which characterize the whole work. E. H. L.

Theory and Applications of Nuclear Induction. By A. K. SAHA and T. P. DAS. (Saha Institute of Nuclear Physics, Calcutta, India.) [Pp. 516.] 40*s*.

NUCLEAR Induction is another name for Nuclear Magnetic Resonance. It used to be said that one's preference for the name of this ever-growing field of study was determined by whether one was situated West or East of the Mississippi. At the present time when the name Nuclear Magnetic Resonance has gained almost universal usage, the authors' choice of title provides a salutary reminder of the alternative approaches to the understanding of the phenomenon.

Six or seven years ago the whole of Nuclear Magnetic Resonance could be reviewed in a book of modest dimensions. The enormous recent growth of activity, particularly in high-resolution chemical applications, makes comprehensive coverage impossible today. Nevertheless this substantial work traverses much ground: Basic theory, experimental methods, relaxation mechanisms, dipolar-broadened spectra, quadrupole-split spectra, chemical shift, electron-coupled nuclear interactions, spin echoes, Overhauser effect, pure quadrupole resonance; indeed all the main topics find their place. The book is addressed to physicists and an account of purely chemical applications is not included. The emphasis throughout is on theory, which occupies the majority of the book. The theoretical treatment is of a high standard and the book is not appropriate as a first introduction to the general reader or to the researcher newly entering the field. On the other hand to the reader already familiar with the subject the presentation of the theory will make stimulating reading. The material of the experimental sections seems rather less well organized, and contains a surprising amount of constructional detail of early apparatus. There are four pages of errata at the end.

The writing and publication of this book in India is commendable and is to be welcomed as a useful addition to the literature of the subject. E. R. A.

Electron Physics: The Physics of the Free Electron. By O. Klemperer. (London: Butterworth's Scientific Publications, 1959.) [Pp. 248+xi.] 32*s.* 6*d.*

With the present-day preoccupation with nuclear phenomena on the one side and with electronic gadgetry on the other, the electron has become something of a Cinderella particle in University courses. Even pre-war texts which did it liberal justice, such as Barton Hoag, have been so swollen with information about the nucleus that the electron has been squeezed out of the original picture in more senses than one. The balance is somewhat restored by the present book, which is based on courses given by the author to Honours students at Imperial College, London.

The fundamental properties of the electron—charge, mass, wavelength, spin and magnetic moment—are discussed in Part II of the book, primarily from the phenomenological standpoint. All the main experiments are described, and at the same time the wave nature of the electron is discussed and the treatment is up-to-date enough to include electron spin resonance and radio frequency spectroscopy. Part I is devoted to the propagation and detection of the electron, much of it clearly condensed from the author's extensive monograph on Electron Optics. The mathematical and the experimental study of trajectories in electrical and magnetic fields are both treated in a clear and concise manner. Space charge flow has a chapter to itself, and that on methods of detection provides an introduction to the principles of different types of counter, even if too short to be very informative about practical matters. However, like the other chapters, it ends with a selected list of references through which details can be hunted up. There are also short selections of problems, mostly from the Special B.Sc. examinations of London University.

The author mentions in his preface that he has had in mind those going on to specialize in electronic engineering, and both his choice of topics and level of treatment seem eminently suited to such students. The book should also find a place in courses in applied physics, and may not be out of place in the reading of the practically minded student of pure physics. He will find here, for instance, an excellent short account of electron optics and an up-to-date discussion of the different methods of measuring e/m. However, as may be inevitable in such an effort of compression, some sections are short to the point of scrappiness. In practice, of course, lectures on electron physics will be dovetailed in with other courses; without this, the average man would not make much of the treatment of the Lamb-Retherford shift, for instance. To get full benefit from the text, a student had best follow up some of the references given and should certainly work through the problems. V. E. C.

Mécanique Quantique, Tome II. By A. Messiah. (Dunod: Paris.) [Pp. 540.] 48 New Francs.

The second volume of this comprehensive treatise takes us though symmetry and invariance, through methods of approximation and collision theory, to the Dirac electron and the elements of quantized fields. On the whole there is probably more here than one might expect every theoretical physicist to know, but it is all said with such accuracy and clarity that there is no excuse for him not knowing it if he has to. Every difficulty is explained, every approximation is justified. In a course of lectures this would be intolerable; in a text book it is invaluable. Moreover there are a number of topics here set forth explicitly which are not at all easy to find in the literature or in the other books. In the problems which are discussed it is entirely up to date, and the general approach reflects standard enlightened opinion amongst professional research workers.

The printing and the writing are impeccable ; great trouble has obviously been taken to eliminate errors and ambiguities. Perhaps I have been misled by the elegant simplicity of the French language. I challenge the author to produce an English translation of like excellence. It will surely become one of the most useful books on the subject. J. M. Z.

Fracture. By B. L. Averbach, D. K. Felbeck, G. T. Hahn and D. A. Thomas (Editors). (Technology Press and John Wiley and Sons, New York.) [Pp. 646.] (No price given by publishers.)

Now that the plastic properties of solids are beginning to be understood people are taking an increased interest in the atomic mechanisms of fracture, a subject that has languished since the great papers of A. A. Griffith. A conference on it was held in April 1959 at Swampscott, U.S.A., and the proceedings are summarized in this book. Particularly valuable features, fully brought out in the book, were the wide survey of various types of fracture produced in different materials under different conditions of temperature and stressing, and the highly critical appraisals of what is really understood in this field. The main advances made at the conference were the recognition that brittle cracks in steel are often nucleated by plastic deformation, that it is usually easier to nucleate them than grow them, and that in ' ductile fracture ' the material probably does not fracture at all but flows plastically into two halves. By contrast, the conference also showed that we still have some way to go in understanding creep fractures and that as regards understanding fatigue fractures, in spite of brilliant observations with the microscope, we are not sure whether we even have started yet. These and many other points are fully brought out in the 28 articles and discussions contributed by those at the conference. This book will undoubtedly become and remain the standard work on the theory of fracture until, at least, another similarly successful conference is held. A. H. C.

Advances in Electronics and Electron Physics, Vol. XI. Edited by L. Marton. (Academic Press.) [Pp. xi+523.] $15.00.

The volume under review is the eleventh of an annual series which has become well established. It follows more or less the form of previous issues, consisting of a number of review articles. The variety of subjects covered in this case is unusually large, ranging from Parity Nonconservation to Radio Telemetering. The articles, however, fall into one or two groups of more closely related subjects.

The first article on *Recent Advances in Photoemission* by P. Görlich gives a short up-to-date account of the interesting advances made in the past few years in the development of compound alkali metal cathodes with a short discussion of the theory of their operation. This may be grouped with the article by O. Hachenberg and W. Brauer on *Secondary Electron Emission from Solids*, which after an all too brief review of recent experimental data gives a rather protracted and sometimes obscure account of developments in the theory. It is interesting to note that data for a number of semiconductors and a good many insulators is given; too often this data is restricted to metals. Less closely related to this group is a long article by R. Clark Jones on *Quantum Efficiency of Detectors for Visible and Infrared Radiation*. This collects together much of the extensive material which the author has written on this subject. For the specialist in this field the article will provide a useful reference but for others it will make rather difficult reading. The article on *Electron Diffraction Structure Analysis and the Investigation of Semiconducting Materials* by Z. G. Pinsker (translated by L. B. Leder) gives an account mainly of Russian work in this field. There is not a great deal of information available on this particular aspect of crystal analysis and the article is a useful addition to the literature on semiconductors.

Articles of a more " electronic " type are those on *Radio Telemetering by* H. B. Riblet, dealing mainly with American practice, and on *Operational Amplifiers* by R. L. Konigsberg. The latter article is mainly theoretical; it covers a good deal of ground well-known to specialists in the field but makes very difficult reading for those not already familiar with it. It is rather typical of a great many articles in this particular field which contain much more abstract theory than practical guidance. Allied to this group of articles is that by G. E. Barlow, J. A. Overstone and F. F. Thonemann on *Automatic Data Processing in the Physical Sciences*. This is rather more discussive than informative, though some interesting examples of data processing are rather briefly described.

Finally, there is an article on *Parity Nonconservation in Weak Interactions*, by R. M. Sternheimer. This is rather more closely allied to Nuclear Physics than to Electronics and will hardly appeal to most electronics engineers. It gives quite a good account of recent work in this field but an extensive knowledge of the theoretical background of quantum mechanics is necessary in order fully to appreciate it.

As with previous issues the volume gives good value for money and both electronics engineers and physicists concerned with electronic techniques will wish to have it available for consultation. P. A. S.

Optics and Spectroscopy (*Optika i Spektroskopia*). Scientific articles translated on the initiative of the Optical Society of America. (The Optical Society of America.) [Pp. 84 per volume.]

This monthly journal of the U.S.S.R. Academy of Sciences commenced publication in 1956. It publishes work in all branches of optics and spectroscopy, (including x-ray, ultra-violet, visible, infra-red and microwave), thin film optics, filters, detectors, diffraction gratings and electroluminescence, and their many other applications in science and industry. The English translation starts from Volume 6, January 1959. At present it appears about six months after the Russian original but it is hoped to reduce the interval to four months. The printing of the translation is clear though rather small.

A typical number contains fourteen papers of average length equivalent to 3800 words and about an equal number of " brief reports " of average length about 1250 words. News items, book reviews and very brief letters are also included. About 40% of the space is occupied by papers on molecular spectroscopy which would be suitable for the Journal of the Faraday Society or the Journal of Chemical Physics. Another 25% of the material is in the field of Solid State Physics (absorption spectra and luminescence). Only about 30% falls within the field of J.O.S.A. or Optica Acta. About half the papers refer almost entirely to Russian journals (including earlier numbers of this journal) and in some cases this is at present a serious obstacle to understanding.

The general scientific standard is high and the translation is very welcome.

R. W. D.

Experimental Nuclear Physics, Vol. III (Editor : E. Segrè). By E. Segrè, G. C. Hanna, M. Deutsch, O. Kofoed-Hansen and E. M. McMillan. (New York : John Wiley and Sons, Inc. ; London : Chapman and Hall.) [Pp. x+811.] 184*s*.

This is the third and final volume in the series. Segrè writes on Radioactive Decay, Hanna on Alpha-Radioactivity, Deutsch and Kofoed-Hansen two parts on Gamma-rays and Beta-rays and McMillan on Particle Accelerators. The case for this type of venture, made by Segrè in his Preface, is that " . . . a summary in book form is becoming even more necessary than it was a few years ago owing to the tremendous swelling of the literature ". This is indeed

a case for a series of summaries prepared by dedicated practitioners of their various fields, but book form imposes unwelcome rigidity and the hard covers give a false air of permanence. When we add to the enormous delays that attend such publications, at least in America, the prohibitive cost, the purpose of such publications as against the standard review series is difficult to see. Books there must still be, but the time has surely come when individual publications on the various sections of the subject, written at an epoch appropriate to each, should take the place of these compendious edited works that themselves arise from the impossibility that a single-author book entitled ' Nuclear Physics ' can ever again take us to the frontiers of knowledge.

Hanna's article is beautifully and conscientiously composed. It is droll that his final ' Note added in proof ' (referring to work done in 1957) should take us back more than 20 years. The chapter on Gamma-rays (for which compilation of material finished in the summer of 1955) is a rather personal account of the subject but contains much valuable information. Beta-rays similarly are cut off in the summer of 1955 for the most part but parity is mercifully caught in time and even V-A. McMillan's article is a delight. It is written from an intimacy with his material that few other than the author can command and that we shall never see again in the field of particle accelerators. D. H. W.

Principles of Optics. By Max Born and Emil Wolf. (London : Pergamon Press, 1959.) [Pp. 803.] £6.

This is a monumental work which should immediately become a standard text. It is intended to fill the same place for the English speaking world as Born's ' Optik ' has held for German readers. It is, however, much more than a translation ; it has been largely rewritten and is completely up to date. The aim, as in the earlier work, is to present optics deductively as a system based on Maxwell's equations. The field covered is narrower than in the earlier work, as classical molecular optics is largely omitted. The discussion is therefore limited to situations in which the atomistic structure of matter plays no decisive part. Within this limitation, the treatment is thorough and comprehensive. There are specialist contributions from seven additional authors : A. B. Bhatia, P. C. Clemmov, D. Gabor, A. R. Stokes, A. M. Taylor, P. A. Wayman and W. L. Wilcock.

Many topics are here presented in a systematic manner for the first time : for example, the treatment of partially coherent light is particularly valuable. The presentation is exceptionally clear, and the printing and illustrations reach a high standard. This book will be needed in every physics library. B. H. B.

Applications of Thermo-Electricity. By H. J. Goldsmid. (London : Methuen.) [Pp. 118.] 10*s.* 6*d.*

This is a neat little book about the practical problem of applying the thermoelectric effect. It deals with the theoretical estimation of the efficiency of thermocouples, and the figure of merit of thermoelectric materials. Attention is then focused on the Bi_2Te_3 type of compound, whose properties are discussed in detail. Finally there is a survey of devices which have been designed or constructed using the Peltier or Seebeck effects. Obviously, with the rapid development of the art (no doubt by the author himself), this part of the text will soon be dated. Meanwhile, it will hold its own as an intelligible and useful review of an interesting application of solid state physics. There is much to be said for its publication here under its own covers at a reasonable price, instead of it being, perhaps, one of a miscellaneous collection of review articles in an expensive and clumsy volume. J. M. Z.

Journal of Nuclear Energy : Part C. Ed. J. V. Dunworth. (London : Pergamon Press.) £7 per volume.

The colossal growth of plasma physics over the last few years may appear to some as a symptom of the instability of plasma physicists, but the present scale of plasma research justifies the initiation by the Pergamon Press of this new journal, which is comfortably shared with accelerator physics ; thermonuclear research is also featured. It is indeed a great benefit to workers in these fields, to have most of their literature concentrated in relatively few journals, and this one offers two other excellent services, namely abstracts of Russian papers and a list of titles of papers from ~100 journals.

While welcoming the new journal, it is fitting to recall our past debt to the dear old *Phil. Mag.* J. W. D.

Theory of Space Time and Gravitation. By V. Fock. (Pergamon Press, 1959.)

This is an outstandingly good book and its publication in English is a major event in the history of relativity. The book is entirely different from all other treatments of general relativity because the theory is treated as the theory of gravitation and the inconsistencies and the emptyness of the general principle of relativity are made clear. Since Professor Fock's Copenhagen lectures, these views have become more widely understood and, in particular, have completely convinced the reviewer. In addition to this uniquely distinguished treatment of the foundations of Einstein's theory of gravitation, the book also contains a superb description of special relativity and a detailed discussion of modern developments in the theory of gravitation due to Professor Fock and others. Although these later chapters are of primary interest to the specialist, the book can be thoroughly recommended to all physicists for its other parts. The author's views on harmonic co-ordinate systems are set out with studied moderation. The translation by Professor Kemmer is worthy of the book and an outstanding model of what a translation should be, conveying the most difficult views with a precision of language only too rarely met in translations. H. B.

The Study of Elementary Particles by the Photographic Method. By C. F. Powell P. H. Fowler, and D. H. Perkins. (Pergamon Press, 1960.) [Pp. 650+xxxv.] £12 10*s*. 0*d*.

The last fifteen years have seen the discovery of a host of unstable particles, which are apparently fundamental to the structure of matter. In the forefront of the techniques for their detection has been the use of nuclear emulsions, pioneered by Professor Powell and his co-workers at Bristol. In this massive book, the authors have succeeded in presenting a detailed history of the discovery of the new particles, and have demonstrated the methods used for their identification by including an extensive collection of microphotographs taken largely from their own experiments. The presentation throughout is lucid, and should be intelligible to anyone with a knowledge of the rudiments of nuclear physics. It sets before the general reader many photographs of historical interest, and imparts much of the excitement of the original discoveries, while the research worker will benefit from the exhaustive discussion of the techniques of measurement and their limitations.

After a general introduction to the history of emulsions, there is an account of their manufacture and processing, including the theory of track formation. In §§ 3 to 5 attention is focused on track densities, scattering, δ-rays, and a multitude of other tricks used to deduce particle momenta and energies. The accuracy possible in emulsions is impressive, particularly when one comes to

hyperfragments, " which it is possible to study in detail only with the photographic method ", as the authors say with obvious pride. The excellent reproduction of 190 microphotographs enables the reader to judge this for himself, and perhaps justifies the lavishness of the production, which has made the price of the book so regrettably high.

Sections 6 to 12 deal in turn with each of the new particles. The detailed discussion of events will appeal to all readers with detective instincts. Complementary information from counter experiments and cloud chambers is included with plentiful diagrams wherever these techniques are superior to emulsions, although the section on hyperons seems rather brief compared with that on K-mesons. The emphasis throughout is on experimental technique, and it seems a pity that a little more space could not have been given to the theoretical schemes into which the elementary particles and their interactions have been fitted. A brief description of the Gell–Mann–Nishijima scheme is given, but the discovery of the non-conservation of parity, in which π- and K-mesons played such an important part, is restricted to five pages. Rather, to the theoreticians, this book will provide an insight into the reliability of experimental data, an invaluable contribution in these days when theoreticians and experimenters are so remote from each other.

Sections 13 to 16 describe interactions of very energetic particles in cosmic rays, and provide the only compact summary of this work of which I am aware. The cosmic rays are the only source of particles with energies above 30 BeV, and emulsions will doubtless still be used for their investigation.

References are conveniently located at the end of each section, and there are good author and subject indexes. D. V. B.

BOOK NOTICES

Advances in Catalysis and Related Subjects, Vol. XI. Edited by D. D. Eley, P. W. Selwood and P. B. Weisz. (Academic Press.) [Pp. x+384.] $12.50.

Modern Physics, Fourth Edition. By H. A. Wilson. (Blackie & Son.) [Pp. xv+473.] 40*s*.

The Theory of Homogeneous Turbulence. By G. K. Batchelor. (Cambridge: University Press, 1959.) Students' Edition. [Pp. xi+197.] 18*s*. 6*d*.

Regression Analysis. By E. J. Williams. (John Wiley & Sons.) [Pp. ix+214.] 60*s*.

Classical Dynamics. By R. H. Atkin. (Heinemann.) [Pp. ix+273.] 30*s*.

Annual Review of Nuclear Science, Vol. 9. Edited by E. Segrè and L. I. Schiff. (Annual Reviews, Inc., 1959.) [Pp. vii+625.]

CORRIGENDA

The Effect of Quenching on the Formation of G.P. Zones and θ' in Al–Cu Alloys, by J. M. Silcock, 1959, *Phil. Mag.*, **4**, 1187.

1. Table 1, column 1, the third temperature should be 300° not 200°.
2. Table 3, column 3, second figure down should be 90 not 30.

[*The Editors do not hold themselves responsible for the views expressed by their correspondents.*]

Fig. 2

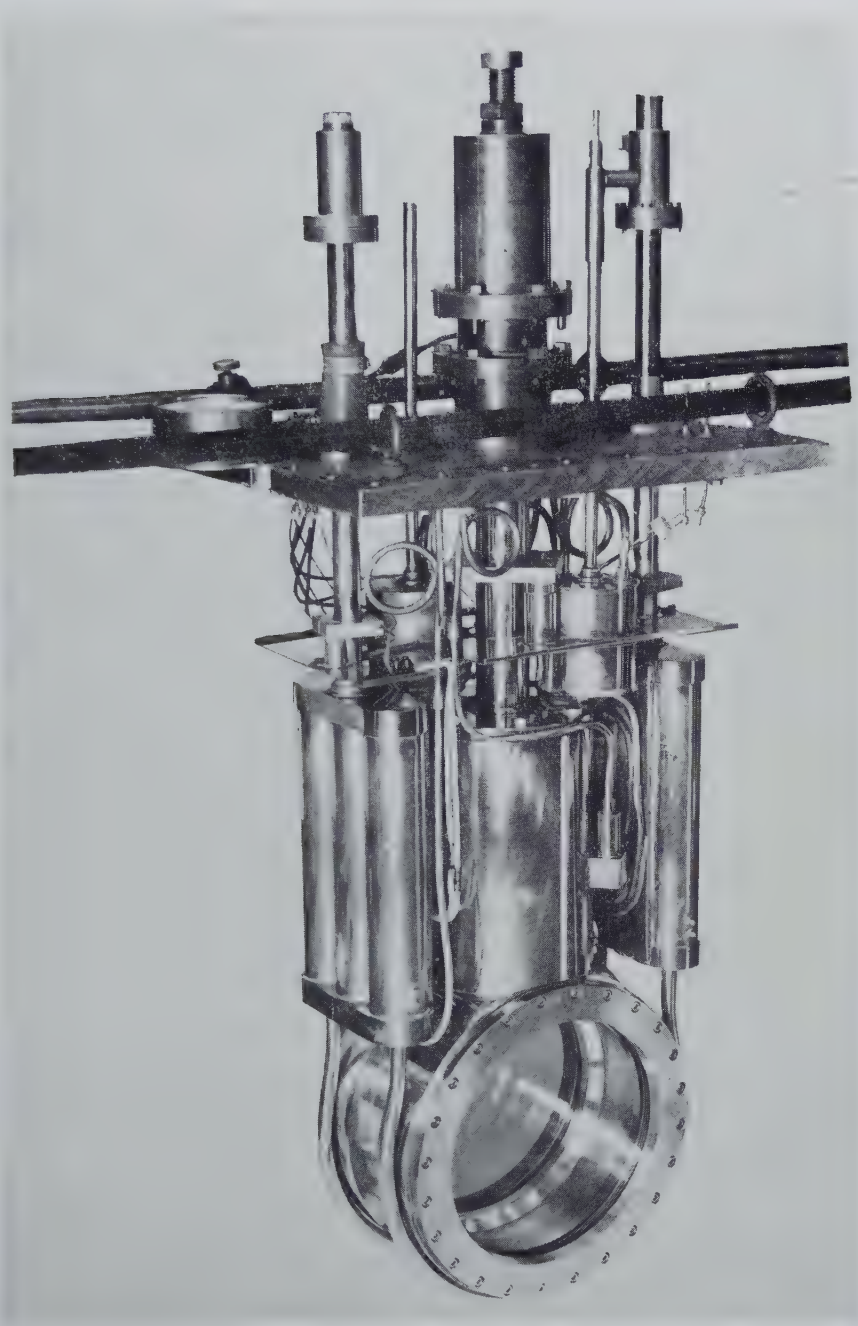

A photograph of the bubble chamber.

Fig. 4

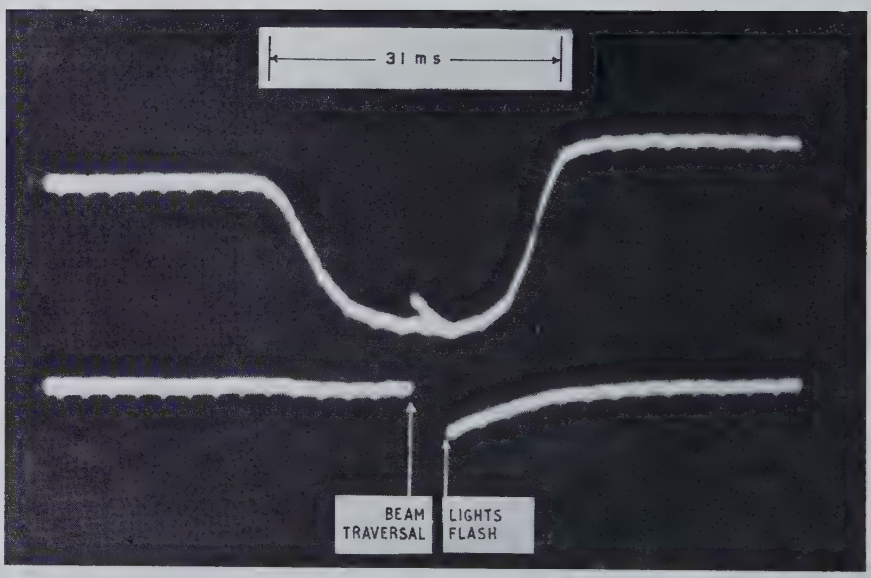

A typical oscilloscope trace showing the expansion cycle.

Fig. 5

π^--mesons stopping in the chamber taken on Kodak R55 recording film at a magnification of 1/20.

Fig. 6

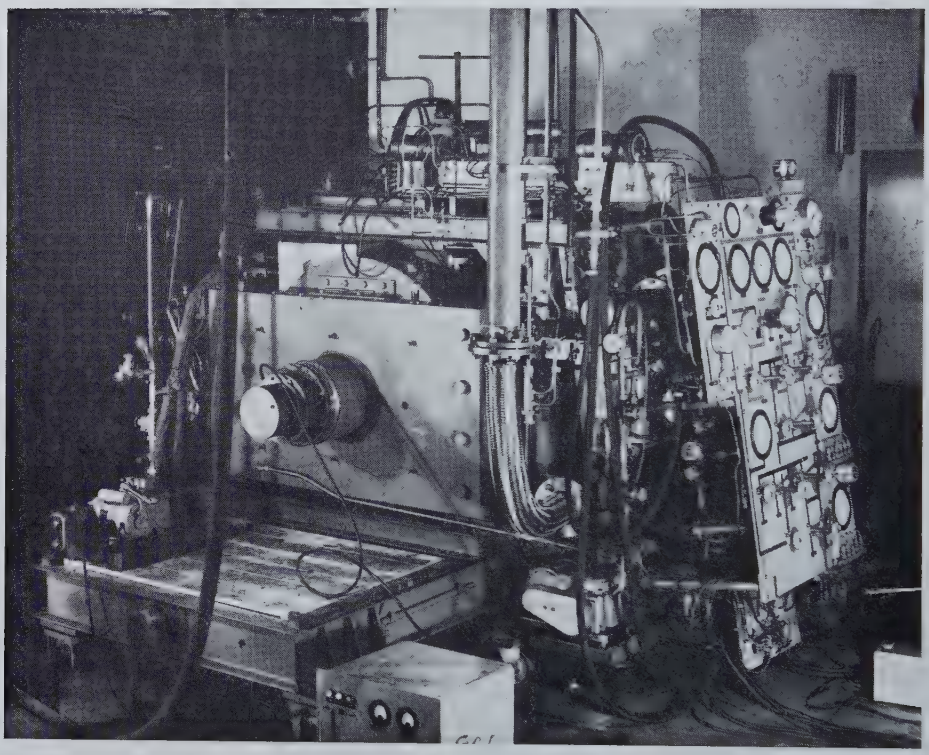

Photograph of the apparatus assembled in the π-meson beam of the 156 in. synchrocyclotron.

Fig. 1

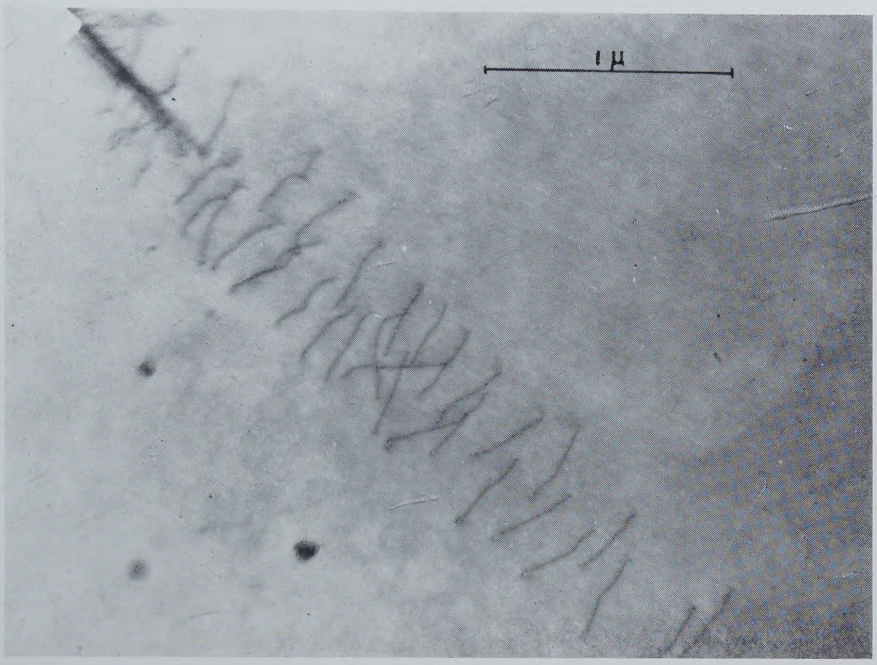

(*a*)

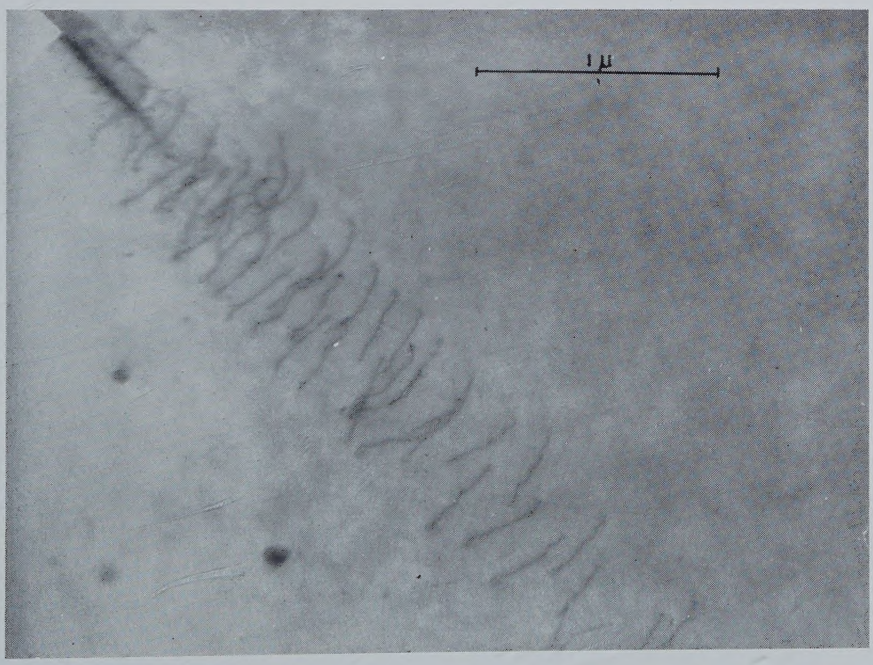

(*b*)

Fig. 1 (*continued*)

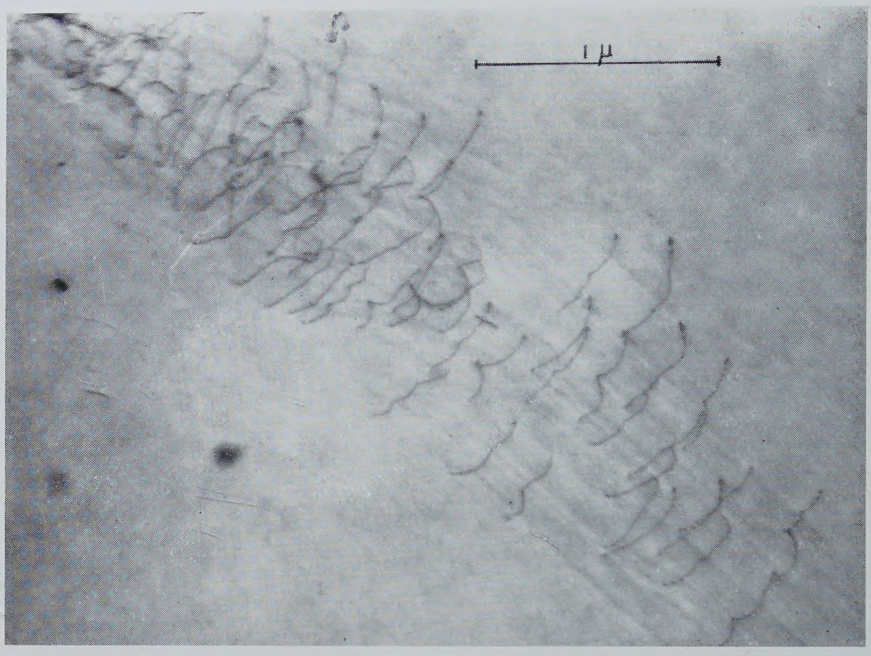

(*c*)

Three successive photographs of the same area of a magnesium oxide crystal showing dislocations moving into the specimen from a crack in the top left hand corner of the micrograph.

Fig. 2

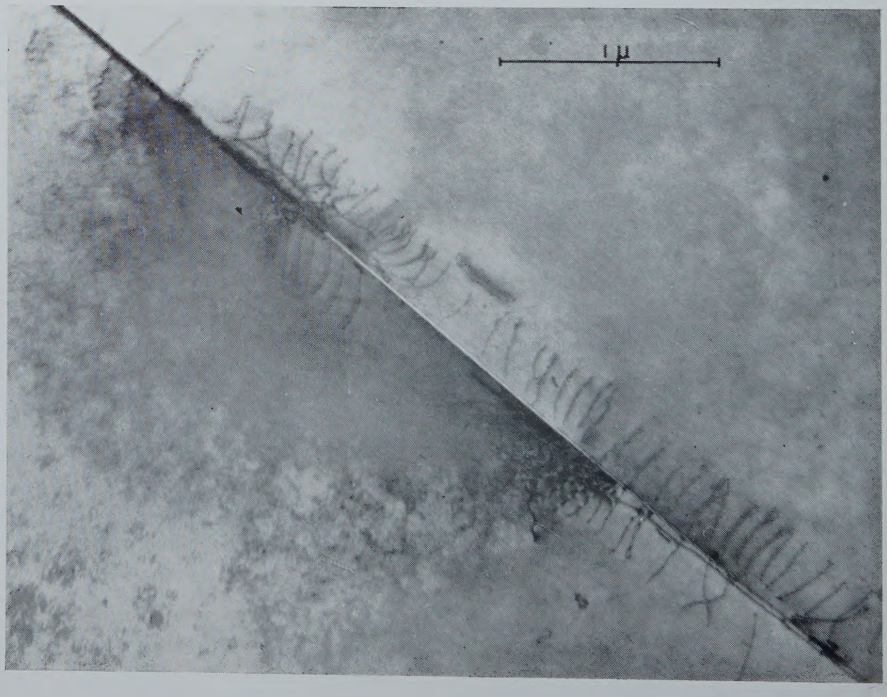

Dislocations associated with a crack in magnesium oxide.

PROCEEDINGS OF THE PHYSICAL SOCIETY

Contents for February 1960

Published monthly: Price 12 guineas per annum

Fellowship of the Society is open to all interested in Physics; Annual Subscription 2 guineas. This entitles Fellows to the *Proceedings* at reduced rates.

For publications and further information apply to:

THE PHYSICAL SOCIETY,

1 Lowther Gardens, Prince Consort Road, London, S.W.7

THE PHILOSOPHICAL MAGAZINE

Vol. 5 February 1960 No. 50

Eighth Series

Contents